The Pennsylvania State University
The Graduate School

DYNAMICAL ELECTRON-PROTON CORRELATION IN THE NUCLEAR-ELECTRONIC ORBITAL FRAMEWORK

A Thesis in
Chemistry
by
Chet Swalina

Submitted in Partial Fulfillment
of the Requirements
for the Degree of

Doctor of Philosophy

December 2006

The thesis of Chet Swalina was reviewed and approved* by the following:

Sharon Hammes-Schiffer
Eberly Professor of Biotechnology and Professor of Chemistry
Thesis Advisor, Chair of Committee

Barbara J. Garrison
Shapiro Professor of Chemistry

James D. Kubicki
Associate Professor of Geochemistry

Karl T. Mueller
Associate Professor of Chemistry

Ayusman Sen
Professor of Chemistry
Head of the Department of Chemistry

*Signatures are on file in the Graduate School.

Abstract

The nuclear-electronic orbital (NEO) approach is a method for including nuclear quantum effects directly into electronic structure calculations. In the NEO approach, specified nuclei are treated quantum mechanically on the same level as the electrons, and mixed nuclear-electronic wavefunctions are calculated using molecular orbital methods. The influence of dynamical electron-proton correlation within the NEO framework is the focus of this dissertation.

A formulation of nuclear-electronic orbital many-body perturbation theory (NEO-MP2) for treating electron-proton correlation is presented. Second-order Rayleigh-Schrödinger perturbation theory based on the NEO-HF (Hartree-Fock) reference Hamiltonian is used to construct corrections for electron-electron and electron-proton correlation.

Fundamental issues associated with the application of the NEO approach to hydrogen transfer systems are addressed. Within the NEO framework, the transferring hydrogen atom can be represented by two basis function centers to allow delocalization of the proton vibrational wavefunction. The NEO approach is applied to the [He-H-He]$^+$ and [He-H-He]$^{++}$ model systems. Analyses of basis center optimization with the NEO-MP2 method demonstrates that electron-proton correlation impacts the delocalized nature of nuclear wavefunctions. Technical issues pertaining to flexibility of the basis set to describe both single and double well proton potential energy surfaces, linear dependency of the hydrogen basis functions, multiple minima in the basis function center optimization, convergence of the number of hydrogen basis function centers, and basis set superposition error are also presented. The accuracy of the NEO approach is tested by comparison to grid calculations for these model systems.

The structural impact of nuclear quantum effects is investigated for a set of bihalides, $[XHX]^-$, X = F, Cl, Br, and hydrogen fluoride clusters, $(HF)_{2-8}$. Structures are calculated with the vibrational self-consistent-field (VSCF) method,

the second-order vibrational perturbation theory method (VPT2), path integral Car-Parrinello molecular dynamics (PICPMD), and the nuclear-electronic orbital (NEO) approach. In the VSCF, VPT2, and PICPMD methods, the vibrationally-averaged geometries are calculated for the Born-Oppenheimer electronic potential energy surface. Electron-electron and electron-proton dynamical correlation effects are included in the NEO approach using NEO-MP2. The nuclear quantum effects are found to alter the distances between the heavy atoms by 0.02−0.05 Å, which is of similar magnitude as electron correlation effects. For the bihalides, inclusion of the nuclear quantum effects with the NEO-MP2 or the VSCF method increases the X−X distance. The bihalide X−X distances are similar for both methods and are consistent with two-dimensional grid calculations and experimental values, thereby validating the use of the computationally efficient NEO-MP2 method for these types of systems.

For the hydrogen fluoride clusters, inclusion of nuclear quantum effects decreases the F−F distance with the NEO-MP2 method. The nuclear quantum effects included with the PICPMD and VPT2 methods result in increased F−F distances for the $(HF)_{2-4}$ clusters and decreased F−F distances for the $(HF)_{5-6}$ clusters. The VPT2 F−F distances for the hydrogen fluoride dimer and the deuterated form are consistent with the experimentally determined values. The NEO-MP2 F−F distance is in excellent agreement with the distance obtained experimentally for a model that removes the large amplitude bending motions. The NEO-MP2 method does not include the large amplitude bending motions properly because it does not recover enough dynamical electron-proton correlation.

A method that includes explicit electron-proton correlation directly into the nuclear-electronic orbital self-consistent-field framework is presented. This nuclear-electronic orbital explicitly correlated Hartree-Fock (NEO-XCHF) scheme is formulated using Gaussian basis functions for the electrons and the quantum nuclei in conjunction with Gaussian-type geminal functions. The description of the nuclear wavefunction is significantly improved by the inclusion of explicit electron-proton correlation. The NEO-XCHF method leads to hydrogen vibrational stretch frequencies that are in excellent agreement with those calculated from grid-based methods.

The results presented indicate that dynamical electron-proton correlation significantly impacts the qualitative characteristics of nuclear wavefunctions. Moreover, dynamical electron-proton correlation is essential for treating systems containing low frequency, large amplitude atomic motions such as hydrogen bonded clusters. Methods based on orbital expansions for recovering dynamical electron-proton correlation suffer from slow convergence reminiscent of that found for precise treatments of electron-electron correlation. Therefore, an explicit treatment of electron-proton correlation is required.

Table of Contents

List of Figures

List of Tables

Acknowledgments

I express my gratitude to my advisor, Professor Sharon Hammes-Schiffer, for her patience and encouragement, and for providing an atmosphere in our research group which has been condusive to my academic and proffesional development.

Some postdoctoral researchers in the Hammes-Schiffer group have been particularly helpful to me throughout my graduate career. I thank Dr. Michael Pak for generously offering his time and expertise over the last four years. Dr. Simon Webb has provided me with many insights regarding the NEO project and electronic structure theory in general. I also thank Dr. Arindam Chakraborty for a great deal of help learning about VSCF, VPT2, and geminals. Last and not least, thanks to Dr. Alexander Soudakov for all of his help.

During my undergraduate work, I was fortunate to learn from some outstanding instructors. I thank my undergraduate advisor, Professor Guillermo Moyna, for introducing me to computational chemistry and scientific research in general. Professor Alan Levin was my organic chemistry professor and I credit him for evoking my interest in science.

Most importantly, thanks to my wife, Lisa, my mother, Marleigh, and my late father, Chet. I appreciate all of your unconditional love and support throughout my graduate career.

Dedication

For my wife, Lisa, and my parents, Marleigh and Chet.

Chapter 1

Introduction

1.1 Nuclear quantum effects

Nuclear quantum effects are defined as zero point energy, anharmonicity, hydrogen tunneling, and vibrational excitations. These effects are important in numerous chemical and biological processes. They impact the energetics, optimized molecular structures, reaction paths, and dynamics of chemical reactions. Nuclear quantum effects are particularly important for studying hydrogen transfer reactions and hydrogen bonding interactions due to the small mass of the hydrogen atom.

Several approaches have been developed to include nuclear quantum effects in electronic structure calculations. Using the harmonic approximation, zero point energies and vibrational frequencies are accounted for by computing and diagonalizing the second derivative, or Hessian matrix. Anharmonic effects can be included for stationary points corresponding to minima on the potential energy surface using vibrational perturbation theory (VPT) [1, 2, 3] or vibrational self-consistent field (VSCF) [4, 5] approaches. Nuclear tunneling effects can be included using the Bell tunneling correction [6]. Tunneling effects can also be accounted for using semi-classical tunneling corrections based on the minimum energy path [7]. Numerical grid-based calculations of the nuclear vibrational wavefunctions for individual geometry configurations are another approach for including nuclear quantum effects [8, 9]. A common thread among these approaches is that they treat the nuclear quantum effects as corrections determined after the generation of the reaction path.

An alternative perspective is provided by the nuclear-electronic orbital (NEO)

approach [10, 11, 12, 13, 14, 15, 16, 17, 18, 19]. Instead of determining nuclear quantum effects as subsequent correction factors, the NEO approach is a method for including nuclear quantum effects *directly* into electronic structure calculations. In the NEO approach, selected nuclei are treated quantum mechanically on equal footing with the electrons. Mixed nuclear-electronic wavefunctions are calculated by solving the time-independent nuclear-electronic Schrödinger equation using molecular orbital techniques. Both the electronic and nuclear molecular orbitals are expressed as linear combinations of Gaussian basis functions. The variational method is used to minimize the energy with respect to all molecular orbitals.

Including nuclear quantum effects via the NEO framework is advantageous for several reasons. In the NEO approach, nuclear quantum effects are included during the electronic structure calculation rather than as a correction. Thus, non-adiabatic effects are included because the Born-Oppenheimer separation [20, 21, 22] between the electrons and quantum nuclei is avoided. Excited *vibronic* states can be calculated. The accuracy of NEO calculations can be improved systematically by increasing the size and quality of the basis set.

1.2 Summary of the nuclear-electronic orbital approach

In the NEO framework, the system is divided into N_c classical nuclei, N_e electrons, and N_p quantum nuclei. The total Hamiltonian for the quantum subsystem is

$$\begin{aligned}\hat{H}_{tot} = &-\sum_{i}^{N_e}\frac{1}{2}\nabla_i^2 - \sum_{i'}^{N_p}\frac{1}{2M_{i'}}\nabla_{i'}^2 - \sum_{A}^{N_C}\sum_{i}^{N_e}\frac{Z_A}{r_{iA}} \\ &+\sum_{A}^{N_C}\sum_{i'}^{N_p}\frac{Z_{i'}Z_A}{r_{i'A}} + \sum_{i}^{N_e}\sum_{j>i}^{N_e}\frac{1}{r_{ij}} + \sum_{i'}^{N_p}\sum_{j'>i'}^{N_p}\frac{1}{r_{i'j'}} - \sum_{i}^{N_e}\sum_{i'}^{N_p}\frac{Z_{i'}}{r_{ii'}}\end{aligned} \tag{1.1}$$

where the unprimed indices i, j refer to electrons, the primed indices i', j' refer to quantum nuclei, and the indices A, B refer to classical nuclei.

At the Hartree-Fock level, the total nuclear-electronic wavefunction is approxi-

mated as a product of single configurational electronic and nuclear wavefunctions:

$$\Psi_{tot}\left(\mathbf{r}^e, \mathbf{r}^p\right) = \Phi_0^e\left(\mathbf{r}^e, \mathbf{r}^p\right) \Phi_0^p\left(\mathbf{r}^e, \mathbf{r}^p\right) \tag{1.2}$$

where $\Phi_0^e\left(\mathbf{r}^e\right)$ and $\Phi_0^p\left(\mathbf{r}^p\right)$ are determinants of spin orbitals representing the electrons and fermionic nuclei. Here $\mathbf{r}^e$ and $\mathbf{r}^p$ represent the spatial coordinates of the electrons and quantum nuclei, respectively.

The resulting Hartree-Fock-Roothaan equations for an RHF treatment of the electrons and a high-spin open shell treatment of the quantum nuclei are

$$\sum_{\nu}^{N_{bf}^e} F_{\mu\nu}^e c_{\nu i}^e = \varepsilon_i^e \sum_{\nu}^{N_{bf}^e} S_{\mu\nu}^e c_{\nu i}^e, \qquad i = 1, \ldots, N_e/2 \tag{1.3}$$

$$\sum_{\nu'}^{N_{bf}^p} F_{\mu'\nu'}^p c_{\nu' i'}^p = \varepsilon_{i'}^p \sum_{\nu'}^{N_{bf}^p} S_{\mu'\nu'}^p c_{\nu' i'}^p, \qquad i' = 1, \ldots, N_p \tag{1.4}$$

where $S_{\mu\nu}^e$ and $S_{\mu'\nu'}^p$ are overlap matrix elements, $F_{\mu\nu}^e$ and $F_{\mu'\nu'}^p$ are Fock matrix elements and $c_{\mu i}^e$ and $c_{\mu' i'}^p$ are coefficients of Gaussian basis fucntions in the expansion of molecular orbitals. There are N_{bf}^e electronic basis functions and N_{bf}^p quantum nuclear basis functions.

The Fock matrix elements are expressed as

$$F_{\mu\nu}^e = h_{\mu\nu}^e + G_{\mu\nu}^e - \sum_{\lambda'\sigma'}^{N_{bf}^p} P_{\lambda'\sigma'}^p (\varphi_\mu^e \varphi_\nu^e | \varphi_{\lambda'}^p \varphi_{\sigma'}^p) \tag{1.5}$$

$$F_{\mu'\nu'}^p = h_{\mu'\nu'}^p + G_{\mu'\nu'}^p - \sum_{\lambda\sigma}^{N_{bf}^e} P_{\lambda\sigma}^e (\varphi_{\mu'}^p \varphi_{\nu'}^p | \varphi_\lambda^e \varphi_\sigma^e) \tag{1.6}$$

where $h_{\mu\nu}^e$ and $h_{\mu'\nu'}^p$ are the core Hamiltonian matrix elements for electrons and protons, respectively, and $G_{\mu\nu}^e$ and $G_{\mu'\nu'}^p$ are the two-particle matrix elements for the electrons and the quantum nuclei. The third contribution to the Fock matrix is from the mixed quantum nuclear-electronic interaction. These mixed terms cou-

ple the electronic and nuclear pieces through the one particle density matrices for the electrons, $P^e_{\lambda\sigma}$ and quantum nuclei, $P^p_{\lambda'\sigma'}$. This leads to the nuclear-electronic self-consistent field (SCF) procedure depicted in Figure 1.1. Note that since at the NEO-HF level the total nuclear-electronic wavefunction is a product of electronic and nuclear wavefunctions the overall wavefunction is separable into quantum nuclear and electronic degrees of freedom. However, this approach still does not invoke the Born-Oppenheimer separation between quantum nuclei and electrons because the electronic and nuclear wavefunctions respond to each other in a mean-field way.

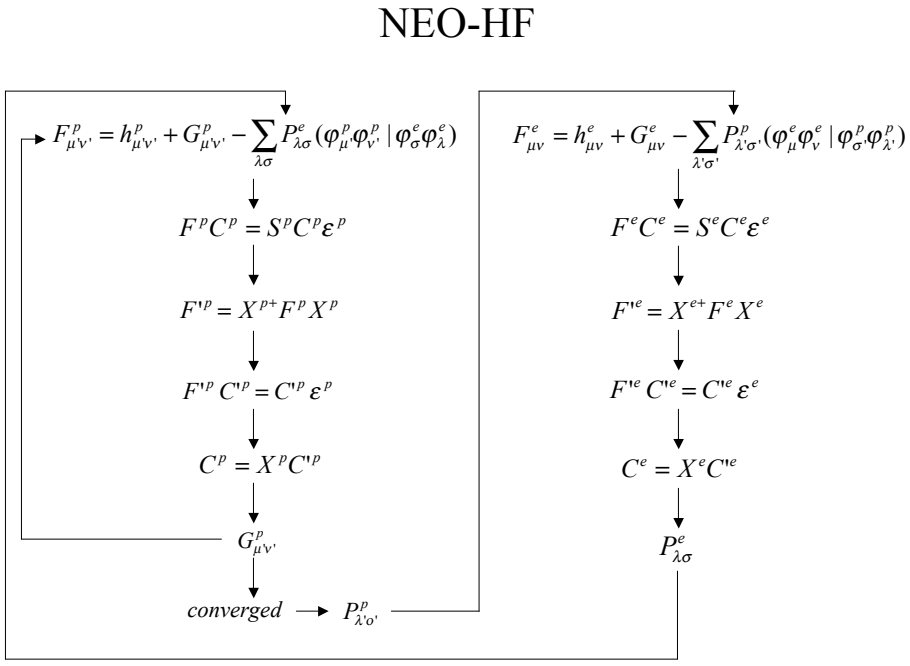

Figure 1.1. A nuclear-electronic orbital self-consistent field scheme. Other NEO SCF schemes are also possible. For instance, the electronic density could be converged for each total SCF cycle instead of the nuclear density.

The NEO-CI wavefunction has the form

$$\Psi_{tot}\left(\mathbf{r}^e,\mathbf{r}^p\right)=\sum_{I}^{N_{CI}^e}\sum_{I'}^{N_{CI}^p}C_{II'}\Phi_I^e\left(\mathbf{r}^e,\mathbf{r}^p\right)\Phi_{I'}^p\left(\mathbf{r}^e,\mathbf{r}^p\right) \tag{1.7}$$

where $\Phi_I^e\left(\mathbf{r}^e\right)$ and $\Phi_I^e\left(\mathbf{r}^e\right)$ are determinants of spin orbitals for the electrons and quantum nuclei, respectively, and $C_{II'}$ are CI coefficients. In the NEO-CI approach, the variational method is used to minimize the total energy with respect to the CI coefficients $C_{II'}$. The resulting secular equation is

$$\sum_{(JJ')}^{N_{CI}}C_{(II')}\left[H_{(II'),(JJ')}-\delta_{(II'),(JJ')}E\right]=0, \tag{1.8}$$

which can be solved by diagonalizing the NEO-CI Hamiltonian, $H_{(II'),(JJ')}$, to obtain the CI coefficients and the corresponding *vibronic* ground and excited state energies. In the NEO-MCSCF approach, the total energy is minimized with respect to both the CI coefficients and the electronic and nuclear MO coefficients.

The NEO method has been implemented in the GAMESS [23] electronic structure program and includes a number of useful options. Several nuclear basis sets are available, coupled with the capability to use multiple basis function centers to represent each quantum nucleus. The positions of the nuclear basis function centers can be optimized variationally during the calculation. The energies at the NEO-HF, NEO-MP2, NEO-CI, and NEO-MCSCF levels can be calculated. Direct SCF methods and an option to form symmetry adapted linear combinations of nuclear molecular orbitals have been implemented at the NEO-HF level. Both RHF and ROHF treatments of electrons are implemented in the code. The NEO-HF gradients [10] are implemented in the code. Numerical Hessians can be calculated [11], and stationary points on the NEO potential energy surface can be identified and characterized.

Other groups have also investigated approaches similar to the NEO method. Thomas and co-workers [24, 25] formulated an approach similar to the NEO method to treat protons and electrons on equal quantum mechanical footing with a molecular orbital approach using Slater-type basis functions. Tachikawa, Nakai and co-workers have developed the nuclear orbital molecular orbital (NOMO) method

[26, 27]. They have implemented the NOMO-HF (Hartree-Fock) [26, 27], NOMO-CIS (configuraton interaction method with singles) [28], NOMO-MBPT (many-body perturbation theory) [29], and the TRF-NOMO (translation and rotation free) method [30, 31]. Kreibich and Gross have developed a nuclear-electronic method based on density functional theory [32] and Shigeta and co-workers have explored similar approaches [33, 34, 35]. Sherrill and co-workers have developed the electronic and nuclear molecular orbitals method [36]. Adamowicz and co-workers have developed a non-Born-Oppenheimer approach to treat atomic or small molecular systems using an explicitly-correlated approach formulated using Gaussian-type geminal basis functions [37, 38, 39].

1.3 Electron-proton correlation

Similar to conventional electronic structure theory [40], electron-proton correlation can be classified as two different effects. Dynamical electron-proton correlation emerges from difficulties accounting for the correlated motions of an electron and a proton due to their instantaneous mutual *attraction*. Moreover, dynamical electron-proton correlation is concerned with accounting for the electron-proton cusp condition which arises from the r^{-1} potential energy interactions that become singular as the electron$-$proton separation distance, r, approaches zero. Within the NEO framework, dynamical electron-proton correlation is even more important than electron-electron correlation due to the attractive Coulomb forces between an electron and proton. This concept has been illustrated analytically using a simple model system in Ref.[12]. Nondynamical or *static* electron-proton correlation is not related to the attraction between an electron and proton. Rather, nondynamical electron-proton correlation arises from strong mixing between the NEO-HF and other configurations which are nearby in energy.

Non-dynamical electron-proton correlation may be incorporated into NEO-CI-based methods by including a few physically relevant electronic and nuclear molecular orbitals in the active space. Dynamical electron-proton correlation can be included in NEO-CI-based calculations by increasing the size of the active space. However, this strategy for including dynamical electron-proton correlation can become computationally intensive for very large active spaces. A more tractable

approach to include both electron-electron and electron-proton dynamical correlation based on many-body perturbation theory is presented in Chapter 2.

We have shown that dynamical electron-proton correlation is important for hydrogen tunneling systems [12, 13]. In addition to hydrogen transfer systems, the influence of dynamical electron-proton correlation will be important for other systems. For instance, nuclear quantum effects stemming from the hydrogen atom motions will be important for studying hydrogen bonded systems. For hydrogen bonded systems, the nuclear wavefunctions are single configurational and will be dominated by dynamical electron-proton correlation.

1.4 Outline

The aim for this thesis is three-fold. One objective is to develop methods for including dynamical electron-proton correlation in the NEO framework. Another is to develop insights regarding the impact of dynamical electron-proton correlation on nuclear wavefunctions. A tertiary goal is to understand how nuclear quantum effects impact hydrogen bonding. This type of understanding is important for applying the NEO method to hydrogen bonded systems.

The remainder of this thesis is organized as follows. Chapter 2 presents the formulation of the nuclear-electronic orbital second-order many-body perturbation theory approach for including dynamical electron-proton correlation. In Chapter 3, a model system is used to explore various issues for treating hydrogen transfer systems with the NEO approach including the number of basis function centers used to represent the hydrogen and the optimization of the positions of the centers. In Chapter 4, the NEO, VSCF, and VPT2 approaches are used to study the structural impact of nuclear quantum effects on hydrogen bonded systems, including bihalides and the hydrogen fluoride dimer. Chapter 5 explores the impact of nuclear quantum effects on hydrogen bonding in general using the path integral Car-Parrinello molecular dynamics [41] approach and the VPT2 method. A method for including explicit dynamical electron-proton correlation in the NEO framework is presented in Chapter 6. Chapter 7 presents conclusions and possible future directions.

Chapter 2

Many-body perturbation theory for electron-proton correlation

Reproduced in part with permission from:
C. Swalina, M. Pak, and S. Hammes-Schiffer "Alternative formulation of many-body perturbation theory for electron-proton correlation,"
Chem. Phys. Lett. **404**, 394-399 (2005).

2.1 Introduction

A wide range of chemically and biologically important processes require the transfer of a hydrogen nucleus[42]. Conventional modeling of these reactions is based on the Born-Oppenheimer separation of the nuclei and the electrons, and the nuclei are represented as classical point charges. However, nuclear quantum effects such as zero point motion and hydrogen tunneling are often significant for such hydrogen transfer reactions[43]. Recently methods have been developed to avoid the Born-Oppenheimer separation and treat nuclei quantum mechanically on the same level as the electrons [26, 33, 44, 32, 29, 10, 11, 12, 13]. In particular, the nuclear-electronic orbital (NEO) approach [10, 11, 12, 13] is designed to treat specified nuclei (e.g., the transferring hydrogen nucleus in hydrogen transfer reactions) quantum mechanically, while the remaining nuclei are treated classically. Electron-proton correlation has been shown to play an essential role in hydrogen transfer reactions[12] and has been incorporated into the NEO approach with multicon-

figurational self-consistent-field methods [10, 12, 13]. Another powerful tool for treating electron-proton correlation is many-body perturbation theory[29].

In this Chapter, we present two distinct formulations of many-body perturbation theory for treating electron-proton correlation. The first formulation is a straightforward extension of many-body perturbation theory for electronic systems [45, 46] and is applicable to all mixed nuclear-electronic systems. The second formulation is based on a reference Hamiltonian that does not include the proton-proton Coulomb-exchange operator and is applicable to systems containing a single quantum nucleus, such as the transferring hydrogen for hydrogen transfer reactions. Although the two formulations are based on different reference Hamiltonians, the ground state Hartree-Fock (HF) wavefunction and the perturbation are identical for both formulations in applications to systems with a single quantum nucleus. We demonstrate that the removal of the proton-proton Coulomb-exchange operator from the reference Hamiltonian for these types of systems does not alter the singly occupied proton orbital but strongly impacts the virtual orbital energies. This procedure is directly related to Huzinaga's improved virtual orbital generation technique[47] and its subsequent extensions[48] for electronic structure calculations. In the present case, the focus is on improving the nuclear rather than the electronic virtual orbitals, and the modified reference Hamiltonian arises naturally for systems with a single quantum nucleus. Moreover, this chapter analyzes the impact of these improved virtual orbitals on the energies obtained from perturbation theory rather than configuration interaction approaches.

Our analysis indicates that the removal of the proton-proton Coulomb-exchange operator from the reference Hamiltonian can lead to a significantly lower second-order energy and potentially faster convergence of the perturbation series for many-electron systems with a single quantum nucleus and many classical nuclei. In addition to the analytical analysis, we provide the numerical results obtained from applications to three chemical systems: $[\mathrm{He-H-He}]^+$, $[\mathrm{F-H-F}]^-$, and $[\mathrm{Cl-H-Cl}]^-$. The results illustrate that this approach can lower the second-order energy by more than 3 kcal/mol.

2.2 Theoretical formulation and analysis

First we present the general derivation of the NEO many-body perturbation theory for a system with N_e paired or high-spin electrons and N_p paired or high-spin protons. Here we define the reference NEO-HF (Hartree-Fock) Hamiltonian as

$$\begin{aligned} H_0^{\mathrm{NEO}} = &\sum_{i}^{N_e} \left\{ h^e(i) + \nu_{ee}^{\mathrm{HF}}(i) + \nu_{ep,e}^{\mathrm{HF}}(i) \right\} \\ &+ \sum_{i'}^{N_p} \left\{ h^p(i') + \nu_{pp}^{\mathrm{HF}}(i') + \nu_{ep,p}^{\mathrm{HF}}(i') \right\} \end{aligned} \tag{2.1}$$

The unprimed indices refer to electrons, and the primed indices refer to the quantum protons. The superscripts e and p denote electrons and quantum protons, respectively. In this expression, h^e and h^p are the one particle terms for the electrons and protons, respectively, and are defined in [10]. The two particle operators are defined as:

$$\begin{aligned} \nu_{ee}^{\mathrm{HF}}(1)\chi_j^e(1) = &\sum_b \langle \chi_b^e(2)| \, r_{12}^{-1} \, |\chi_b^e(2)\rangle \chi_j^e(1) \\ &- \sum_b \langle \chi_b^e(2)| \, r_{12}^{-1} \, \big|\chi_j^e(2)\big\rangle \chi_b^e(1) \end{aligned} \tag{2.2}$$

$$\begin{aligned} \nu_{pp}^{\mathrm{HF}}(1')\chi_{j'}^p(1') = &\sum_{b'} \langle \chi_{b'}^p(2')| \, r_{1'2'}^{-1} \, |\chi_{b'}^p(2')\rangle \chi_{j'}^p(1') \\ &- \sum_{b'} \langle \chi_{b'}^p(2')| \, r_{1'2'}^{-1} \, \big|\chi_{j'}^p(2')\big\rangle \chi_{b'}^p(1') \end{aligned} \tag{2.3}$$

$$\nu_{ep,e}^{\mathrm{HF}}(1)\chi_j^e(1) = -\sum_{b'} \langle \chi_{b'}^p(1')| \, r_{11'}^{-1} \, |\chi_{b'}^p(1')\rangle \chi_j^e(1) \tag{2.4}$$

$$\nu_{ep,p}^{\mathrm{HF}}(1')\chi_{j'}^p(1') = -\sum_{b} \langle \chi_b^e(1)| \, r_{11'}^{-1} \, |\chi_b^e(1)\rangle \chi_{j'}^p(1') \tag{2.5}$$

where the spin orbitals are referred to by the symbol χ, and the summations $\sum_{b}$ and $\sum_{b'}$ are over the occupied electronic and proton spin orbitals, respectively. Thus, $\nu_{ee}^{\mathrm{HF}}(i)$ and $\nu_{pp}^{\mathrm{HF}}(i')$ are the Coulomb-exchange operators for the electrons and protons respectively, and $\nu_{ep,e}^{\mathrm{HF}}(i)$ and $\nu_{ep,p}^{\mathrm{HF}}(i')$ are the electron-proton Coulomb operators for the electrons and protons, respectively. The electronic and nuclear Fock equations are

$$f^e(1)\chi_i^e(1) = \left(h^e(1) + \nu_{ee}^{\mathrm{HF}}(1) + \nu_{ep,e}^{\mathrm{HF}}(1)\right)\chi_i^e(1) = \varepsilon_i^e\chi_i^e(1) \tag{2.6}$$

$$f^p(1')\chi_{i'}^p(1') = \left(h^p(1') + \nu_{pp}^{\mathrm{HF}}(1') + \nu_{ep,p}^{\mathrm{HF}}(1')\right)\chi_{i'}^p(1') = \varepsilon_{i'}^p\chi_{i'}^p(1') \tag{2.7}$$

The orbital energies can be expressed as

$$\varepsilon_i^e = \langle i\,|h^e|\,i\rangle + \sum_b \left[\langle ib|ib\rangle - \langle ib|bi\rangle\right] - \sum_{b'}\langle ib'|ib'\rangle \tag{2.8}$$

$$\varepsilon_{i'}^p = \langle i'\,|h^p|\,i'\rangle + \sum_{b'} \left[\langle i'b'|i'b'\rangle - \langle i'b'|b'i'\rangle\right] - \sum_{b}\langle bi'|bi'\rangle \tag{2.9}$$

where $\langle ij|kl\rangle = \int d\mathbf{x}_1 d\mathbf{x}_2 \chi_i^{e*}(\mathbf{x}_1)\chi_j^{e*}(\mathbf{x}_2) r_{12}^{-1}\chi_k^e(\mathbf{x}_1)\chi_l^e(\mathbf{x}_2)$.

The perturbations for electron-electron, proton-proton, and electron-proton correlation are

$$W_{ee} = \sum_{i<j}^{N_e} r_{ij}^{-1} - \sum_{i}^{N_e}\nu_{ee}^{\mathrm{HF}}(i) \tag{2.10}$$

$$W_{pp} = \sum_{i'<j'}^{N_p} r_{i'j'}^{-1} - \sum_{i'}^{N_p}\nu_{pp}^{\mathrm{HF}}(i') \tag{2.11}$$

$$W_{ep} = -\sum_{i}^{N_e}\sum_{i'}^{N_p} r_{ii'}^{-1} - \sum_{i}^{N_e}\nu_{ep,e}^{\mathrm{HF}}(i) - \sum_{i'}^{N_p}\nu_{ep,p}^{\mathrm{HF}}(i') \tag{2.12}$$

The combined perturbation for electron-electron, proton-proton, and electron-proton correlation is $W = W_{ee} + W_{pp} + W_{ep}$.

Using Rayleigh-Schrödinger perturbation theory[49], the NEO-MP2 (second-order many-body perturbation theory) energy expression for mixed electronic-nuclear wavefunctions is

$$E_0^{(2)} = \sum_{(nn')\neq(00)} \frac{\left|\langle \Phi_0^e \Phi_0^p \left| W \right| \Phi_n^e \Phi_{n'}^p \rangle\right|^2}{E_{00}^{(0)} - E_{nn'}^{(0)}} \tag{2.13}$$

Here the zeroth-order wavefunctions (i.e., the eigenfunction of H_0^{NEO} given in Eq. 2.1) are $|\Phi_0^e \Phi_0^p\rangle$ for the ground state and $|\Phi_n^e \Phi_{n'}^p\rangle$ for excited states. The zeroth-order energy $E_{nn'}^{(0)}$ is the sum of the energies corresponding to the occupied electronic and proton spin orbitals for the state $|\Phi_n^e \Phi_{n'}^p\rangle$. The notation under the summation in Eq. 2.13 indicates that both n and n' cannot simultaneously correspond to the ground state electronic and nuclear determinants, respectively.

The second-order energy correction within the nuclear-electronic framework can be expressed as

$$\begin{aligned} E_0^{(2)} = &\sum_{n\neq 0} \frac{\left|\langle \Phi_0^e \left| W_{ee} \right| \Phi_n^e \rangle\right|^2}{E_0^e - E_n^e} + \sum_{n'\neq 0} \frac{\left|\langle \Phi_0^p \left| W_{pp} \right| \Phi_{n'}^p \rangle\right|^2}{E_0^p - E_{n'}^p} \\ &+ \sum_{(nn')\neq(00)} \frac{\left|\langle \Phi_0^e \Phi_0^p \left| W_{ep} \right| \Phi_n^e \Phi_{n'}^p \rangle\right|^2}{E_0^e + E_0^p - E_n^e - E_{n'}^p} \end{aligned} \tag{2.14}$$

The W_{ee} term becomes the standard MP2 equation[49, 50] for electron-electron correlation in electronic structure theory

$$E_{ee}^{(2)} = \frac{1}{4} \sum_{abrs} \frac{\left|\langle ab \left| \right. rs \rangle - \langle ab \left| \right. sr \rangle\right|^2}{\varepsilon_a^e + \varepsilon_b^e - \varepsilon_r^e - \varepsilon_s^e} \tag{2.15}$$

where a and b refer to occupied electronic spin orbitals, and r and s refer to virtual electronic spin orbitals. Analogously, the W_{pp} term becomes

$$E_{pp}^{(2)} = \frac{1}{4} \sum_{a'b'r's'} \frac{\left|\langle a'b' \mid r's' \rangle - \langle a'b' \mid s'r' \rangle\right|^2}{\varepsilon_{a'}^p + \varepsilon_{b'}^p - \varepsilon_{r'}^p - \varepsilon_{s'}^p} \tag{2.16}$$

The only non-zero matrix elements for $\langle \Phi_0^e \Phi_0^p \left| W_{ep} \right| \Phi_n^e \Phi_{n'}^p \rangle$ include single excita-

tions in both the proton and electron determinants, leading to the second-order electron-proton correlation correction

$$E_{ep}^{(2)} = \sum_{aa'rr'} \frac{|\langle aa' \mid rr' \rangle|^2}{\varepsilon_a^e + \varepsilon_{a'}^p - \varepsilon_r^e - \varepsilon_{r'}^p} \tag{2.17}$$

where a and a' denote occupied electron and proton spin orbitals respectively, and r and r' denote virtual electron and proton spin orbitals respectively. The Goldstone diagrams corresponding to the second-order electron-electron and electron-proton correlation [49, 29] corrections are depicted in Figure 2.1. Note that the electron-proton correlation correction (Figure 2.1 (b)) only contains a Coulomb contribution since electrons and quantum protons are distinguishable particles. The total NEO-MP2 energy is $E^{\text{NEO-MP2}} = E^{\text{NEO-HF}} + E_{ee}^{(2)} + E_{pp}^{(2)} + E_{ep}^{(2)}$.

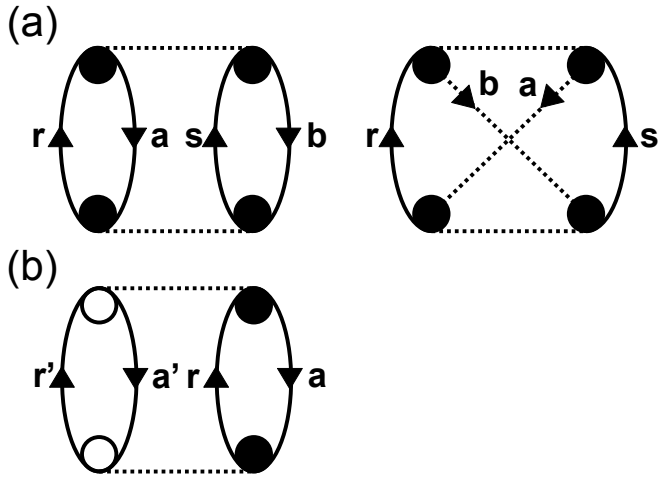

Figure 2.1. Goldstone diagrams corresponding to the second-order electron-electron (a) and electron-proton (b) correlation corrections[29].

Systems containing only one electron or one proton merit special attention when perturbation theory is used to calculate the electron-proton correlation energy. For simplicity, here we consider a system containing one electron and one proton. In this case, the perturbations corresponding to electron-electron and proton-proton correlation vanish. Thus, we need to consider only the electron-proton correlation. For this special case, the second-order electron-proton correlation correction in Eq.

2.17 simplifies to

$$E_{ep}^{(2)} = \sum_{rr'} \frac{|\langle 11' \mid rr' \rangle|^2}{\varepsilon_1^e + \varepsilon_{1'}^p - \varepsilon_r^e - \varepsilon_{r'}^p} \tag{2.18}$$

The occupied and virtual electronic orbital energies determined from Eq. 2.8 are $\varepsilon_1^e = \langle 1| h^e |1\rangle - \langle 11' \mid 11' \rangle$ and $\varepsilon_r^e = \langle r| h^e |r\rangle + \langle r1|r1\rangle - \langle r1|1r\rangle - \langle r1' \mid r1' \rangle$. The occupied and virtual proton orbital energies determined from Eq. 2.9 are $\varepsilon_{1'}^p = \langle 1'| h^p |1'\rangle - \langle 11' \mid 11' \rangle$ and $\varepsilon_{r'}^p = \langle r'| h^p |r'\rangle + \langle r'1'|r'1'\rangle - \langle r'1'|1'r'\rangle - \langle 1r' \mid 1r' \rangle$.

For a system with only one electron and one proton, an alternative reference Hamiltonian that does not include the electron-electron and proton-proton Coulomb-exchange operators can be used for the NEO-MP2 calculations. The expression for this alternative reference Hamiltonian is

$$\tilde{H}_0^{\mathrm{NEO}} = h^e(1) + \nu_{ep,e}^{\mathrm{HF}}(1) + h^p(1') + \nu_{ep,p}^{\mathrm{HF}}(1') \tag{2.19}$$

For this alternative reference Hamiltonian, the Fock equations in Eqs. 2.6 and 2.7 become

$$\tilde{f}^e(1)\tilde{\chi}_i^e(1) = \left(h^e(1) + \nu_{ep,e}^{\mathrm{HF}}(1)\right)\tilde{\chi}_i^e(1) = \tilde{\varepsilon}_i^e \tilde{\chi}_i^e(1) \tag{2.20}$$

$$\tilde{f}^p(1')\tilde{\chi}_{i'}^p(1') = \left(h^p(1') + \nu_{ep,p}^{\mathrm{HF}}(1')\right)\tilde{\chi}_{i'}^p(1') = \tilde{\varepsilon}_{i'}^p \tilde{\chi}_{i'}^p(1') \tag{2.21}$$

The nuclear Fock matrix with elements $\tilde{F}_{ij}^p = \left\langle \tilde{i}' \middle| \tilde{f}^p \middle| \tilde{j}' \right\rangle$ corresponding to the reference Hamiltonian $\tilde{H}_0^{\mathrm{NEO}}$ in the basis of the canonical spin orbitals $\tilde{\chi}_{i'}^p$ is

$$\tilde{\mathbf{F}}^p = \begin{pmatrix} \tilde{\varepsilon}_{1'}^p & 0 & \cdots & 0 \\ 0 & \tilde{\varepsilon}_{2'}^p & & \vdots \\ \vdots & & \ddots & 0 \\ 0 & \cdots & 0 & \tilde{\varepsilon}_{N'}^p \end{pmatrix} \tag{2.22}$$

For comparison, we also calculate the nuclear Fock matrix with elements $F_{ij}^p = \left\langle \tilde{i}' \middle| f^p \middle| \tilde{j}' \right\rangle$ corresponding to the reference Hamiltonian H_0^{NEO} in the basis of these

spin orbitals $\tilde{\chi}^p_{i'}$:

$$\mathbf{F}^p = \begin{pmatrix} \tilde{\varepsilon}^p_{1'} & 0 & \cdots & 0 \\ 0 & \tilde{\varepsilon}^p_{2'} + (\nu^{\mathrm{HF}}_{pp})_{22} & \cdots & (\nu^{\mathrm{HF}}_{pp})_{N2} \\ \vdots & \vdots & \ddots & \vdots \\ 0 & (\nu^{\mathrm{HF}}_{pp})_{2N} & \cdots & \varepsilon^p_{N'} + (\nu^{\mathrm{HF}}_{pp})_{NN} \end{pmatrix} \tag{2.23}$$

where $\left(\nu^{\mathrm{HF}}_{pp}\right)_{ij} = \left\langle \tilde{i}' \left| \nu^{\mathrm{HF}}_{pp} \right| \tilde{j}' \right\rangle$. This Fock matrix is block diagonal with respect to the occupied and virtual orbitals. Since the occupied orbital space is diagonal in both Eqs. 2.22 and 2.23, the occupied nuclear orbital and the corresponding orbital energy are the same for the two reference Hamiltonians given in Eqs. 1 and 19: $\tilde{\varepsilon}^p_{1'} = \langle 1' | h^p | 1' \rangle - \langle 11' \mid 11' \rangle = \varepsilon^p_{1'}$. Since the traces of these Fock matrices differ by $\sum_{i=2}^{N} \left(\nu^{\mathrm{HF}}_{pp}\right)_{ii}$, however, these two Fock matrices are not related by a unitary transformation. Thus, the virtual nuclear orbital energies are different for the two reference Hamiltonians. Specifically, the virtual nuclear orbital energies for the reference Hamiltonian $\tilde{H}^{\mathrm{NEO}}_0$ are $\tilde{\varepsilon}^p_{\tilde{r}'} = \langle \tilde{r}' | h^p | \tilde{r}' \rangle - \langle 1\tilde{r}' \mid 1\tilde{r}' \rangle$. In general, the relation between $\varepsilon^p_{r'}$ and $\tilde{\varepsilon}^p_{r'}$ is not straightforward due to the differences in the virtual orbitals.

The physical meaning of the virtual orbital energies is different for the two reference Hamiltonians. For the reference Hamiltonian $\tilde{H}^{\mathrm{NEO}}_0$, the virtual proton orbital energies correspond to the wavefunction in which the proton is transferred from the occupied orbital to the virtual orbital. In this case, the negative of the virtual orbital energy is the ionization potential for removing the proton from this orbital. These virtual orbital energies are generally negative[49]. For the reference Hamiltonian H^{NEO}_0, however, the virtual proton orbital energies correspond to the wavefunction in which a second proton is added to the virtual orbital. In this case, the second proton interacts with the first proton, which remains in the ground state occupied orbital, and the negative of the virtual orbital energy is the affinity for adding a proton to the virtual orbital. For neutral molecules, these virtual orbital energies are typically positive[49].

The analogous analysis is applicable to the electronic orbital energies for the two reference Hamiltonians. As for the proton, the occupied electronic orbital and the corresponding orbital energy are the same for the two reference Hamiltonians,

and the virtual electronic orbital energies are different for the two reference Hamiltonians. Note that conventional electronic structure calculations use the analog of H_0^{NEO} as the reference Hamiltonian for perturbation theory calculations because of the presence of more than one electron when electron-electron correlation is included. For conventional electronic structure calculations of the hydrogen atom, where only the electron is treated quantum mechanically, typically the electron-electron Coulomb-exchange operator is included in the Fock operator, and the virtual orbital energies are positive.

These analyses indicate that the electron-electron and proton-proton Coulomb-exchange operators do not alter the occupied orbital energies but strongly impact the virtual orbital energies. Differences in the virtual orbital energies associated with $\tilde{H}_0^{\mathrm{NEO}}$ and H_0^{NEO} will lead to different values of the second-order electron-proton correlation corrections. Although this effect is related to the effect of level shifting[51], in this case the alternative reference Hamiltonian is physically meaningful.

To illustrate the differences in the second-order electron-proton correlation corrections, consider a calculation for this system of one electron and one proton represented by two electronic and two nuclear basis functions. In this case, the electronic and nuclear Fock matrices are 2×2 (i.e., there are two electronic spin orbitals and two nuclear spin orbitals). The occupied electronic and nuclear spin orbitals are the same for the two reference Hamiltonians. For this small basis set, the virtual electronic and nuclear spin orbitals must also be the same for the two reference Hamiltonians because the virtual orbitals are determined by orthogonality with respect to the occupied orbitals. Thus, only the virtual orbital energies are different for the two reference Hamiltonians. In this case, the second-order electron-proton correlation corrections using H_0^{NEO} and $\tilde{H}_0^{\mathrm{NEO}}$, respectively, as the reference Hamiltonians are

$$E_{ep}^{(2)} = \frac{|\langle 11' \mid 22' \rangle|^2}{\varepsilon_1^e + \varepsilon_{1'}^p - \varepsilon_2^e - \varepsilon_{2'}^p} \tag{2.24}$$

$$\tilde{E}_{ep}^{(2)} = \frac{|\langle 11' \mid 22' \rangle|^2}{\varepsilon_1^e + \varepsilon_{1'}^p - \tilde{\varepsilon}_2^e - \tilde{\varepsilon}_{2'}^p} \tag{2.25}$$

where $\varepsilon_2^e = \tilde{\varepsilon}_2^e + \langle 21|21\rangle - \langle 21|12\rangle$ and $\varepsilon_{2'}^p = \tilde{\varepsilon}_{2'}^p + \langle 2'1'|2'1'\rangle - \langle 2'1'|1'2'\rangle$. In general, $\langle 21|21\rangle \geqslant \langle 21|12\rangle$, so for this system, $\tilde{\varepsilon}_2^e < \varepsilon_2^e$ and $\tilde{\varepsilon}_{2'}^p < \varepsilon_{2'}^p$, leading to $\left|\tilde{E}_{ep}^{(2)}\right| > \left|E_{ep}^{(2)}\right|$. The second-order electron-proton correlation correction is generally negative. Thus, for this special case of one electron and one proton represented by two electronic and two nuclear basis functions, we have proven that the total NEO-MP2 energy is lower with the reference Hamiltonian $\tilde{H}_0^{\text{NEO}}$ than with the reference Hamiltonian H_0^{NEO}.

We expect that the relation $\left|\tilde{E}_{ep}^{(2)}\right| > \left|E_{ep}^{(2)}\right|$ is maintained for larger electronic and nuclear basis sets as well. For the reasons discussed above, $\tilde{\varepsilon}_r^e, \tilde{\varepsilon}_{r'}^p < 0$, and typically $\varepsilon_r^e, \varepsilon_{r'}^p > 0$. When these relations hold, the denominators of the terms in the second-order electron-proton correlation correction expression given in Eq. 2.18 are significantly smaller for $\tilde{E}_{ep}^{(2)}$ than for $E_{ep}^{(2)}$. If the numerators do not counteract this trend, we would expect that $\left|\tilde{E}_{ep}^{(2)}\right| > \left|E_{ep}^{(2)}\right|$. (Note that the numerators depend on the virtual orbitals, which may be different for the two reference Hamiltonians.) This analysis indicates that the reference Hamiltonian $\tilde{H}_0^{\text{NEO}}$ is likely to lead to a lower NEO-MP2 energy. We have demonstrated empirically that this reference Hamiltonian leads to a significantly lower NEO-MP2 energy for a number of systems, such as HF (hydrogen fluoride) and $[\text{He} - \text{H} - \text{He}]^+$. Note that the exact Hamiltonian, the ground state Hartree-Fock wavefunction and energy, and the perturbation are identical for the two reference Hamiltonians. As a result, the two perturbation series will converge to the same energy if they converge. The choice between these two reference Hamiltonians will impact only the speed of convergence. Note also that we have not proven that the perturbation series converges faster for the reference Hamiltonian $\tilde{H}_0^{\text{NEO}}$ even if the NEO-MP2 energy is lower. In many cases, however, a lower NEO-MP2 energy is associated with faster convergence of the perturbation series.

Table 2.1 presents the second-order electron-proton correlation corrections for three chemical systems: $[\text{He} - \text{H} - \text{He}]^+$, $[\text{F} - \text{H} - \text{F}]^+$, and $[\text{Cl} - \text{H} - \text{Cl}]^+$. In all cases, only the H nucleus was treated quantum mechanically within the NEO framework. The geometry of each system was optimized at the NEO-MP2 level using numerical gradients. At these equilibrium geometries, the hydrogen moves in a single well potential with maximum nuclear density at the midpoint between the two heavy atoms. Thus, the hydrogen nucleus is represented with a single

Table 2.1. The second-order electron-proton correlation corrections for three chemical systems. The correction $E_{ep}^{(2)}$ corresponds to the reference Hamiltonian that includes the proton-proton Coulomb exchange operator, and the correction $\tilde{E}_{ep}^{(2)}$ corresponds to the reference Hamiltonian that does not include the proton-proton Coulomb exchange operator. The energies are given in kcal/mol.

	$E_{ep}^{(2)}$	$\tilde{E}_{ep}^{(2)}$	$\tilde{E}_{ep}^{(2)} - E_{ep}^{(2)}$
$[\mathrm{He-H-He}]^+$	-2.572	-4.671	-2.099
$[\mathrm{F-H-F}]^-$	-3.134	-6.051	-2.917
$[\mathrm{Cl-H-Cl}]^-$	-3.056	-6.543	-3.487

basis function center located at this midpoint. The double-zeta nuclear basis set including s, p, and d functions, DZSPDN[10], was used for the quantum hydrogen. Dunning′s correlation consistent valence triple-split basis set augmented with diffuse functions, aug-cc-pVTZ[52, 53, 54], was used for the electrons. The numerical results illustrate that the removal of the proton-proton Coulomb-exchange operator can lower the second-order energy by more than 3 kcal/mol.

2.3 Conclusions

We have shown that many-body perturbation theory for including electron-proton correlation in systems with a single quantum nucleus can be formulated in terms of two reference Hamiltonians that differ by only the proton-proton Coulomb-exchange operator. When the reference Hamiltonian includes the proton-proton Coulomb-exchange operator, the virtual nuclear orbital energy corresponds to the negative of the affinity for adding a proton to the virtual orbital and is typically positive for neutral molecules. In contrast, when the reference Hamiltonian does not include the proton-proton Coulomb-exchange operator, the virtual nuclear orbital energy corresponds to the negative of the ionization potential for removing the proton from this orbital and is generally negative.

We have proven analytically that the removal of the proton-proton Coulomb-exchange operator from the reference Hamiltonian leads to a lower NEO-MP2 energy for a system with one electron and one proton represented by two electronic and two nuclear basis functions. Our analysis indicates that the removal of the

proton-proton Coulomb-exchange operator from the reference Hamiltonian can lead to a significantly lower NEO-MP2 energy and potentially faster convergence of the perturbation series for general systems with a single quantum nucleus and many classical nuclei[12, 13]. We have applied this approach to the three chemical systems $[He - H - He]^+$, $[F - H - F]^-$, and $[Cl - H - Cl]^-$. The results illustrate that removal of the proton-proton Coulomb-exchange operator from the reference Hamiltonian can lower the second-order energy by more than 3 kcal/mol.

In conventional electronic structure theory, typically Hartree-Fock calculations on neutral molecules give positive virtual orbital energies that are related to the electron affinity for adding an electron to the virtual orbital[49]. According to this convention, the electron-electron Coulomb-exchange operator is included in the Fock operator even for systems with only a single electron. Thus, the removal of the proton-proton Coulomb-exchange operator to obtain negative virtual orbital energies related to ionization potentials represents a departure from the basic framework of conventional electronic structure calculations. This conceptual issue has been addressed previously for electronic structure calculations by Huzinaga's improved virtual orbital generation technique[47] and its subsequent extensions[48]. Within the NEO framework, the modified reference Hamiltonian arises naturally for a single quantum nucleus. Analogous to Huzinaga′s method, in principle this general procedure could be applied to systems with more than one quantum nucleus.

The analysis presented elucidates the fundamental physical principles underlying the two distinct formulations of many-body perturbation theory for treating electron-proton correlation in systems with a single quantum nucleus and many classical nuclei. The insights provided by this analysis have important implications for the investigation of hydrogen transfer reactions in a wide range of chemical and biological systems.

Chapter 3

Analysis of the nuclear-electronic orbital approach for model hydrogen transfer systems

3.1 Introduction

Hydrogen transfer reactions are important for a wide range of chemical and biological processes[42]. Due to the quantum nature of the hydrogen nucleus, conventional calculations of the electronic wavefunction in a field of nuclei represented as classical point charges are not adequate for the description of hydrogen transfer systems. Invoking the Born-Oppenheimer separation between the proton and the electrons, the proton vibrational wavefunctions can be calculated for the nucleus moving in the electronic ground state potential corresponding to each instantaneous conformation of the environment. This approach is the foundation of multidimensional grid-based quantum dynamical calculations[55, 56] which provide structural, energetic, and spectroscopic information.

An alternative perspective is provided by the nuclear-electronic orbital (NEO)

method[10, 11, 12, 13] which avoids the Born-Oppenheimer separation between the proton and the electrons through the calculation of mixed nuclear-electronic wavefunctions with molecular orbital methods. In the NEO approach, specified nuclei are treated quantum mechanically on the same level as the electrons, and both the electronic and nuclear molecular orbitals are expressed as linear combinations of Gaussian basis functions. In the application of the NEO approach to chemical reactions, the coordinates of the nuclear basis function centers are optimized variationally during the self-consistent-field procedure. When the NEO method is applied to hydrogen transfer reactions, the transferring proton and all electrons are treated quantum mechanically. Typically the transferring hydrogen atom is represented by two basis function centers to allow delocalization of the proton vibrational wavefunction. A variety of molecular orbital methods, including Hartree-Fock (HF), configuration interaction (CI), multiconfigurational self-consistent-field (MCSCF), and second-order perturbation theory (MP2) have been implemented within the NEO framework[10, 13, 14]. A number of related mixed nuclear-electronic molecular orbital methods[26, 27, 29, 32, 33, 34, 35, 44, 36] have been developed but have not been applied to hydrogen transfer systems.

In this chapter, we apply the NEO approach to the $[\text{He-H-He}]^{+}$ and $[\text{He-H-He}]^{++}$ model systems to investigate a number of fundamental issues arising in applications to hydrogen transfer processes. These systems were chosen as models because they have few enough electrons to be treated at the NEO-full CI level, which includes all electron-electron and electron-proton correlation. Only the transferring hydrogen nucleus is treated quantum mechanically in our NEO calculations on this system. The quantum mechanical treatment of the helium nuclei as well as the hydrogen nucleus would be appropriate for quantitative studies of the dynamical and spectroscopic aspects of these chemical systems. Our objective, however, is not to perform such quantitative studies but rather to use these systems as models for the illustration of fundamental physical principles underlying the NEO approach.

We address a number of important technical aspects relevant to the application of the NEO approach to hydrogen transfer reactions. First we investigate the flexibility of two hydrogen basis function centers for the description of chemical reactions involving both single and double well proton potential energy surfaces.

We also examine possible difficulties with linear dependency of the hydrogen basis functions and multiple minima for the basis function center positions during the variational optimization. In addition, we analyze the convergence of the number of basis function centers by comparision of calculations with two and three hydrogen basis function centers. Finally, we study the significance of intramolecular basis set superposition error (BSSE) with respect to the hydrogen basis function centers. We also test the accuracy of the NEO approach by comparison to conventional grid calculations for the model systems. The NEO approach will be computationally practical for much larger systems than can be studied with grid-based methods. Moreover, the NEO approach is advantageous over grid-based methods in that it includes the impact of the nuclear wavefunction on the electronic structure and nonadiabatic effects arising from the breakdown of the Born-Oppenheimer approximation.

The remainder of the Chapter is organized as follows. In Section 2, we summarize the NEO-HF and NEO-CI approaches. In Section 3, we investigate a number of technical issues pertaining to the application of the NEO approach to hydrogen transfer systems and benchmark the method by comparison to grid calculations. In Section 4 we investigate the influence of dynamical correlation on nuclear wavefunctions. Section 5 presents conclusions and a discussion of future directions.

3.2 Methods

In the NEO approach, the system is divided into three parts: N_e electrons, N_p quantum nuclei, and N_c classical nuclei. The NEO-HF and NEO-full CI approaches have been described in detail elsewhere[13, 14]. At the Hartree-Fock level, the total nuclear-electronic wavefunction can be approximated as a product of single configurational electronic and nuclear wavefunctions:

$$\Psi_{tot}(\mathbf{r}^e, \mathbf{r}^p) = \Phi_0^e(\mathbf{r}^e)\Phi_0^p(\mathbf{r}^p) \tag{3.1}$$

where $\Phi_0^e(\mathbf{r}^e)$ and $\Phi_0^p(\mathbf{r}^p)$, respectively, are antisymmetrized wavefunctions (determinants of spin orbitals) representing the electrons and fermionic nuclei such as protons. (Here $\mathbf{r}^e$ and $\mathbf{r}^p$ denote the spatial coordinates of the electrons and quan-

tum nuclei, respectively.) The spatial orbitals for the electrons and the quantum nuclei are expanded in Gaussian basis sets, and the variational method is used to minimize the total energy with respect to both the electronic and nuclear molecular orbitals.

The NEO-CI wavefunction has the form

$$\Psi_{tot}(\mathbf{r}^e, \mathbf{r}^p) = \sum_{I}^{N_{CI}^e} \sum_{I'}^{N_{CI}^p} C_{(II')} \Phi_I^e(\mathbf{r}^e) \Phi_{I'}^p(\mathbf{r}^p) \tag{3.2}$$

where $\Phi_I^e(\mathbf{r}^e)$ and $\Phi_{I'}^p(\mathbf{r}^p)$ are determinants of spin orbitals representing the electrons and quantum nuclei, respectively, and $C_{(II')}$ are CI coefficients. Here there are N_{CI}^e electronic determinants and N_{CI}^p quantum nuclear determinants, leading to a total of $N_{CI} = N_{CI}^e * N_{CI}^p$ nuclear-electronic configurations. For the NEO-CI method, the variational method is used to minimize the total energy with respect to the CI coefficients $C_{(II')}$. In NEO-full CI, a complete active space is used for both the electrons and the quantum nuclei.

The NEO methodology has been implemented in the GAMESS electronic structure program[23]. The nuclear basis set previously developed for hydrogen nuclei within the NEO framework was optimized for a set of five simple diatomic molecules that each contained one hydrogen atom. This DZSPDN basis set[10] includes two each of *s*-,*p*-, and *d*-type Gaussians, resulting in a total of 20 nuclear basis functions per hydrogen center. For simplicity, the DZSNB basis set, which includes only *s*-type Gaussians with the exponents from the DZSPDN basis set, was used to study the technical issues in this chapter. A range of different nuclear basis sets were used for the benchmarking calculations. The 6-31G electronic basis set[57], which includes two *s*-type orbitals for each helium and hydrogen atom, was used for all calculations. Note that these electronic and nuclear basis sets are not optimized for hydrogen tunneling systems. In the future, electronic and nuclear basis sets including *s*-, *p*-, and *d*-type Gaussians will be developed for hydrogen tunneling systems.

3.3 Results

In this section, we analyze the properties of the $[\text{He-H-He}]^+$ and $[\text{He-H-He}]^{++}$ systems to address a number of technical issues. Figure 3.1 illustrates the basic properties of proton transfer systems. The electronic ground state potential energy curves as functions of the proton coordinate and the corresponding ground state hydrogen nuclear wavefunctions are depicted for the $[\text{He-H-He}]^+$ system with He−He distances of 1.8, 2.2, and 2.6 Å.

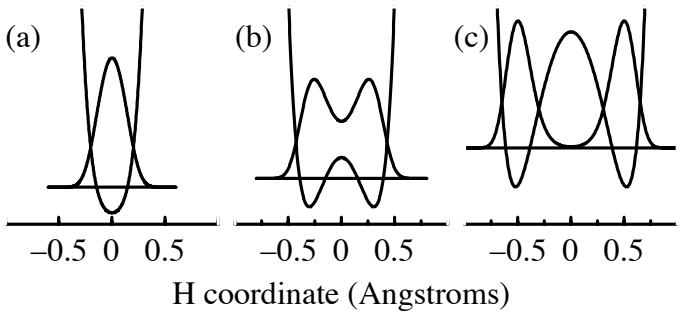

Figure 3.1. One-dimensional proton potential energy curves and the coresponding ground state nuclear wavefunctions for the $[\text{He-H-He}]^+$ system with He−He distances of (a) 1.8, (b) 2.2, and (c) 2.6 Å. These curves were calculated on a one-dimensional grid along the He−He axis at the full CI/6-31G level, and the proton vibrational wavefunctions were calculated with the FGH method.

The potential energy curves were calculated at the full CI/6-31G level on a one-dimensional grid along the hydrogen coordinate, and the one-dimensional hydrogen nuclear wavefunctions were calculated with the Fourier grid Hamiltonian (FGH) method[56, 8]. Note that the resulting wavefunction is based on an adiabatic Born-Oppenheimer separation between the electrons and the transferring hydrogen nucleus (i.e., the electrons are assumed to respond instantaneously to the motion of the hydrogen nucleus). In the NEO approach, the electronic and nuclear wavefunctions are solved self-consistently, and the Born-Oppenheimer approximation is removed in the multiconfigurational NEO methods. Moreover, the NEO approach provides three-dimensional hydrogen wavefunctions. Nevertheless, these one-dimensional adiabatic nuclear wavefunctions are useful for illustrative purposes. At shorter He−He distances, the potential energy curve is a single well, and the nuclear wavefunction is localized in the middle. At longer distances, the

potential energy curve becomes a double well, and the nuclear wavefunction is bilobal. As the He−He distance increases, the barrier height increases and the bilobal nature of the nuclear wavefunction becomes more pronounced.

Figure 3.2 depicts the ground state energies of the $[\text{He-H-He}]^{+}$ and $[\text{He-H-He}]^{++}$ systems as functions of the He−He distance at the NEO-full CI level. The

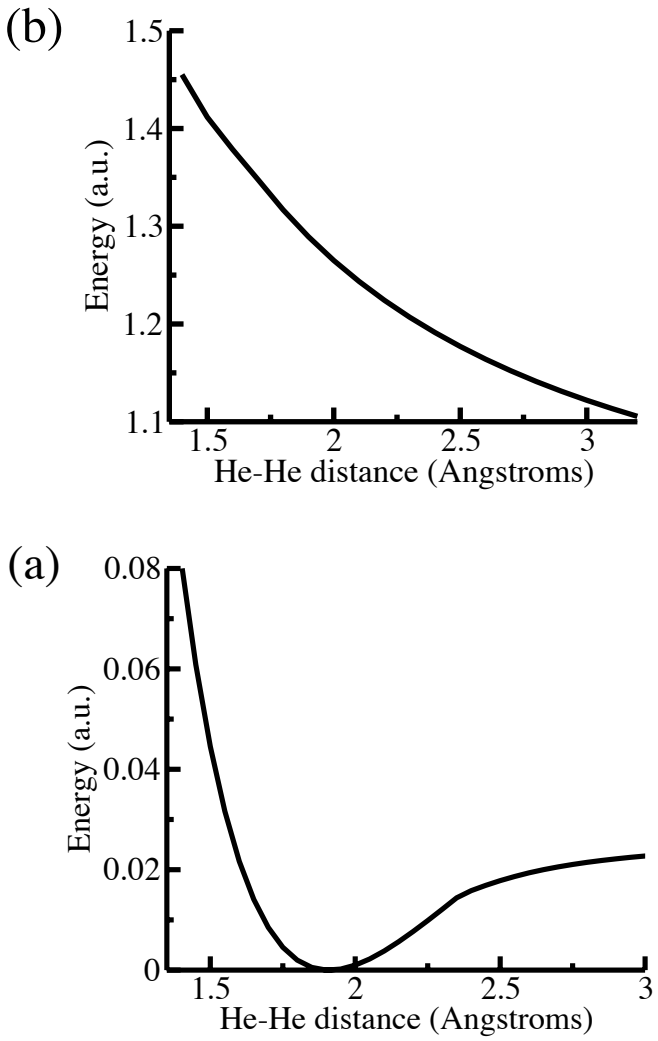

Figure 3.2. NEO-full CI ground state energies as functions of the He−He distance for (top) $[\text{He-H-He}]^{++}$ and (bottom) $[\text{He-H-He}]^{+}$ relative to the minimum of the $[\text{He-H-He}]^{+}$ system.

hydrogen atom is represented by two basis function centers, and the positions of

these centers are optimized variationally at the NEO-full CI level. The nuclear wavefunction is delocalized equally over both nuclear basis function centers at the NEO-full CI level[12, 13]. In the NEO approach, the nuclear basis function centers include both electronic and nuclear basis functions. For the $[He\text{-}H\text{-}He]^+$ system, the electronic density is localized predominantly on the helium nuclei, and the nuclear basis function centers do not contain significant electronic density (i.e., the double well system corresponds to H^+ between two He atoms). This system has a stable minimum at a He−He distance of 1.86 Å and dissociates into HeH^+ and He. For the $[He\text{-}H\text{-}He]^{++}$ system, the proton potential energy profile is double well at all relevant He−He distances, and the nuclear basis function centers contain significant electronic density (i.e., the double well system corresponds to H between two He^+ ions). This system dissociates into HeH^+ and He^+, and the energy increases monotonically as the He−He distance decreases because of the repulsive electrostatic interactions.

An important issue that arises in the application of the NEO approach to chemical reactions is that the nuclear basis set must be flexible enough to describe both single and double well proton potential energy surfaces. Figure 3.2 illustrates that the NEO-full CI energy varies smoothly as the He−He distance is varied, even though the proton potential changes qualitatively from single to double well along this coordinate for the $[He\text{-}H\text{-}He]^+$ system. For He−He distances with double well proton potential energy curves (Figure 3.1 (b) and (c)), the optimized basis function positions are approximately at the minima of the potential energy curves. For He−He distances with single well proton potential energy curves (Figure 3.1 (a)), a single nuclear basis function center would provide a qualitatively reasonable wavefunction. In general, however, the removal and addition of basis function centers could create singularities in the potential energy surface. In order to maintain a continuous potential energy surface, the hydrogen atom can be represented by two nuclear basis function centers for these shorter distances as well. We found that the variationally optimized positions of the two nuclear basis function centers are near the midpoint but not at the midpoint for He−He distances with single well proton potential energy curves.

We also examine possible difficulties arising from linear dependency of the hydrogen basis functions. Table 3.1 gives the positions of the two nuclear basis

Table 3.1. Optimized nuclear basis function separations for a range of relatively short He−He distances in the [He-H-He]$^+$ system. The two hydrogen basis function center positions were optimized variationally at the NEO-full CI level. The smallest eigenvalue from diagonalization of the electronic overlap matrix is also given for each He−He distance.

He−He distance (Å)	r_{HBFC} (Å) [a]	S_{min} [b]
2.0	0.185	7.144×10^{-4}
1.8	0.150	4.412×10^{-4}
1.6	0.115	2.700×10^{-4}
1.4	0.070	1.132×10^{-4}

[a]Hydrogen basis function center separation
[b]Smallest eigenvalue of overlap matrix

function centers optimized variationally at the NEO-full CI level for a range of He−He distances for the [He-H-He]$^+$ system. As the separation between the helium atoms is reduced, the second derivative of the proton potential energy along the He−He axis increases, and the nuclear wavefunction becomes narrower. Consistent with this trend, the separation between the NEO basis function centers is reduced as the He−He distance decreases. We also find that linear dependence in the electronic basis functions is not problematic at these nuclear basis function center distances. Linear dependency problems would appear in the electronic basis before the nuclear basis because the electronic basis functions are more diffuse. Table 3.1 gives the smallest eigenvalue from diagonalization of the electronic overlap matrix for each He−He distance. These values are well above the standard tolerance of 10^{-6} that indicates linear dependence of the basis set in the GAMESS electronic structure package[23]. As for conventional electronic structure calculations, the NEO program checks for linear dependency of the basis functions during the calculations. Although linear dependency may be problematic for some systems in conjunction with certain electronic and nuclear basis sets, the basis sets can be designed to avoid such difficulties. For example, the use of extremely diffuse electronic basis functions to represent transferring hydrogen atoms is not advisable within the NEO framework.

In addition, we investigate the possible difficulties arising from multiple minima for the optimization of the hydrogen basis function centers. For the [He-H-He]$^+$

system with intermediate He−He distances, we observe two minima for the basis function center separation. At these intermediate He−He distances, the hydrogen nuclear wavefunctions are of the type depicted in Figure 3.1 (b) (i.e., the wavefunctions are intermediate between being localized in the middle and distinctly bilobal). The multiple minima arise from a competition between describing the middle and the outer regions of hydrogen nuclear wavefunctions of the type depicted in Figure 3.1 (b). The energies in Figure 3.2 correspond to the global minimum for each He−He distance. At a He−He distance of 2.2 Å, the global minimum corresponds to the smaller basis function center separation, whereas at a He−He distance of 2.6 Å, the global minimum corresponds to the larger basis function center separation. As discussed below, when a third hydrogen basis function center is placed in the middle, only a single minimum is observed for the separation of the outer hydrogen basis function centers. This observation indicates that the potential difficulties with multiple minima are eliminated when the electronic and nuclear basis sets are enhanced.

Our next step is to determine if two nuclear basis function centers are sufficient to describe the nuclear wavefunction corresponding to hydrogen moving in a double well potential. A greater number of basis function centers representing each hydrogen atom would enhance the accuracy, but the computational expense would increase and the advantages over grid-based methods would diminish. The objective of the NEO approach is to incorporate the essential nuclear quantum effects in a computationally tractable manner. As for conventional electronic structure calculations, however, the basis sets must be adequately converged to obtain the desired level of accuracy.

To test the convergence of our calculations with two hydrogen basis function centers, we study the impact of including three hydrogen basis function centers. Figure 3.3 provides a comparison of the NEO-full CI ground state energy as a function of the hydrogen basis function separation for two and three hydrogen basis function centers, where the third basis function center is placed at the midpoint. For both the $[\text{He-H-He}]^{+}$ and $[\text{He-H-He}]^{++}$ systems, the behavior is qualitatively similar with two and three basis function centers in the physically meaningful region but becomes qualitatively different for larger basis function center separations. As shown in Fig. 3.3 (b) for the $[\text{He-H-He}]^{++}$ system, the energy no longer

changes with basis function center separation at larger separations when three basis function centers are used because the hydrogen nuclear and electronic densities are predominantly on the middle basis function center. When two basis function centers are used, the energy continues to increase as the basis function centers approach the He atoms due to repulsive interactions. As shown in Fig. 3.3(a) for the $[He\text{-}H\text{-}He]^+$ system, the energy decreases with basis function center separation at larger separations when three basis function centers are used because the proximity of the basis function centers improves the electronic basis set for the He atoms. In this case, the hydrogen nuclear density is predominantly on the middle basis function center, and electronic density is shared among the helium and hydrogen electronic basis functions.

This decrease in the energy at larger basis function center separations is an example of intramolecular basis set super position error (BSSE), which is an error in the relative energy between two configurations of a molecule due to enhanced quality of the basis set for one configuration relative to the other[58]. Intramolecular BSSE is expected to be significant for these calculations because a relatively small basis set is used. The electronic basis functions on each nuclear basis function center improve the description of electronic density around the He atoms, and this effect becomes more pronounced as the nuclear basis function centers move closer to the He atoms. In other words, the quality of the electronic basis set is reduced as the NEO basis function centers are moved away from the He atoms. Figure 3.3 illustrates that BSSE is more significant for the $[He\text{-}H\text{-}He]^+$ system than for the $[He\text{-}H\text{-}He]^{++}$ system. As discussed above, the $[He\text{-}H\text{-}He]^+$ system may be viewed as a proton between two He atoms, whereas the $[He\text{-}H\text{-}He]^{++}$ system may be viewed as a hydrogen between two He^+ atoms. Figure 3.4 depicts the full CI ground state energy as a function of the distance between the He nucleus and a ghost hydrogen electronic basis function center for both the He atom and the He^+ cation. This figure indicates that the intramolecular BSSE is much more significant for He than for He^+. This difference arises because the two electrons on the He atom are not held as tightly as the single electron on the He^+ cation and therefore benefit more from the additional electronic basis function centers on the ghost hydrogen electronic basis function center.

We performed additional calculations to further quantify the BSSE for the [He-

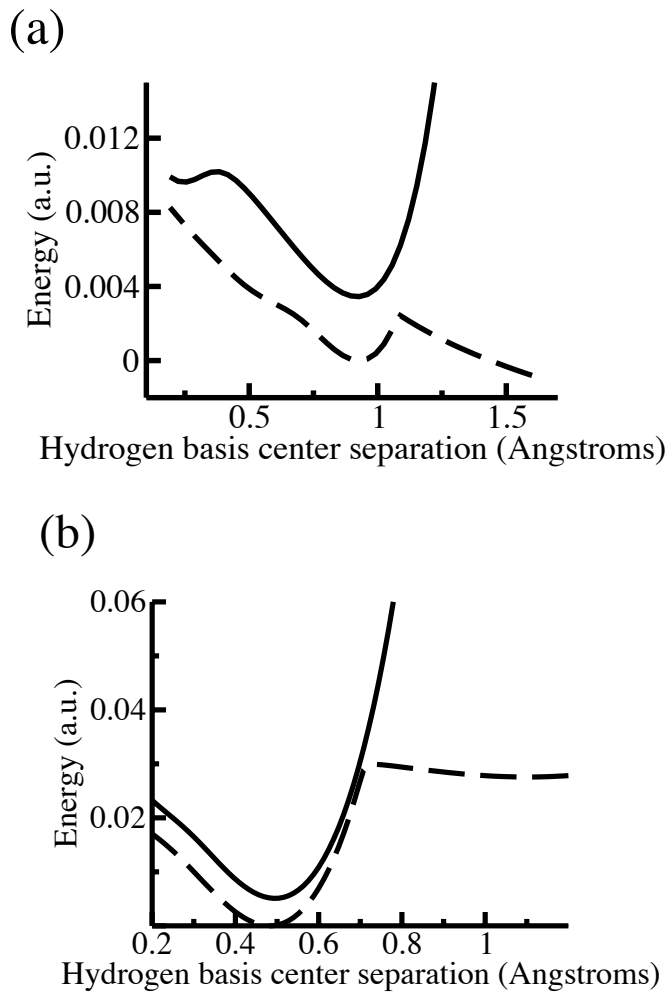

Figure 3.3. NEO-full CI ground state energy as a function of the hydrogen basis function center separation for two (solid) and three (dashed) hydrogen basis fucntion centers, where the third basis function center is placed at the midpoint. The results are given for the (a) [He-H-He]$^{+}$ system with He−He distance of 2.6 Å and (b) [He-H-He]$^{++}$ system with He−He distance of 1.8 Å.

H-He]$^{+}$ model system with a fixed He−He distance of 2.6 Å. Figure 3.5 (a) depicts this system with two different nuclear basis function center separations of 1.60 and 0.928 Å. The difference in NEO-HF energy for these two different configurations is 0.1837 a.u. We repeated the calculations with the addition of two electronic basis function centers positioned to maintain a consistent electronic basis set, as shown in Figure 3.5 (b). Thus, there were four electronic basis function centers in both

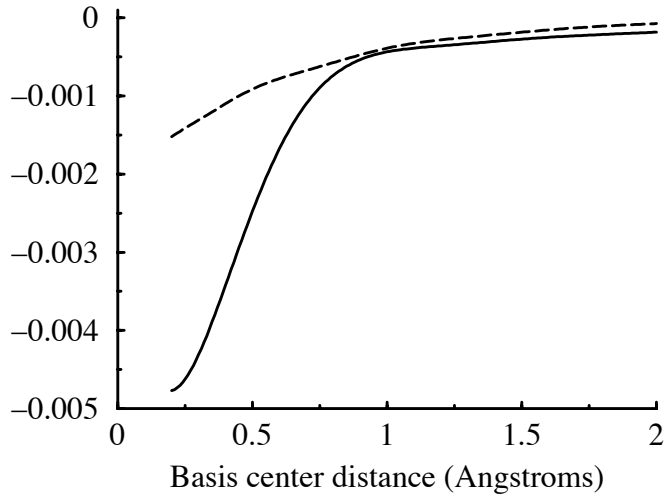

Figure 3.4. Full CI ground state energy as a function of the distance between the He nucleus and a ghost hydrogen electronic basis function center for the He atom (solid) and the He^+ cation (dashed). Note that the intramolecular BSSE is much larger for the He atom. The energies are relative to the energy of the He and He^+ atoms in the absence of ghost hydrogen electronic basis function center.

calculations. The difference in NEO-HF energy for these two nuclear basis function center separations is 0.1931 a.u. The intramolecular BSSE is estimated to be the difference between the relative energies of the configurations in Figure 3.5. At the NEO-HF level, the intramolecular BSSE was determined to be -0.0094 a.u., which is ~ 5 percent of the relative energy between the configurations in Figure 3.5 (a). When we increased the electronic basis set for the helium atoms by adding p orbitals (corresponding to adding polarization to the 6-31G electronic basis set for the helium atoms), the BSSE decreased to -0.0022 a.u., which is ~ 1 percent of the relative energy between the configurations in Figure 3.5 (a). In general, the BSSE is expected to decrease as the electronic basis set is improved.

To test the accuracy of the NEO approach, we compare the NEO and one-dimensional grid methods for calculation of the energy splittings between the lowest two vibronic states corresponding to the hydrogen stretch for the $[He\text{-}H\text{-}He]^+$ and $[He\text{-}H\text{-}He]^{++}$ model systems. The NEO calculations were performed at the NEO-full CI level using the 6-31G electronic basis set and the nuclear basis sets listed in Table 3.2 and Table 3.3. For the NEO calculations, the hydrogen basis function center positions were optimized for the ground and excited states. The grid cal-

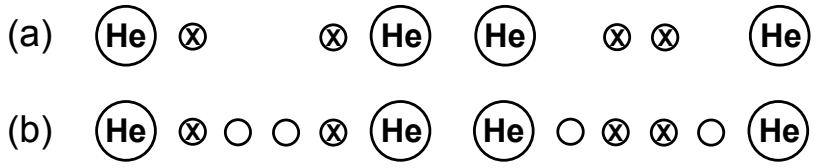

Figure 3.5. A schematic representation of the system used to estimate the intramolecular BSSE for NEO-HF calculations on the [He-H-He] $^+$ system with a He−He distance of 2.6 Å. The X's represent the nuclear basis function centers and the open circles represent the electronic basis function centers. In (a) the proton and electronic basis function centers are identical, as in typical neo calculations. the separation between basis function centers is 1.6 Å on the left and 0.928 Å on the right. In (b) two additional basis function centers are included, so each calculation includes four electronic and two nuclear basis function centers. The additional electronic basis function centers ensure a consistent electronic basis set. The intramolecular BSSE is estimated to be the difference between the relative energies of the configurations in (a) and (b).

culations were performed with the FGH method[56, 8] for a one-dimensional grid potential obtained at the full CI/6-31G level. In contrast to the NEO approach, the grid method does not include the response of the electronic wavefunction to the nuclear wavefunction or nonadiabatic effects. In particular, the nuclear-electronic wavefunction is clearly multiconfigurational for the [He-H-He]$^{++}$ system[12, 13]. Thus, the grid method may not be an ideal benchmark for this system but still provides useful insights. Moreover, the grid method is expected to be highly accurate for the [He-H-He]$^+$ system.

The vibronic energy level splittings obtained with the NEO method agree well with those obtained with the grid method for both model systems. The results for the [He-H-He]$^+$ system with a He−He distance of 1.9 Å are given in Table 3.2. At this distance, the potential along the hydrogen coordinate is a flat, anharmonic single well, as depicted in Figure 3.1 (a). Although the hydrogen potential is single well, two hydrogen basis function centers are required to obtain a reasonable splitting due to the anharmonicity of this potential. The results demonstrate that systematic improvement of the nuclear basis set leads to convergence of the NEO energy splitting toward the one-dimensional grid result. The results for the [He-H-He]$^{++}$ system with a He-He distance of 1.6 Å are given in Table 3.3. At this distance, the potential along the hydrogen coordinate is a double well similar to

Table 3.2. Energy differences between the lowest two vibronic states coresponding to the hydrogen stretch for the $[\text{He-H-He}]^+$ system with a He−He distance of 1.9 Å. The numbers in parenthesis indicate the number of hydrogen basis function centers. The DZSPDN nuclear basis set includes two each of *s*-, *p*-, and *d*-type Gaussians, resulting in a total of 20 nuclear basis functions per hydrogen center. The DZSNB (or DZSPNB) include only *s*- (or *s*- and *p*-) type Gaussians, and the DZSPDN' nuclear basis set includes two each of *s*- and *p*-type Gaussians and one set of *d*-type Gaussians. The grid calculations were performed with the FGH method for a one-dimensional grid potential obtained at the full CI level. The 6-31G electronic basis set was used for all calculations.

Method	Splitting (cm^{-1})
NEO/DZSPDN(1)	4508
NEO/DZSNB(2)	2229
NEO/DZSPNB(2)	1655
NEO/DZSPDN'(2)	1579
Grid	1400

Table 3.3. Energy differences between the lowest two vibronic states coresponding to the hydrogen stretch for the $[\text{He-H-He}]^{++}$ system with a He−He distance of 1.6 Å. Two hydrogen basis function centers were used for the NEO calculations. The DZSPDN nuclear basis set includes two each of *s*-, *p*-, and *d*-type Gaussians, resulting in a total of 20 nuclear basis functions per hydrogen center. The DZSNB (or DZSPNB) include only *s*- (or *s*- and *p*-) type Gaussians. The grid calculations were performed with the FGH method for a one-dimensional grid potential obtained at the full CI level. The 6-31G electronic basis set was used for all calculations.

Method	Splitting (cm^{-1})
NEO/DZSNB	1189
NEO/DZSPNB	428
NEO/DZSPDN	417
Grid	462

the one depicted in Figure 3.1 (b). Two hydrogen basis function centers were used in these NEO calculations. As for the other model, systematic improvement of the nuclear basis set leads to convergence of the NEO energy splitting near the one-dimensional grid result.

3.4 Influence of dynamical correlation on nuclear wavefunctions

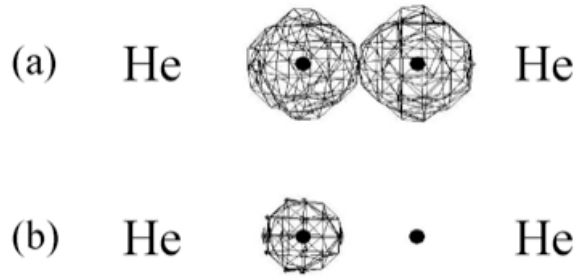

Figure 3.6. Schematic picture of delocalized and localized proton molecular orbitals for the $[He\text{-}H\text{-}He]^+$ system. The nuclear basis function centers are indicated with solid black circles, and the wavefunctions are depicted as contour plots.

As shown in Figure 3.1 (b) and (c) the hydrogen nuclear wavefunction is delocalized and bilobal for He−He distances larger than $\sim$ 2.0 Å. At the NEO-HF level, the nuclear wavefunction for the $[He\text{-}H\text{-}He]^+$ system is localized on one of the nuclear basis function centers due to the neglect of electron-proton correlation (Figure 3.6 (b)). At the NEO-full CI level, all electron-electron and electron-proton correlation is included, and the nuclear wavefunctions are delocalized equally over the two nuclear basis function centers (Figure 3.6 (a)). The variational optimization of the nuclear basis function center positions is also strongly influenced by electron-proton correlation. In this section, we use the NEO-MP2 method to investigate the effects of electron-electron and electron-proton correlation on the optimization of the nuclear basis function centers and the nuclear wavefunction delocalization for the $[He\text{-}H\text{-}He]^+$ system.

The initial calculations are performed for the $[He\text{-}H\text{-}He]^+$ system under $D_{\infty h}$ symmetry to avoid the localization of the nuclear wavefunction at the NEO-HF level. The energy is calculated at the NEO-HF, NEO-MP2, and NEO-full CI levels as a function of the separation of the two nuclear basis function centers. The results are depicted in Figure 3.7 for a He−He distance of 2.6 Å. At the NEO-HF level, the optimized nuclear basis function center positions approach the midpoint between the two helium atoms. Thus, the variational NEO-HF solution with $D_{\infty h}$ symmetry

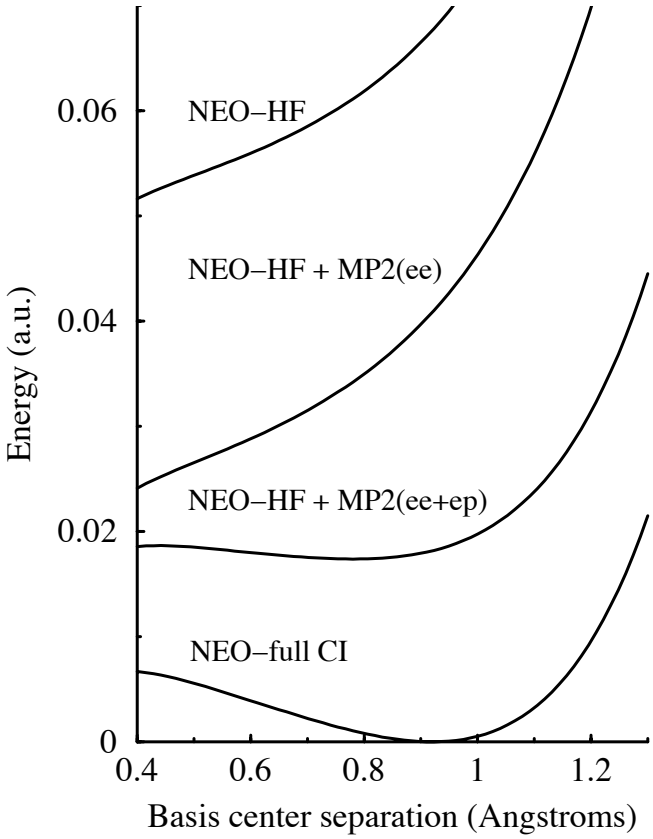

Figure 3.7. Relative energies as a function of nuclear basis function center separation for a He−He separation of 2.6 Å. The results are given for NEO-HF, NEO-HF + MP2 (ee), NEO-HF + MP2 (ee+ep), and NEO-full CI. The NEO-HF and NEO-MP2 calculations were performed by enforcing $D_{\infty h}$ symmetry to ensure a delocalized nuclear wavefunction. The variational NEO-full CI solution with C_1 symmetry corresponds to a delocalized nuclear wavefunction.

is localized on a single nuclear basis function center at the midpoint. The addition of only electron-electron correlation with NEO-MP2 also leads to localization at the midpoint. The addition of electron-electron and electron-proton correlation with NEO-MP2, however, leads to a variational solution in which the optimized nuclear basis function centers are separated by 0.78 Å, which is similar to the separation determined at the NEO-full CI level.

Next we compare the calculations with $D_{\infty h}$ symmetry to calculations performed with no symmetry constraints (i.e., C_1 symmetry). For the variational NEO-HF solution with C_1 symmetry, the nuclear wavefunction is localized on one

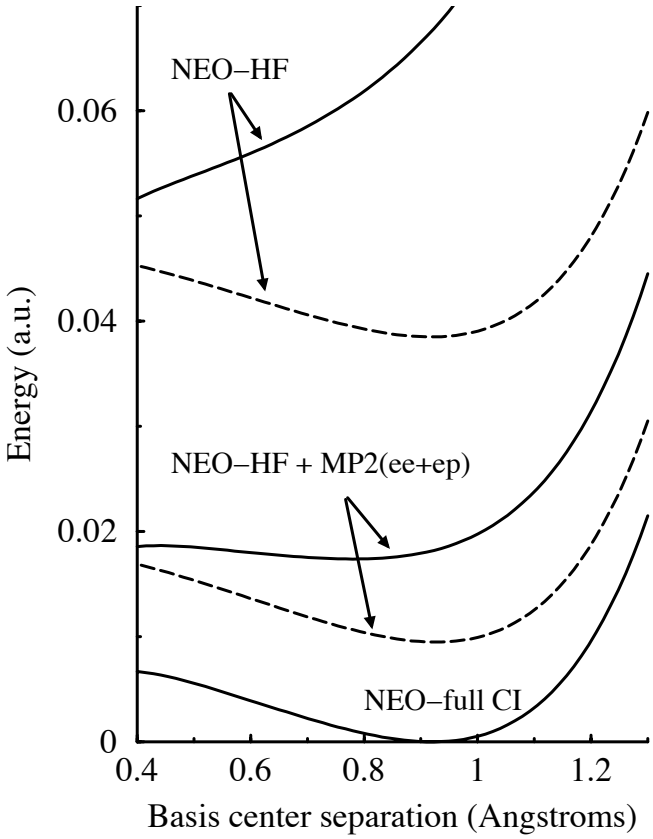

Figure 3.8. Relative energies as a function of nuclear basis function center separation for a He−He separation of 2.6 Å. The results are given for NEO-HF, NEO-HF + MP2 (ee+ep), and NEO-full CI. The solid lines correspond to delocalized nuclear wavefunctions obtained by enforcing $D_{\infty h}$ symmetry for NEO-HF and NEO-MP2. The dashed lines correspond to localized nuclear wavefunctions obtained with C_1 symmetry for NEO-HF and NEO-MP2. The variational NEO-full CI solution with C_1 symmetry corresponds to a delocalized nuclear wavefunction.

of the nuclear basis function centers, as depicted in Figure 3.6 (b). Figure 3.8 depicts the energies at the NEO-HF and NEO-MP2 levels as a function of the separation of the two nuclear basis function centers for both the localized (C_1) and delocalized ($D_{\infty h}$) nuclear wavefunctions for a He−He distance of 2.6 Å. Although the addition of electron-proton correlation using NEO-MP2 narrows the energy gap between the localized and delocalized solutions, the localized solution remains lower in energy.

Table 3.4 compares the energetics of the localized and delocalized solutions

Table 3.4. Energetics for the [He-H-He]$^+$ system with a He−He distance of 2.6 Å. The two nuclear basis function centers are at the positions optimized variationally at the NEO-full CI level. The total NEO-HF and NEO-MP2 energies are given relative to the variational NEO-HF solution. The electron-electron and electron-proton MP2 corrections $E_{ee}^{(2)}$ and $E_{ep}^{(2)}$, respectively, are also given. All energies are in atomic units.

	NEO-HF	NEO-MP2	$E_{ee}^{(2)}$	$E_{ep}^{(2)}$
localized	0.0000	−0.0290	−0.0288	−0.0002
delocalized	0.0293	−0.0203	−0.0268	−0.0228

for the [He-H-He]$^+$ system at a He−He distance of 2.6 Å. For all results given in this table, the two nuclear basis function centers are at the positions optimized variationally at the NEO-full CI level. At the NEO-HF level, the delocalized solution is 0.0216 a.u. higher in energy than the localized solution. At the NEO-MP2 level, the delocalized solution is still higher in energy than the localized solution, but the energy gap between the localized and delocalized solutions is reduced to 0.0067 a.u. The MP2 correction for electron-electron correlation slightly widens the energy gap between the localized and delocalized solutions. In contrast, the MP2 correction for electron-proton correlation reduces this energy gap, and the amount of electron-proton correlation is two orders of magnitude greater for the delocalized NEO-HF reference than for the localized NEO-HF reference. Thus, the electron-proton correlation is responsible for the narrowing of the energy gap between the delocalized and localized solutions with NEO-MP2. Qualitatively similar results were obtained with larger electronic and nuclear basis sets.

3.5 Conclusions

The NEO approach allows the calculation of mixed nuclear-electronic wavefunctions with molecular orbital methods. The objective of this approach is to incorporate the essential nuclear quantum effects into electronic structure calculations in a computationally practical manner. In this chapter, we addressed a number of fundamental technical issues related to the application of the NEO approach to hydrogen transfer reactions. We discussed the challenges associated with the variational optimization of the nuclear basis function centers and the representation

of each hydrogen with multiple basis function centers. Analogous to conventional electronic structure calculations, the electronic and nuclear basis sets used in NEO calculations must be adequately converged to obtain the desired level of accuracy for each system studied. We demonstrated that two nuclear basis function centers can adequately describe both single and double well proton potential energy surfaces. This flexibility of the nuclear basis set is advantageous for the generation of minimum energy paths and the calculation of direct dynamics within the NEO framework because hydrogen transfer reactions often sample a range of both single and double well proton potential energy surfaces.

Furthermore, we compared the NEO approach to grid-based methods for the model systems. Our results indicate that the vibronic energy level splittings calculated with the NEO approach converge to those calculated with a grid-based method as the nuclear basis set is systematically improved. Although we used the NEO-full CI method to study these model systems, we have developed a computationally efficient NEO-nonorthogonal CI approach to enable the calculation of accurate vibronic energy level splittings for more complex systems with larger electronic and nuclear basis sets. The efficiency of the NEO approach will render it computationally practical for much larger systems than feasible for grid-based quantum dynamical calculations. Moreover, the NEO approach includes the effects arising from the impact of the nuclear wavefunctions on the electronic structure, as well as nonadiabatic effects. These effects are not included in conventional grid-based methods. Additional benchmarking of the NEO approach has been performed for bihalide systems $[XHX]^-$ with X=F,Cl, and Br [17]. For these systems, the NEO-MP2 (second-order perturbation theory) approach [14] provides structures that are in excellent agreement with grid-based calculations and experimental data. These results will be discussed in Chapter 4. The NEO approach has also reproduced the experimentally observed trends in isotope effects for a wide range of systems [16].

Chapter 4

Impact of nuclear quantum effects on the molecular structure of bihalides and the hydrogen fluoride dimer

4.1 Introduction

Hydrogen bonding plays an important role in biomolecular structure and function[59], molecular self-assembly[60], and solvation[61]. Theoretical studies of hydrogen-bonded systems are challenging due to the low-frequency, anharmonic, intermolecular vibrations[62, 63]. Moreover, nuclear quantum effects of the hydrogen atom motions significantly impact the structures and spectroscopic properties of these systems. Conventional molecular dynamics and electronic structure calculations of hydrogen-bonded systems typically neglect the nuclear quantum effects.

Recently, the role of nuclear quantum effects in hydrogen-bonded systems has been investigated with a variety of theoretical methods. The quantum diffu-

sion Monte Carlo approach has been used to study the impact of nuclear quantum effects on donor-acceptor distances, rotational constants, and hydrogen bond energies in gas phase hydrogen-bonded clusters[63, 64, 65]. A disadvantage of the quantum diffusion Monte Carlo method is that it requires analytical potentials to describe the potential energy surfaces of larger systems. The vibrational self-consistent-field (VSCF)[66, 5], the multimode vibrational configuration interaction[63, 67], and the second-order vibrational perturbation theory (VPT2)[2, 3, 68] approaches have been used to investigate anharmonic effects on frequencies and interaction energies in hydrogen-bonded systems. Although these methods can utilize *ab initio* potential energy surfaces, they are computationally demanding for larger systems. Path integral methods have been applied to study hydrogen bonding in solution. For example, the Car-Parrinello molecular dynamics approach combined with a path integral treatment of the nuclei[69] has been used to analyze the structural impact of nuclear quantum effects on hydrogen bonding in liquid hydrogen fluoride and water[70, 71].

The nuclear-electronic orbital (NEO) method is an alternative approach for including nuclear quantum effects directly into electronic structure calculations[10, 11, 12, 13, 14, 15, 16]. In the NEO approach, selected nuclei are treated quantum mechanically on the same footing as the electrons, and mixed nuclear-electronic wavefunctions are calculated variationally using molecular orbital techniques. Both the nuclear and electronic wavefunctions are expanded in terms of Gaussian basis functions. The nuclear basis set typically includes s, p, and d-type Gaussians. In the NEO treatment of hydrogen-bonded systems, only the hydrogen nuclei are treated quantum mechanically. Dynamical electron-electron and electron-proton correlation effects are included in the NEO framework using second-order perturbation theory (NEO-MP2)[14]. Other groups[72, 73, 74, 75] have also studied hydrogen bonded systems using a related nuclear molecular orbital method, but their studies used only a single 1s basis function for the hydrogen nucleus and did not include electron-electron or electron-nuclear correlation.

The NEO method possesses several advantages over other methods for including nuclear quantum effects. Anharmonic properties of the potential energy surface are included directly in NEO calculations. Moreover, the impact of nuclear quantum effects on the electronic wavefunction is inherently included in NEO calculations

because the nuclear and electronic wavefunctions are calculated simultaneously. This type of response is not fully included in methods that calculate nuclear wavefunctions on Born-Oppenheimer electronic potential energy surfaces with no feedback between the nuclear and electronic wavefunctions. In addition, the NEO approach is more computationally efficient for the calculation of vibrationally averaged molecular structures than the grid-based methods such as VSCF and the VPT2 method. NEO calculations at the Hartree-Fock (NEO-HF) or second-order perturbation theory (NEO-MP2) levels are approximately as expensive as the corresponding conventional RHF or MP2 analogues.

In this paper, we utilize three different approaches to study the impact of nuclear quantum effects on molecular structure. The NEO-MP2 and VSCF approaches are applied to a set of bihalide compounds, $[XHX]^-$ (X = F, Cl, Br), and the NEO-MP2, VSCF, and VPT2 approaches are applied to the hydrogen fluoride dimer, $(HF)_2$. These systems are depicted in Figures 4.1 and 4.2. Our objective is to compare the geometries calculated with a variety of quantum mechanical approaches to available experimental data. Additionally, we analyze the significance of electron-electron and electron-proton correlation, anharmonicity of the vibrational modes, and nonadiabatic effects for these hydrogen-bonded systems. Bihalides exhibit anharmonic potential energy surfaces that must be described accurately to recover vibrationally-averaged molecular properties. Experimental bond lengths and frequencies are available for the bihalides with fluorine and chlorine. These bihalide systems have also been studied by Del Bene and Jordan using a two-dimensional grid-based approach[76]. The hydrogen fluoride dimer exhibits an asymmetric hydrogen bond that strongly influences vibrationally-averaged molecular properties. Experimental F−F distances are available for the hydrogen fluoride dimer and the deuterated form of the dimer[77, 78].

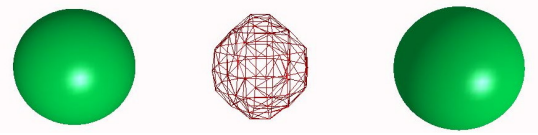

Figure 4.1. The bifluoride ion. The hydrogen atom is represented by nuclear wavefunctions calculated using the NEO approach.

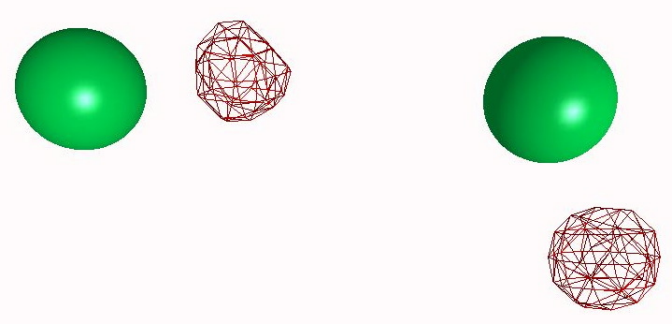

Figure 4.2. The hydrogen fluoride dimer. The hydrogen atoms are represented by nuclear wavefunctions calculated using the NEO approach.

The remainder of the chapter is organized as follows. Section 2 provides a summary of the NEO-HF, NEO-MP2, VSCF, and VPT2 methods. Section 3 presents the results for the bihalides and the hydrogen fluoride dimer. The final section presents conclusions and future directions.

4.2 Theory and methods

4.2.1 Nuclear-electronic orbital aproach

The NEO methodology has been implemented in the GAMESS electronic structure program[23]. The DZSPDN hydrogen nuclear basis set was used for the NEO calculations presented in this chapter. This DZSPDN nuclear basis set[10] includes two each of s, p, and d-type Gaussians, resulting in a total of 20 nuclear basis functions per hydrogen center. The aug'-cc-pVTZ electronic basis set[52, 53, 54], in which the prime indicates that diffuse functions were placed only on the heavy atoms, was used for the bihalide calculations, and the aug-cc-pVTZ electronic basis set was used for the HF dimer calculations. At the NEO-HF level, analytical gradients[10] were used to carry out all geometry optimizations. Structures were identified as minima on the NEO potential energy surface by computing and diagonalizing the NEO Hessian matrix[11]. At the NEO-MP2 level, all geometry optimizations were performed using numerical gradients. A criteria of 10^{-5} Hartree/Bohr was used for all geometry optimizations, and all SCF densities were converged to within 10^{-7}.

A significant source of error present in electronic structure calculations on

hydrogen-bonded dimers is basis set superposition error (BSSE). BSSE is the mutual improvement of the electronic basis sets on the monomers in the overall basis of the dimer. Since BSSE can impact structures of hydrogen-bonded dimers[79], we have estimated the magnitude of BSSE with the counterpoise correction[80] using both the NEO-MP2(ee+ep) and conventional MP2 methods for the HF dimer. Both the NEO and conventional counterpoise correction calculations were performed using the MP2/aug-cc-pVTZ optimized HF dimer geometry. The NEO-MP2(ee+ep) and conventional MP2 counterpoise corrections are ~ 0.55 and ~ 0.48 kcal/mol, respectively. Thus, the amount of BSSE is similar for the conventional MP2 and NEO-MP2 calculations.

4.2.2 Vibrational self-consistent field

The VSCF method as implemented by Chaban, Jung, and Gerber[66] was used to calculate vibrationally-averaged geometries for the bihalides and the HF dimer. An option to calculate vibrationally-averaged molecular structures within the VSCF framework is not implemented in the distributed version of GAMESS[23]. Therefore, we have incorporated this capability into an experimental version of the GAMESS code. At the VSCF level, the total molecular vibrational wavefunction is constructed as a product of vibrational normal mode wavefunctions.

$$\Psi_0^{VSCF}\left(Q_1, Q_2, ..., Q_N\right) = \prod_i^N \varphi_i^0\left(Q_i\right) \tag{4.1}$$

The expectation value of the displacement coordinate for normal mode i over the VSCF wave function is

$$\langle Q_i \rangle = \frac{\left\langle \Psi_0^{VSCF} \right| Q_i \left| \Psi_0^{VSCF} \right\rangle}{\left\langle \Psi_0^{VSCF} \mid \Psi_0^{VSCF} \right\rangle} \tag{4.2}$$

The expectation value for a mass weighted cartesian displacement coordinate is calculated using the expectation values of the mass weighted normal coordinates as

$$\langle x_j \rangle = \sum_i L_{ji} \langle Q_i \rangle \tag{4.3}$$

where L_{ji} are the eigenvectors of the mass weighted Cartesian force constant matrix. The Cartesian displacement coordinates need to be un-mass weighted:

$$\langle \tilde{x}_j \rangle = \mathrm{M}_{jj}^{1/2} \langle x_j \rangle \tag{4.4}$$

where $\tilde{x}$ denotes an un-mass weighted Cartesian coordinate. The effective un-mass weighted Cartesian coordinate can now be calculated as

$$x_j^{\mathrm{eff}} = x_j^0 + \langle \tilde{x}_j \rangle \tag{4.5}$$

Here x_j^0 and x_j^{eff} are the equilibrium and effective Cartesian coordinates, respectively.

In the GAMESS implementation of VSCF, the VSCF potential is computed using standard un-mass weighted Cartesian displaced coordinates. In practice, the eigenvectors of the mass weighted force constant matrix are un-mass weighted

$$\tilde{\mathbf{L}} = \mathbf{M}^{1/2}\mathbf{L} \tag{4.6}$$

Here the tilde denotes un-mass weighting. In our implementation of the caluclation of effective geometries the the un-mass weighted Cartesian dispacement expectation values are calculated using

$$\langle \tilde{x}_j \rangle = \sum_i \tilde{L}_{ji} \langle Q_i \rangle \tag{4.7}$$

For all of the VSCF calculations, 16 directly-computed quadrature points along each normal mode were used to construct the VSCF potential. The potentials were calculated at the MP2/aug'-cc-pVTZ level for the bihalides and at the MP2/aug-cc-pVTZ level for the HF dimer. Geometries obtained at the VSCF level and frequencies obtained at the VSCF and CC-VSCF levels[66] are reported. The CC-VSCF (correlation corrected VSCF) level includes a second-order perturbation theory correction to include dynamical correlation between the vibrational modes.

4.2.3 Vibrational perturbation theory

The VPT2 method as implemented by Barone[2, 3] in the Gaussian03 package[81] was used to calculate vibrationally-averaged geometries for the HF dimer at the MP2/aug-cc-pVTZ level. This method was not available for linear molecules such as the bihalides. In the VPT2 method, the zeroth-order vibrational wavefunctions are generated from the harmonic approximation, and the second-order perturbation theory corrections are calculated from the cubic force constants and semidiagonal quartic force constants. The required cubic and quartic force constants are obtained by numerical differentiation of the analytical Hessians. Vibrationally-averaged molecular structures are standard output for VPT2 calculations in Gaussian03[81].

4.3 Results and discussion

4.3.1 Bihalides

In this subsection, we analyze calculations for a set of $[XHX]^-$ systems with X = F, Cl, and Br. We compare the X−X distances obtained with the NEO approach to the distances obtained with two-dimensional grid methods by Del Bene and Jordan[76] and to distances obtained with the VSCF method. To enable this comparison, we used the aug'-cc-pVTZ electronic basis set and included electron-electron correlation at the MP2 level for all calculations. For the NEO calculations, only the hydrogen nucleus was treated quantum mechanically, and it was represented by a single nuclear basis function center with the DZSPDN nuclear basis set (i.e., 20 nuclear basis functions). The NEO-MP2 method was used to include both electron-electron and electron-proton correlation. The geometries were optimized at the NEO-MP2(ee) and NEO-MP2(ee+ep) levels. To include the X−X mode quantum effects in the NEO calculations, we implemented the NEO-MP2/1D grid approach. In this approach, the NEO-MP2 energy is calculated along a grid representing the X−X distances, and the Fourier grid Hamiltonian (FGH) method[56] is used to calculate the wavefunction corresponding to the X−X mode. The NEO-MP2/1Dgrid approach assumes an adiabatic separation between the hydrogen motion and the X−X motion (i.e., the hydrogen nucleus and the electrons are assumed

to respond instantaneously to the motion of the heavy nuclei).

We emphasize that the NEO calculations are much faster than the two-dimensional grid and VSCF calculations. The two-dimensional potential energy surface used for the $[FHF]^-$ grid calculation of Del Bene and Jordan required 206 single point conventional MP2 energy calculations, and 1,601 quadrature points were used to construct the VSCF potential. In contrast, only 32 NEO-MP2 calculations were used to construct the NEO-MP2/1D grid potential for $[FHF]^-$. For this system, a single NEO-MP2 energy calculation requires only about 15 seconds of CPU time, which is similar to a conventional MP2 energy calculation.

Table 4.1 presents the X−X distances calculated with a number of different approaches. The two-dimensional grid method includes the nuclear quantum effects of the hydrogen and the X−X modes, as well as the coupling between these modes. The VSCF method includes the quantum effects of the two bending modes, in addition to the hydrogen stretch and X−X modes, and describes the couplings among the modes in an approximate manner. The two-dimensional grid and VSCF methods do not include the response of the electronic wavefunction to the nuclear wavefunction or a rigorous treatment of electron-proton correlation because the nuclear wavefunctions are calculated on a Born-Oppenheimer electronic potential energy surface. In contrast, the quantum nuclear and electronic wavefunctions are calculated self-consistently in the NEO approach, and the NEO-MP2(ee+ep) method includes a significant amount of electron-proton dynamical correlation. The NEO-MP2(ee) and NEO-MP2(ee+ep) methods include the nuclear quantum effects of the hydrogen but not the X−X motion, whereas the NEO-MP2(ee)/1Dgrid and NEO-MP2(ee+ep)/1Dgrid methods include the nuclear quantum effects of the hydrogen and the X−X motions but not the coupling between these motions.

The NEO approach is capable of including the nuclear quantum effects of the bending mode with an adequate nuclear basis set, sufficient electron-proton correlation, and inclusion of nonadiabatic effects between the classical and quantum nuclei. The present implementation is aimed at an accurate description of the stretching modes, however, so the nuclear basis set is not optimized for the description of the lower-frequency bending modes. Inclusion of electron-proton correlation at the NEO-MP2(ee+ep) level provides an approximate description of these bending modes within the context of this nuclear basis set and in the absence

Table 4.1. Experimental and theoretical X−X distances in Å for bihalide systems, $[XHX]^-$ with X=F,Cl,Br.

	$[FHF]^-$	$[ClHCl]^-$	$[BrHBr]^-$
method[a]	R_{FF}	R_{ClCl}	R_{BrBr}
experimental R_e	2.27771[b]	3.1122(26)[c]	N/A
experimental R_0	2.304[d]	3.14676(5)[b]	N/A
MP2	2.288	3.110	3.408
2D grid[e]	2.324	3.152	3.430
VSCF-MP2	2.311	3.131	3.424
NEO-MP2(ee)	2.321	3.150	3.449
NEO-MP2(ee)/1Dgrid	2.325	3.151	3.451
NEO-MP2(ee+ep)	2.313	3.139	3.437
NEO-MP2(ee+ep)/1Dgrid	2.318	3.142	3.440

[a]The aug'-cc-pVTZ electronic basis set and MP2 level of including electron-electron correlation were used in all calculations. The DZSPDN nuclear basis set was used in all of the NEO calculations.

[b]Ref.[82]

[c]Ref.[83]

[d]Calculated using the rigid rotor approximation and B_0 from Ref.[82]

[e]Ref.[76]

of nonadiabatic effects between the classical and quantum nuclei.

The results provided in Table 4.1 indicate that inclusion of the nuclear quantum effects of the hydrogen significantly increases the X−X distance relative to the conventional MP2 method. Comparison of the NEO-MP2 and NEO-MP2/1Dgrid results illustrates that the quantum effects of the X−X motion are not as significant as those of the hydrogen motion. Specifically, the X−X distance is altered by nearly an order of magnitude more by the quantum effects of the hydrogen nucleus than by the quantum effects of the heavy nuclei. The NEO-MP2(ee)/1D grid method leads to an X−X distance within 0.001 Å of the distance obtained with the two-dimensional grid method for X = F and X = Cl. This excellent agreement provides validation for the NEO approach.

Analysis of the results for the three different halides indicates that the difference between the NEO-MP2(ee)/1Dgrid and the two-dimensional grid X−X distances is significantly greater for X = Br than for X = F and Cl. To verify that the hydrogen nuclear basis set is not the source of the discrepancies, we optimized

the exponents in the nuclear basis functions for each system and found that the results did not change significantly. A source of error in the NEO-MP2/1Dgrid calculations is the adiabatic separation of the H and X−X motions. This error is expected to decrease as the mass of X increases. A source of error in the two-dimensional grid calculations of Del Bene and Jordan is the neglect of the impact of the nuclear wavefunctions on the electronic structure. This error is expected to increase as the number of electrons in X increases and is most likely responsible for the discrepancies when X = Br.

Inclusion of electron-proton dynamical correlation in the NEO calculations decreases the X−X distances by ~ 0.01 Å. Similarly, the X−X distances calculated with the VSCF method are ~ 0.01 Å shorter than the distances calculated with the two-dimensional grid method. The smaller X−X distances for the VSCF calculations are most likely due to the inclusion of the bending motions. As discussed above, the inclusion of electron-proton dynamical correlation improves the description of the bending modes within the NEO approach. An improved description of the bending modes through either VSCF or NEO-MP2(ee+ep) leads to better agreement of the calculated distances with the experimental R_0 values[82, 83].

The agreement between the NEO-MP2(ee+ep)/1D grid method and the experimental R_0 values provides further validation for the NEO approach. For X = F, the X−X distances obtained from the NEO-MP2(ee+ep)/1D grid and VSCF methods are ~ 0.02 Å above the experimental R_0 value. The differences between the X−X distance obtained with the conventional MP2 method and the experimental R_e suggest that the remaining discrepancies may be due in part to limitations of the electronic basis set and level of electron correlation. Another potential source of error for the VSCF calculations is the approximate treatment of the couplings among the vibrational modes. A possible source of the discrepancy for the NEO calculations is the limited treatment of the bending modes due to the choice of nuclear basis set and level of electron-proton correlation. An additional source of error in the NEO approach is the adiabatic separation of the hydrogen and heavy atom motions. This error decreases as the mass of X increases. For $[ClHCl]^-$, the difference between the experimental R_0 value and the NEO-MP2(ee+ep)/1Dgrid distance decreases to 0.005 Å.

The frequencies corresponding to the X−X symmetric stretch mode are pre-

sented in Table 4.2. The conventional MP2 frequencies are significantly greater than the experimental values due to the neglect of anharmonic effects. The two-dimensional grid and CC-VSCF frequencies are much closer to the experimental values. The VSCF frequencies are greater than the CC-VSCF frequencies due to the lack of dynamical correlation among the vibrational modes in VSCF. The NEO-MP2/1Dgrid frequencies are smaller than the conventional MP2 frequencies but larger than the two-dimensional grid and CC-VSCF frequencies. The larger errors in the X−X symmetric stretch frequencies calculated with the NEO approach compared to those calculated with the two-dimensional grid and CC-VSCF methods are most likely due to a combination of the adiabatic separation of the hydrogen and X−X motions and an inadequate nuclear basis set in the outer regions of the NEO potential energy surfaces (i.e., for large X−X distances). The potential along the proton coordinate becomes a double well at large X−X distances. As shown in Ref. [15], an additional nuclear basis function center may be required for an accurate description of these types of potentials. The inclusion of an additional nuclear basis function center is expected to decrease the energy in the outer region of the potential energy surface along the X−X mode and thereby lead to a lower frequency for this mode. Although these types of calculations are straightforward, the level of accuracy provided in Table 4.2 is satisfactory for the present purposes.

Table 4.2. Experimental and theoretical symmetric stretch mode frequencies in cm^{-1} for $[XHX]^-$ with X = F, Cl, Br.

method	$[FHF]^-$	$[ClHCl]^-$	$[BrHBr]^-$
experiment	583[a]	318[b]	N/A
MP2-harmonic	633	345	208
2D grid[c]	589	317	195
VSCF-MP2	618	343	205
CC-VSCF-MP2	591	327	197
NEO-MP2(ee)/1Dgrid	606	334	212
NEO-MP2(ee+ep)/1Dgrid	611	334	206

[a]Ref.[82]
[b]Ref.[83]
[c]Ref.[76]

The asymmetric stretch and bending mode frequencies for the bihalides are given in Table 4.3. Note that the stretching and bending mode frequencies are of similar magnitude for the bihalides. The bending mode frequencies for $[FHF]^-$ calculated with the VSCF and CC-VSCF methods are in excellent agreement with the experimental value. The asymmetric stretch mode frequencies calculated with the VSCF and two-dimensional grid[76] methods are somewhat larger than the experimental values for all of the bihalides. The hydrogen stretching and bending mode frequencies are not calculated with the NEO-MP2 method because this method does not provide accurate excited vibronic states. Multiconfigurational NEO methods are being developed to enable the calculation of these frequencies.

Table 4.3. Experimental and theoretical bending (ν_2) and asymmetric stretch (ν_3) mode frequencies in cm^{-1} for $[XHX]^-$ with X = F, Cl, Br.

	$[FHF]^-$		$[ClHCl]^-$		$[BrHBr]^-$	
method	ν_2	ν_3	ν_2	ν_3	ν_2	ν_3
experiment	1286[a]	1331[a]	N/A	723[b]	N/A	646[c]
MP2-harmonic	1334	1280	843	629	725	663
2D grid[d]	N/A	1485	N/A	881	N/A	846
VSCF-MP2	1283	1485	816	939	701	901
CC-VSCF-MP2	1277	1464	811	925	698	894

[a]Ref.[82]
[b]Ref.[83]
[c]Ref.[84]
[d]Ref.[76]

4.3.2 Hydrogen fluoride dimer

In this subsection, we analyze calculations for the hydrogen fluoride (HF) dimer, which is depicted in Figure 4.3. The HF dimer is a prototypical hydrogen-bonded system for comparing electronic structure results to experimental structural and vibrational data[85, 86]. In contrast to the $[XHX]^-$ systems, the hydrogen participating in the hydrogen bond in the HF dimer is not equally shared between the two fluorine atoms, and the potential for this hydrogen is highly asymmetric. Klemperer and coworkers have performed molecular beam experiments on this

system[77, 78]. They have calculated the F−F distance using a model that removes the large amplitude hydrogen bond exchange motion (i.e., the tunneling motions between equivalent hydrogen-bonded structures) but retains the stretching and bending motions about a single equilibrium geometry. Thus, the HF dimer is an ideal benchmark for the NEO, VSCF, and VPT2 approaches. In the NEO calculations for this system, both hydrogen nuclei were treated quantum mechanically.

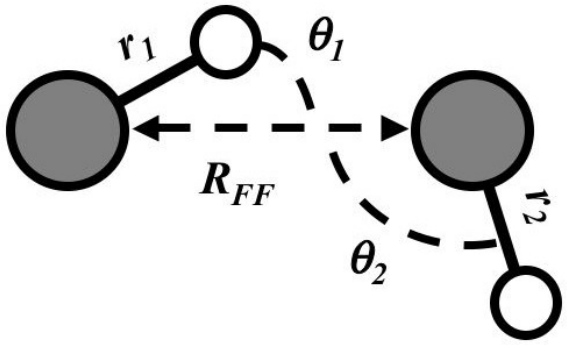

Figure 4.3. Definitions of structural parameters for the hydrogen fluoride dimer.

Table 4.4 provides the HF dimer F−F distances determined from conventional electronic structure methods, the VSCF and VPT2 methods, the NEO approach, and experimental data. The conventional RHF, MP2, and CCSD(T) calculations indicate that the F−F distance decreases as the amount of electron-electron correlation is increased. The NEO-HF calculation suggests that the F−F distance is also reduced when nuclear quantum effects are included. The impact of nuclear quantum effects on the F−F distance is on the same order as the impact of electron-electron correlation on this distance. When both electron-electron correlation and nuclear quantum effects are included in the NEO-MP2(ee) calculation, the F−F distance is further reduced. The NEO-MP2(ee) result illustrates that nuclear quantum effects and electron-electron correlation effects on the F−F distance are approximately additive for this system. Furthermore, when only the hydrogen-bonded hydrogen nucleus is treated quantum mechanically, the F−F distance is 2.733 Å with the reference Hamiltonian in Eq. 2.19 and 2.730 Å with the reference Hamiltonian in Eq. 2.1. Thus, relative to the CCSD(T) calculations, the nuclear quantum effects due to the terminal hydrogen in the HF dimer have the same

impact on the F−F distance as those due to the hydrogen-bonding hydrogen.

Table 4.4. Experimental and theoretical structural data for the HF dimer. Definitions for the structural parameters are given in Figure 4.3. Distances are in Å, and angles are in degrees. The aug-cc-pVTZ electronic basis set was used in all calculations. The DZSPDN nuclear basis set was used in all of the NEO calcualtions. Distances and angles involving the hydrogen nuclei were computed as expectation values with respect to the NEO hydrogen nuclear wavefunctions.

method	R_{FF}	r_1	r_2	θ_1	θ_2
experiment[a]	2.72 ± 0.03[b]	N/A	N/A	10 ± 6[c]	117 ± 6[c]
	2.7913[d]				
RHF	2.830	0.903	0.902	6.77	119.70
MP2	2.746	0.928	0.925	6.37	111.15
CCSD(T)[e]	2.742	0.927	0.924	6.66	110.79
NEO-HF	2.787	0.925	0.922	6.29	119.76
NEO-MP2(ee)	2.717	0.931	0.928	6.53	110.92
NEO-MP2(ee+ep)	2.717	0.930	0.926	6.30	111.40
VSCF2-MP2	2.772	0.926	0.928	6.92	111.78
VPT2-MP2	2.801	0.902	0.905	7.01	116.42

[a]Ref.[78]
[b]The large amplitude bending motions are removed.
[c]In Ref. [78], these angles are interpreted to be associated with the equilibrium geometry.
[d]The stretching and bending motions are included.
[e]Ref.[86]

As given in Table 4.4, the NEO-MP2(ee+ep) and NEO-MP2(ee) calculations yield the same F−F distance for the HF dimer. This observation indicates that electron-proton correlation is not significant with this nuclear basis set for this system. In contrast, for the $[XHX]^-$ systems discussed in the previous subsection, electron-proton correlation significantly altered the X−X distances with this nuclear basis set. Note that the reference Hamiltonian in Eq. 2.19 was used for the bihalide systems, which include only a single quantum nucleus, whereas the reference Hamiltonian in Eq. 2.1 was used for the HF dimer, which includes two quantum nuclei. We verified that the impact of electron-proton correlation on the X−X distances in the bihalides is still significant when the reference Hamiltonian in Eq. 2.1 is used. Thus, the greater impact of electron-proton correlation on the bihalides than on the HF dimer is not due to the different reference Hamiltonians

but rather is due to the different types of proton potentials. The proton potentials for the bihalides are flat, symmetric single wells, whereas the proton potential for the HF dimer is a tighter, asymmetric single well along the donor-acceptor axis. Electron-proton correlation is more important for the bihalides because the proton nuclear wavefunction is more delocalized along the donor-acceptor axis. As discussed below, however, electron-proton correlation may be important for calculations of the HF dimer with a nuclear basis set designed to describe the lower frequency bending modes.

In addition to the F−F distance, the two angles and the H−F bond lengths defined in Figure 4.3 are also provided in Table 4.4. For the NEO approach, these quantities were calculated as expectation values with respect to the nuclear wavefunctions. The H−F bond lengths for both HF molecules increase when electron-electron correlation and nuclear quantum effects are included. The increase in the H−F bond lengths due to electron-electron correlation is of similar order as the increase due to nuclear quantum effects. The increased H−F distances result in larger dipole moments in each of the interacting HF molecules, thereby enhancing the electrostatic interaction between the HF monomers and decreasing the F−F distance. Thus, inclusion of nuclear quantum effects using the NEO approach strengthens the hydrogen bond in the HF dimer.

In contrast to the NEO-MP2 results, the F−F distances calculated with the VSCF and VPT2 methods are larger than the conventional electronic structure F−F distance. To evaluate the accuracy of the VSCF and VPT2 approaches for this system, we analyzed the vibrational frequencies calculated at the VSCF, CC-VSCF, and VPT2 levels. These frequencies are provided in Table 4.5. The frequencies calculated at the CC-VSCF and VPT2 levels are in reasonable agreement with the experimental frequencies compiled by Collins and coworkers[85]. The frequencies calculated at the VSCF level do not agree as well with these experimental frequencies. These discrepancies are most likely due to the omission of some important higher order terms in the implementation of VSCF in the GAMESS package[66]. As a result, the vibrationally-averaged geometries calculated with the VPT2 method are expected to be more reliable than those calculated with this VSCF method.

The qualitative difference between the NEO results and the VSCF and VPT2

Table 4.5. Experimental and theoretical vibrational frequencies in cm^{-1} for the HF dimer.

method[a]	stretch	stretch	bend	*o/p* bend	bend	F−F stretch
experiment[b]	3931	3868	N/A	400	394	125, 128
VPT2	3916	3846	456	406	153	130
CC-VSCF	3866	3744	743	690	568	227
VSCF	3866	3744	743	690	568	227
harmonic	4082	3989	578	474	219	159

[a]The theoretical frequencies were calculated at the MP2/aug-cc-pVTZ level.
[b]Ref.[85]

results for the F−F distance arises from the treatments of the bending-type modes. Previous studies[87] have suggested that librational motions in the water dimer increase the O−O distance. An analogous effect is expected to be observed in the HF dimer. As the separation between the two HF monomers is decreased slightly from equilibrium, the bending motions become more confined, increasing the zero point energy of these modes. In contrast, the stretching potential of the shared hydrogen becomes flatter, reducing the zero point energy of this mode. The vibrationally-averaged F−F distance is determined by a balance between the opposing effects of the stretching and bending modes, as well as the electrostatic effects. The VPT2 F−F distance of 2.801 Å is in excellent agreement with the vibrationally-averaged F−F distance of 2.7913 Å determined experimentally by Klemperer and coworkers[78] for a model that includes all stretching and bending motions about a single equilibrium structure. The F−F distance of 2.717 Å calculated with the NEO-MP2 method is in excellent agreement with the distance of 2.72 Å obtained experimentally from a model that removes the large amplitude bending motions[78].

We also studied the impact of isotopic substitution on the geometry of the HF dimer. Specifically, we calculated the F−F distance for the HF and DF dimers using the NEO-MP2, VSCF, and VPT2 approaches. The structural data for the DF dimer are presented in Table 4.6, and the calculated vibrational frequencies are presented in Table 4.7. For the NEO-MP2 calculations of the DF dimer, the DZSPDN(D) basis set optimized for deuterium[16] was used. The NEO-MP2(ee)

F−F distance in the DF dimer was calculated to be 2.726 Å, which is $\sim$ 0.01 Å longer than the NEO-MP2(ee) distance for the HF dimer. As discussed in Ref. [16], this weakening of the hydrogen bond upon deuteration arises from the decrease in the H−F bond lengths and therefore the dipole moments of the HF monomers. Conversely, the VPT2 F−F distance in the DF dimer was calculated to be $\sim$ 0.01 Å shorter than the VPT2 distance for the HF dimer. A similar trend was found with the VSCF method. This decrease in the F−F distance by $\sim$ 0.01 Å upon deuteration was also observed experimentally by Klemperer and coworkers[78] for the model that includes all stretching and bending motions about a single equilibrium structure.

Table 4.6. Experimental and theoretical structural data for the DF dimer. Definitions for the structural parameters are given in Figure 4.3. Distances are in Å, and angles are in degrees. The aug-cc-pVTZ electronic basis set was used in all calculations.

method	R_{FF}	r_1	r_2	θ_1	θ_2
experiment[a]	2.778[b]	N/A	N/A	N/A	N/A
VSCF-MP2	2.765	0.924	0.925	6.75	111.55
VPT2-MP2	2.794	0.909	0.910	6.79	115.03

[a]Ref.[85]
[b]The stretching and bending motions are included.

Table 4.7. Theoretical vibrational frequencies in cm^{-1} for the DF dimer.

method[a]	stretch	stretch	bend	*o/p* bend	bend	F−F stretch
VPT2	2872	2818	354	306	153	114
CC-VSCF	2831	2782	502	429	51	79
VSCF	2839	2758	519	463	305	296
harmonic	2958	2892	417	341	180	137

[a]The theoretical frequencies were calculated at the MP2/aug-cc-pVTZ level.

These results suggest that the NEO-MP2 calculations accurately account for the stretching motions of the hydrogen atoms but may not adequately describe the bending motions, which significantly impact the F−F distance for the HF dimer. The bending modes have a greater structural impact on the HF dimer than on the

bihalides because the HF dimer bending modes have lower frequencies. Moreover, the stretching and bending frequencies in the HF dimer differ by an order of magnitude, whereas the stretching and bending frequencies in the bihalides are of similar magnitudes. The DZSPDN nuclear basis set was designed for higher-frequency stretching motions[10]. Thus, the DZSPDN basis set adequately describes the hydrogen vibrational ground state in the bihalide systems, but it may not give the correct hydrogen vibrational ground state in the HF dimer due to the significant difference between the bending and stretching frequencies. We performed NEO-MP2 calculations on the hydrogen fluoride dimer with a larger nuclear basis set (i.e., quadruple-zeta s and p and double-zeta d) with frequencies ranging from 400 - 4000 cm^{-1}, and the results were virtually identical to those obtained with the DZSPDN nuclear basis set. We also found that including proton-proton correlation at the NEO-full CI level[10, 13] did not alter the qualitative trends. These results suggest that additional electron-proton dynamical correlation or multiconfigurational nuclear-electronic wavefunctions[10, 13] may be required to accurately predict geometries for these types of systems. Note that these large amplitude bending motions will be damped in large clusters and condensed phase environments. The path-integral CPMD results of Raugei and Klein for liquid HF indicate that inclusion of nuclear quantum effects decreases the F−F distance in solution[70].

4.4 Conclusions

We have investigated the structural impact of nuclear quantum effects for a set of bihalides, $[XHX]^-$ with X = F, Cl, Br, and the hydrogen fluoride dimer. These two types of hydrogen bonding systems are fundamentally different because the proton potential along the donor-acceptor axis is flat and symmetric for the bihalides but tighter and asymmetric for the HF dimer. Moreover, the difference between the bending and stretching mode frequencies is significantly greater for the HF dimer than for the bihalides. We compared structural parameters obtained from conventional electronic structure methods, multidimensional grid methods, the VSCF and VPT2 methods, the NEO-MP2 approach, and experimental data. Our analysis provides insight into key physical principles governing the structural

properties of hydrogen-bonded systems.

For the bihalides $[XHX]^-$, inclusion of the nuclear quantum effects of the hydrogen significantly increases the X−X distance. The quantum effects of the hydrogen motion impact the X−X distance by nearly an order of magnitude more than the quantum effects of the X−X motion. The X−X distances calculated with the NEO-MP2(ee)/1D grid method are in excellent agreement with the distances calculated with the Born-Oppenheimer two-dimensional grid method[76]. The differences between the X−X distances calculated with these two methods are only ~ 0.001 Å for X = F and Cl. The slightly larger discrepancies for X = Br are most likely due to the neglect of the impact of the nuclear wavefunctions on the electronic structure in the two-dimensional grid method. The NEO-MP2(ee+ep) and VSCF methods lead to smaller X−X distances that are in better agreement with the experimental R_0 values available for X = F and Cl. This improvement is due to a more accurate description of the bending modes, which are neglected in the two-dimensional grid method. The difference between the NEO-MP2(ee+ep)/1D grid and experimental X−X distances is only ~ 0.005 Å for X = Cl. This agreement is slightly better for X = Cl than for X = F because the adiabatic separation between the hydrogen and heavy atom motions is a more valid approximation for X = Cl.

The HF dimer is a more challenging system for these approaches because it exhibits bending motions that have much lower frequencies than the stretching motions. Inclusion of the hydrogen quantum effects using the NEO-MP2 approach decreases the F−F distance in the HF dimer. The physical basis for this observation is that the H−F bond lengths of both HF molecules increase when nuclear quantum effects are included, resulting in larger dipole moments in each molecule and therefore a stronger electrostatic interaction between the HF monomers. The NEO-MP2 F−F distance of 2.717 Å is in excellent agreement with the distance of 2.72 Å obtained experimentally for a model that removes the large amplitude bending motions[78]. These results illustrate that the NEO-MP2 approach accurately describes the stretching motions. In contrast to the NEO-MP2 results, the inclusion of nuclear quantum effects with the VSCF and VPT2 methods increases the F−F distance. The VPT2 F−F distance of 2.802 Å is in excellent agreement with the distance of 2.7913 Å obtained experimentally with a model that includes all stretching and bending motions around a single equilibrium structure[78]. For

the isotopically substituted DF dimer, the VPT2 method predicts a decrease in the F−F distance by ~ 0.01 Å. This decrease in the F−F distance upon deuteration is consistent with the experimental data[78]. These results indicate that the VPT2 method accurately describes both the stretching and the low-frequency bending motions.

Our analysis provides a comprehensive evaluation of the applicability of the NEO approach to the investigation of hydrogen-bonded systems. The agreement of the NEO-MP2 calculations with multidimensional grid, VSCF, and VPT2 calculations, as well as experimental data, illustrates the potential of the NEO approach for calculating quantitatively accurate structures. The NEO approach is substantially more efficient than the multidimensional grid, VSCF, and VPT2 methods and therefore will enable the inclusion of nuclear quantum effects for much larger systems. In large clusters and condensed phase environments, the low-frequency bending modes are not expected to impact the geometries as significantly. Future work will focus on the extension of the NEO approach to describe low-frequency bending motions more accurately. These extensions will involve the development of more flexible nuclear basis sets and methods that include additional electron-proton correlation and nonadiabatic couplings between the hydrogen and heavy atom motions.

Chapter 5

Analysis of nuclear quantum effects on hydrogen bonding

5.1 Introduction

The impact of nuclear quantum effects on the molecular structures of bihalides and the hydrogen fluoride dimer were discussed in Chapter 4. This chapter is an extension of Chapter 4. Here, the impact of nuclear quantum effects on hydrogen bonding in hydrogen fluoride clusters, $(HF)_{n=2-6}$, and a partially solvated fluoride anion, $F^-(H_2O)$ are studied. In addition to the second-order vibration perturbation theory (VPT2) and vibrational self-consistent field (VSCF) approaches used in Chapter 4, we also use the path integral Car-Parrinello molecular dynamics (PICPMD) approach to include nuclear quantum effects for the hydrogen fluoride clusters.

Our main objective is to study the impact that nuclear quantum effects have on the interactions between the subunits of hydrogen bonded systems. We also investigate the robustness of the VSCF and VPT2 approaches for studying hydrogen bonded systems. These investigations will hopefully provide useful benchmarks for

the nuclear-electronic orbital approach to be applied to hydrogen bonded systems in the future.

Recently Klein and coworkers have studied the impact of nuclear quantum effects on the structure of hydrogen bonded liquids including hydrogen fluoride (HF) [70] and water [71] by comparing density functional theory (DFT)-based path integral [41] (PI) and classical Car-Parrinello [88] molecular dynamics (CPMD) simulations. For both liquids, inclusion of nuclear quantum effects with PICPMD resulted in shorter hydrogen bond donor−acceptor distances compared to the corresponding classical CPMD simulations. The shorter donor−acceptor distances in the PICPMD simulations reflect strengthened hydrogen bonds which arise from enhanced electrostatic interactions between individual monomers. The enhanced electrostatics present in the PICPMD simulations stem from the quantum delocalization of the hydrogen atoms. The delocalization of the hydrogen atoms increases the dipole moments in the individual monomers causing enhanced electrostatic interactions between the hydrogen bonded subunits.

The impact of nuclear quantum effects on the structures of water clusters has also been investigated using the quantum diffusion Monte Carlo approach [64, 65]. In contrast to the results obtained with the PICPMD simulations for liquid water, the inclusion of nuclear quantum effects in water clusters produced increased O−O distances for clusters containing up to six water monomers.

The impact of nuclear quantum effects on the structures of HF clusters has been studied only for the HF dimer [17]. Inclusion of nuclear quantum effects in the HF dimer resulted in an increased F−F distance consistent with experiment [78]. The increase in the F−F distance in the HF dimer is due to the librational, or bending-type, modes. As the separation between the two HF monomers is decreased slightly from equilibrium, the bending motion becomes more confined, increasing the zero point energy of this mode. In contrast, the stretching potential of the shared hydrogen becomes flatter, reducing the zero point energy of this mode. The vibrationally averaged F−F distance is determined by a balance between the opposing effects of the bending and stretching modes, as well as the electrostatic effects. Previous studies have shown that the same combination of effects also leads to increased O−O distances in the water dimer [87].

Considering the qualitatively different impacts of nuclear quantum effects on

the hydrogen bonding between gas and condensed phase hydrogen fluoride and water, we decided to investigate the impact of nuclear quantum effects for a series of hydrogen fluoride clusters. HF clusters have cyclic structures [89, 90], Figure 5.1, while the liquid form consists of zigzag hydrogen bonded chains [70]. However, as the HF clusters increase in size they can acquire characteristics present in the liquid since the larger rings are approximately zigzag hydrogen bonded chains which are connected at both ends. In order to be consistent with the trends for donor−acceptor distances in the gas and condensed phases, for the smaller HF clusters inclusion of nuclear quantum effects must lead to increased F−F distances between hydrogen bonded subunits and the larger clusters must have decreased F−F distances.

Previous theoretical investigations of HF clusters using conventional electronic structure methods have focused on effects related to the increase in hydrogen bond cooperativity with cluster size [91, 92]. In particular, as the size of the HF clusters increases, additional electronic density accumulates around the fluorine atoms and the hydrogen atoms develop increased partial positive charges. The electronic redistribution seems to converge between $(HF)_4$ and $(HF)_5$ sized clusters and results in substantial non-additive increases in the binding energies [92].

In order to gain further insights about the impact of nuclear quantum effects on hydrogen bonding, we also study a partially solvated fluoride anion, $F^-(H_2O)$. The hydrogen bonding in this system is fundamentally different than in the HF dimer since the hydrogen interacts with a polarizable anion. The $F^-(H_2O)$ system is more strongly bound than the HF dimer (the D_0 for $F^-(H_2O)$ is 26.2 ± 0.8 kcal/mol [93] and D_0 for $(HF)_2$ is 4.6 kcal/mol [86]). For $F^-(H_2O)$, the hydrogen bonding is expected to be dominated by electrostatics, so zero point effects arising from librational motions are not the dominant nuclear quantum effect in this system.

5.2 Methods

We utilize two fundamentally different approaches to study the impact of nuclear quantum effects on the structures of HF clusters. First, we compare DFT-based PICPMD and classical CPMD results for $(HF)_{n=2-6}$. In the PICPMD approach [41, 69], path integrals are combined with Car−Parrinello [88] molecular dynamics.

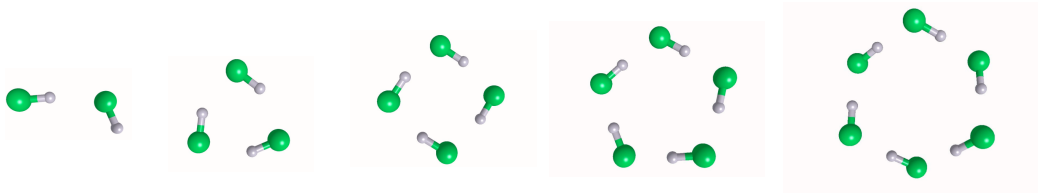

Figure 5.1. Hydrogen fluoride clusters

In the path integral formulation, each quantum nucleus is represented by a ring of p quasi-particles. Each quasi-particle interacts with the two adjacent quasi-particles via a harmonic potential corresponding to the quantized kinetic energy, and each quasi-particle feels only $1/p$ of the actual potential energy.

For the PICPMD simulations $p = 16$ for all quantum nuclei. The PICPMD and CPMD simulations were carried out using the PINY-MD[94] simulation package at 290 K with a 0.1 fs time-step. An MT-BLYP pseudopotential to describe the atomic core of the fluorine atoms and a BLYP-PP30 pseudopotential for hydrogens was used. The valence wavefunctions were expanded in plane-waves up to an energy cutoff of 80 Ry. An energy cutoff of 90 Ry was used for the HF dimer and trimer to check the influence of the cutoff. The overall trend is the same as seen for 80 Ry for the dimer. The BLYP exchange-correlation functional was used.

In addition to the CPMD approach, we use the second-order vibrational perturbation theory (VPT2) approach as implemented [2, 3] in Gaussian03 [81] to calculate vibrationally averaged molecular structures for $(HF)_{n=2-8}$ and compare these to the corresponding equilibrium structures. In the VPT2 method, the zeroth order vibrational wavefunctions are generated from the harmonic approximation, and the second-order perturbation theory corrections are calculated from the cubic and semidiagonal quartic force constants.

The VPT2 calculations were performed using the BLYP [95, 96] and B3LYP [97, 98] exchange-correlation functionals. For all calculations, the aug-cc-pVDZ [53] basis set was used. We have verified that this electronic basis set is suitable for comparing differences between the vibrationally averaged and equilibrium molecular structures for hydrogen fluoride clusters by calculating the difference between vibrationally averaged and equilibrium F−F and F−H distances for the

HF trimer at the BLYP level using a series of basis sets, aug-cc-pVnZ for n = 2−4. The variance in these distances for this series of basis sets was no greater than 0.003 Å. An ultrafine grid was used for the numerical quadrature in the Kohn−Sham procedure. Geometries were optimized using a tolerance of 10^{-6} Hartree/Bohr. The displacement size used for the numerical differentiation of analytical second derivatives in the VPT2 procedure was 0.01 Å.

Two different implementations of the VPT2 approach were used to study nuclear quantum effects in $F^-(H_2O)$. The VPT2 method as implemented by Barone [2, 3] in Gaussian03 [81] was used to calculate anharmonic vibrational frequencies. Vibrationally averaged molecular structures and isotropic nuclear magnetic shielding constants were calculated using the VPT2 approach as implemented [1, 99, 100] in the DALTON [101] electronic structure program. For this system, all calculations were performed at the B3LYP/aug-cc-pVTZ level of theory.

5.3 Results

5.3.1 Hydrogen fluoride clusters

The impact of nuclear quantum effects on the donor-acceptor F−F distances is calculated as

$$\Delta R_{FF}(n) = R^{Q}_{FF}(n) - R^{C}_{FF}(n) \tag{5.1}$$

for each of the HF clusters. The superscript Q indicates that the F−F distance was calculated with PICPMD or VPT2, whereas C indicates the F−F distance was calculated using classical CPMD or the equilibrium value calculated from a conventional electronic structure optimization. An analogous expression is used for the F−H distances.

The results for the F−F distances are depicted in Figure 5.2. For the HF dimer the PICPMD ΔR_{FF} is almost 0.04 Å smaller than for the VPT2 calculations. This difference arises because the CPMD simulations sample two equivalent hydrogen bonded conformers corresponding to exchange of the hydrogen bonded and free FH monomers, whereas the VPT2 calculations are based on expansions for a single equilibrium conformation. However, the VPT2 and PICPMD methods

are qualitatively consistent since they both result in positive ΔR_{FF} values indicating that inclusion of nuclear quantum effects using two fundamentally different approaches results in increased F−F distances for the HF dimer.

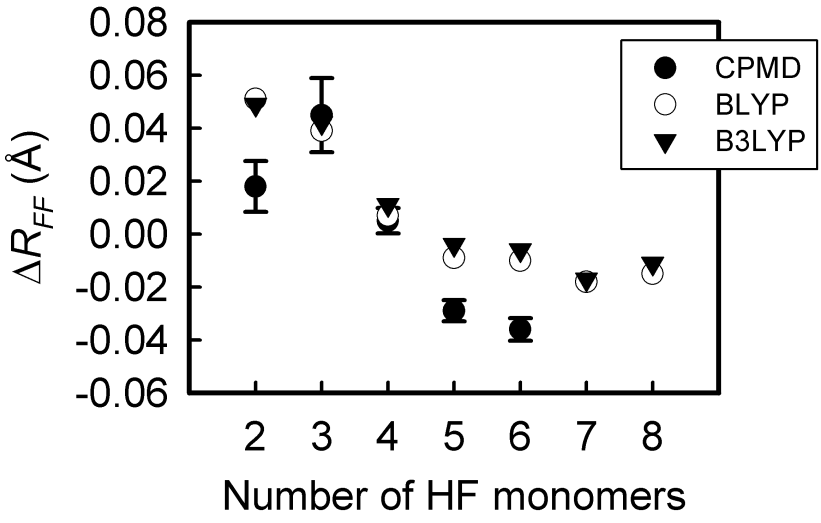

Figure 5.2. Differences between quantum and classical F−F distances for hydrogen fluoride clusters.

The PICPMD ΔR_{FF} values for the $(HF)_{3,4}$ clusters show that nuclear quantum effects result in increased F−F distances. For the $(HF)_{5,6}$ clusters the PICPMD method produces contracted F−F distances indicating a strengthening in the hydrogen bonding. Thus, as the HF clusters evolve toward the condensed phase, a directional change in the impact of the nuclear quantum effects on the hydrogen bonding occurs between $(HF)_4$ and $(HF)_5$. The decrease in F−F distances for the larger HF clusters is consistent with the PICPMD results obtained by Raugei and Klein for liquid HF [70].

The ΔR_{FF} values obtained with the VPT2 approaches agree well with the ones obtained using PICPMD for the $(HF)_{3,4}$ clusters. The directional change in ΔR_{FF} on going from $(HF)_4$ to $(HF)_5$ with PICPMD is also seen with VPT2, but the effect is smaller than at the PICPMD level.

The trends for ΔR_{FF} in Figure 5.2 can be understood by analyzing the ΔR_{FH} values presented in Figure 5.3. At the PICPMD level, the ΔR_{FH} values consistently increase with respect to the size of the HF cluster. Therefore, the quantum

delocalization of the hydrogen atoms increases with the size of the HF clusters. This trend correlates well with the systematic decrease in ΔR_{FF} in Figure 5.2. Moreover, the trends for the ΔR_{FH} and ΔR_{FF} distances demonstrate that as the size of the HF clusters increases, the interactions between the individual subunits is enhanced when nuclear quantum effects are included at the PICPMD level for the larger HF clusters.

The directional change in the impact of nuclear quantum effects on the hydrogen bonding in the HF clusters is due to competition between two effects. In the smaller clusters, zero point energy contributions stemming from librational modes are the dominant energetic factors resulting in increases in distances between individual HF monomers. For the larger HF clusters, electrostatic interactions become the dominant contributor to the interactions between individual HF monomers. The electrostatics become more dominant in the larger HF clusters because as the HF clusters increase in size electron density shifts from the hydrogen atoms to the fluorine atoms [92]. Thus, the interaction between the partial negative charge on the fluorine atoms and the quantum delocalized proton is greater in the larger HF clusters.

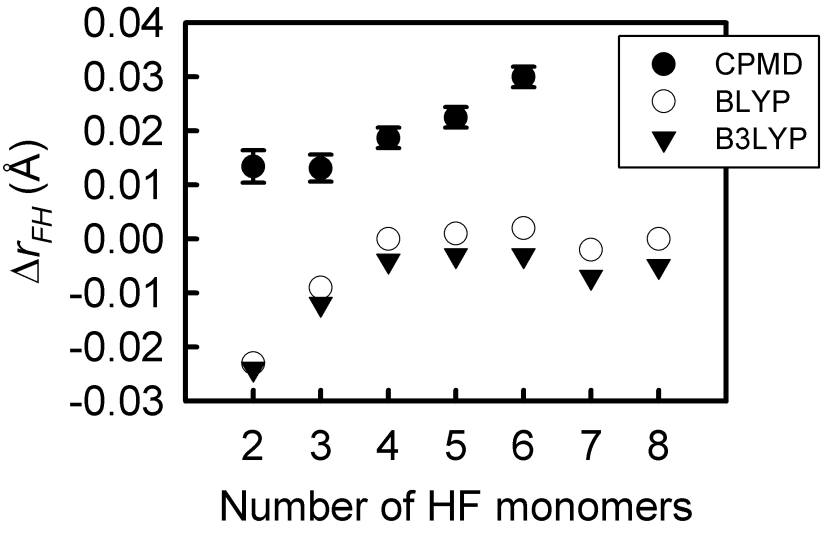

Figure 5.3. Differences between quantum and classical covalent F−H distances for hydrogen fluoride clusters.

In contrast to the PICPMD results, at the VPT2 level the ΔR_{FH} values for all of the HF clusters are consistently negative indicating a contraction of the F−H distances when nuclear quantum effects are included. This trend is not physical due to the asymmetry in the F−H stretching modes which should result in delocalization of the protons along these modes producing increased F−H distances. The differences in the ΔR_{FF} distances between the VPT2 and PICPMD methods in Figure 5.2 for the $n = 5$, 6 clusters are due to the non-physical contraction of the F−H distances at the VPT2 level.

The contraction in F−H distance is also present for the VPT2/MP2/aug-cc-pVTZ level calculations on the HF dimer in Chapter 4. In the next section we present an analysis using the HF dimer which addresses the contraction of the quantum F−H distances at the VPT2 level. Our analysis indicates that the contraction of the vibrationally averaged F−H distances arises from attractive terms in the many-mode potential in conjunction with a truncation of the many-mode potential. The contraction in the vibrationally averaged covalent F−H distances serves as an indicator for problems associated with truncation of the many-mode expansion potential.

5.3.2 VSCF analysis of $(HF)_2$ and $F^-(H_2O)$

In order to further investigate the cause for the contraction of the vibrationally averaged F−H distances in the HF clusters, we used a variational method, vibrational self-consistent field (VSCF), to examine the problem. In the VSCF approach [4, 5, 66, 102], for an N-mode system, the N-dimensional vibrational wavefunction is represented as a product of N single-mode vibrational wavefunctions. This approximation permits the N-dimensional vibrational Schrödinger equation to be simplified to the self-consistent solution of N single-mode vibrational equations.

For the HF dimer the full may-mode potential is

$$V(Q_1,...,Q_6) = \sum_{i}^{6} V_i^{(1)}(Q_i) + \sum_{i<j}^{6} V_{ij}^{(2)}(Q_i,Q_j) + \sum_{i<j<k}^{6} V_{ijk}^{(3)}(Q_i,Q_j,Q_k) + \sum_{i<j<k<l}^{6} V_{ijkl}^{(4)}(Q_i,Q_j,Q_k,Q_l) + \sum_{i<j<k<l<m}^{6} V_{ijklm}^{(5)}(Q_i,Q_j,Q_k,Q_l,Q_m) + \sum_{i<j<k<l<m<n}^{6} V_{ijklmn}^{(6)}(Q_i,Q_j,Q_k,Q_l,Q_m,Q_n) \quad (5.2)$$

In practice, for VSCF implementations which are based on direct computations of the VSCF quadrature points using electronic structure theory methods [66, 103], the VSCF many-mode potential in Equation 5.2 is truncated to include up to the first three terms.

We have performed a series of VSCF calculations on the HF dimer and the partially solvated fluoride anion, $F^-(H_2O)$, where the number of terms in the VSCF many-mode potential in Equation 5.2 is systematically increased from 1 to 3. These calculations were performed using the VSCF method implemented [66, 103] in the GAMESS [23] electronic structure program. For all calculations, 16 directly computed quadrature points along each mode were used to construct the VSCF$(n)_{n=1-3}$ many-mode potentials at the B3LYP/aug-cc-pVDZ level.

The frequencies and vibrationally averaged molecular structures for the HF dimer are presented in Tables 5.1 and 5.2, respectively. For the four low frequency modes, all of the VSCF calculations result in frequencies which are 90 cm^{-1} or more, greater than the corresponding harmonic values. This trend indicates that the truncated VSCF potentials used in these calculations contain attractive contributions due to the low frequency modes. The vibrationally averaged covalent F−H distances computed at the VSCF(2,3) levels are contracted relative to the corresponding equilibrium (harmonic) values. Thus, the VSCF approach has the same problem as the VPT2 method.

The frequencies and vibrationally averaged structural parameters for the $F^-(H_2O)$ system are listed in Tables 5.3 and 5.4, respectively. In contrast to the HF dimer, for $F^-(H_2O)$, four of the six vibrational modes are above 1000 cm^{-1}. For the two low frequency modes, the VSCF calculations produce frequencies which

Table 5.1. Theoretical vibrational frequencies in cm^{-1} for the HF dimer at the VSCF/B3LYP/aug-cc-pVDZ level using 1, 2, and 3-mode expansions for the VSCF potentials.

mode	VSCF(1)	VSCF(2)	VSCF(3)	Harmonic
stretch	3847	3790	3777	4016
stretch	3683	3627	3607	3882
bend	782	745	715	578
o/p bend	789	686	567	465
bend	584	547	500	233
F−F stretch	220	246	257	167

Table 5.2. Theoretical structural data for the HF dimer at the VSCF/B3LYP/aug-cc-pVDZ level using 1, 2, and 3-many-mode expansions in the VSCF potentials.

method	R_{FF}	${r_1}^a$	${r_2}^b$
Equilibrium	2.732	0.9337	0.9289
VSCF(1)	2.7397	0.9492	0.9469
VSCF(2)	2.7532	0.9324	0.9322
VSCF(3)	2.7506	0.9304	0.9263

[a]Hydrogen bonded F−H distance.
[b]Free F−H distance.

are higher than the corresponding harmonic values. The vibrationally averaged covalent O−H distances computed at the VSCF(1-3) levels are all greater than the corresponding equilibrium (harmonic) values. Thus, for this system, truncation of the many-mode expansion is a more valid approximation than for the HF dimer.

In order to obtain further insight about the behavior of the higher order terms in the VSCF many-mode potentials for the $(HF)_2$ and $F^-(H_2O)$ systems, we have evaluated the VSCF$(n)_{n=1-6}$ potential for a single quadrature point in displaced normal mode coordinates for both systems. As a convenient choice for such a location we have used vibrationally averaged geometries for each system which have been calculated at the VSCF(2)/B3LYP/aug-cc-pVDZ level.

Values for each of the six terms comprising the full many-mode potential in Equation 5.2 evaluated at single quadrature points corresponding to vibrationally averaged geometries for the HF dimer and $F^-(H_2O)$ systems are presented in Figure

Table 5.3. Theoretical vibrational frequencies in cm^{-1} for the $F^-(H_2O)$ system at the VSCF/B3LYP/aug-cc-pVDZ level using 1, 2, and 3-mode expansions for the VSCF potentials.

mode	VSCF(1)	VSCF(2)	VSCF(3)	Harmonic
1	3680	3620	3625	3845
2	1649	1618	1629	2216
3	1657	1617	1619	1676
4	1166	1126	1130	1122
5	729	612	624	461
6	376	421	420	387

Table 5.4. Theoretical structural data for the $F^-(H_2O)$ system at the VSCF/B3LYP/aug-cc-pVDZ level using 1, 2, and 3-many-mode expansions in the VSCF potentials.

method	R_{F-O}	r_{F-H}	${r_1}^a$	${r_2}^b$
Equilibrium	2.465	1.4059	1.06	0.9632
VSCF(1)	2.4818	1.3760	1.108	0.98
VSCF(2)	2.4576	1.3569	1.1012	0.9707
VSCF(3)	2.4563	1.3545	1.1025	0.9710

[a]Hydrogen bonded O−H distance.
[b]Free O−H distance.

5.4. For the HF dimer, the higher order terms in the many-mode expansion are up to three orders of magnitude larger than the corresponding terms for the $F^-(H_2O)$ system. The second and fourth order contributions to the many-mode potential in the HF dimer are negative, indicating an attractive contribution to the overall potential. This oscillation, coupled with the fact that the higher order terms (2-4) are larger in magnitude than the first order term indicates that the many-mode potential for the HF dimer converges non-monotonically.

Overall, this analysis indicates that the contraction of vibrationally averaged F−H distances in the HF clusters is not related to the specific method used to include the anharmonic effects, but instead, arises from truncation of the full many-mode potential, which is an approximation used in both the VSCF and VPT2 approaches. Further, at the VSCF level, convergence of the many-mode potential

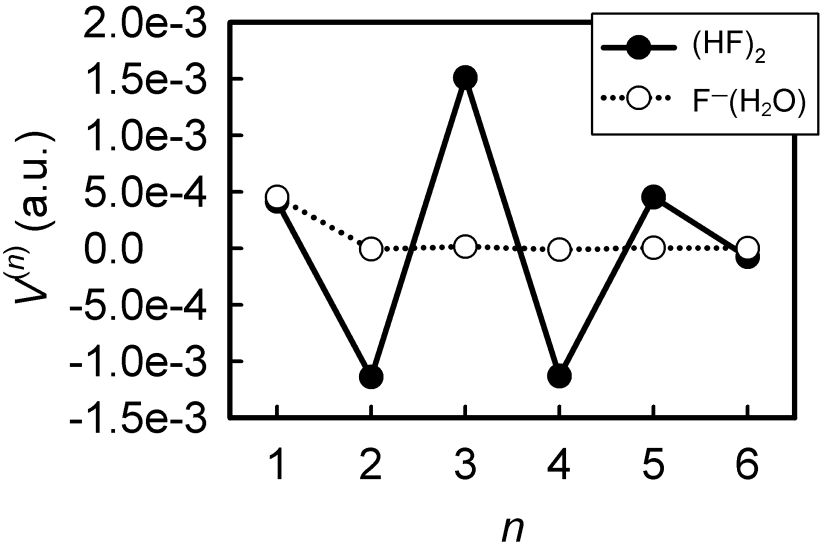

Figure 5.4. The six individual terms in the many-mode potential in Equation 5.2 for the hydrogen fluoride dimer and the $F^-(H_2O)$ system evaluated at the corresponding VSCF(2)-B3LYP/aug-cc-pVDZ vibrationally averaged geometries.

for the HF dimer requires up to five terms. Therefore, the vibrational perturbation series requires higher order terms to converge, if it converges at all. Since the $F^-(H_2O)$ system is more tightly bound and contains fewer low frequency modes, the terms in the many-mode expansion are more well-behaved and truncation of the potential is a valid approximation for this system. Care must be taken when applying VPT or truncated VSCF methods to loosely bound systems such as the HF dimer. Vibrationally averaged structural effects such as the contraction of F−H distances can be used as a diagnostic for identifying such non-convergent behavior in hydrogen bonded systems.

5.3.3 Partially solvated fluoride anion

In this section we present an analysis of the impact of nuclear quantum effects on hydrogen bonding using a simple system, $F^-(H_2O)$, depicted in Figure 5.5. This is a different type of hydrogen bonded system than the HF dimer because the donor hydrogen interacts with a polarizable anion. Unlike the HF clusters, for $F^-(H_2O)$, the vibrationally averaged covalent O−H distances are not contracted relative to

the equilibrium values at the VPT2 or VSCF levels. Therefore, it is reasonable to examine the impact of nuclear quantum effects on this system using the VPT2 approach. Thus, a more detailed analysis of the impact of nuclear quantum effects on the hydrogen bonding in this system can be obtained by calculating vibrationally averaged magnetic properties.

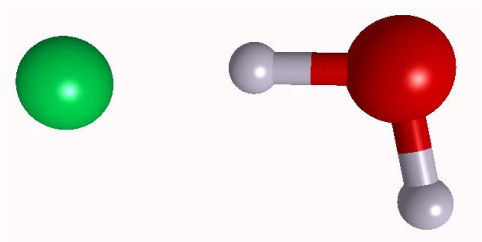

Figure 5.5. The $F^-(H_2O)$ system.

The harmonic and anharmonic vibrational frequencies for the $F^-(H_2O)$ system and its deuterated analog, $F^-(D_2O)$ are presented in Table 5.5. For the $F^-(H_2O)$ system the anharmonic correction is 1050 cm^{-1} for the hydrogen stretching mode involving the hydrogen bonded H. This correction is significantly greater than the anharmonic corrections for any of the other vibrational frequencies. The large anharmonic correction indicates that the hydrogen bonded hydrogen is heavily delocalized between the oxygen and the fluorine atoms due to the high asymmetry in the potential for this mode. For the $F^-(D_2O)$ system the anharmonic correction for the corresponding mode is reduced by a factor of 2. Thus, the deuterium participating in the hydrogen bond is less delocalized than hydrogen, due to the increased mass of deuterium. For both systems, the anharmonic effects result in increased delocalization of the shared hydrogen or deuterium.

The equilibrium and vibrationally averaged structures for the $F^-(H_2O)$ and $F^-(D_2O)$ systems are presented in Table 5.6. The r_{O-H} distance for the hydrogen bonded H increases by $\sim$ 0.04 Å and the corresponding r_{O-D} distance increases by slightly less. These trends are qualitatively consistent with the anharmonic corrections to the vibrational frequencies given in Table 5.5. The R_{F-H} (hydrogen bond) distance decreases by 0.057 Å (0.035 Å) for the $F^-(H_2O)$ ($F^-(D_2O)$) system. There is a similar trend for the R_{F-O} distance.

These trends indicate that the nuclear quantum effects stemming from the hy-

Table 5.5. Vibrational frequencies in cm^{-1} for $F^-(H_2O)$ and $F^-(D_2O)$ computed at the B3LYP/aug-cc-pVTZ level.

mode	experiment[a]	$F^-(H_2O)$ harmonic	$F^-(H_2O)$ anharmonic	$F^-(D_2O)$ harmonic	$F^-(D_2O)$ anharmonic
ν_f[b]	3687	3849	3664	2800	2701
ν_{IHB}[c]	1523	2138	1088	1569	925
ν_b[d]	1650	1689	1607	1228	1188
ν_{oop}[e]	1083−1250	1146	1010	823	833
ν_{ip}[f]		574	568	416	411
ν_{iw}[g]		390	408	375	384

[a]Frequencies for $F^-(H_2O)$ from Ref. [104]
[b]free O−H stretch
[c]ionic H bond
[d]HOH bend
[e]out-of-plane wag
[f]in-plane wag
[g]ion-water stretch

Table 5.6. Vibrationally averaged structural parameters for $F^-(H_2O)$ and $F^-(D_2O)$ computed at the B3LYP/aug-cc-pVTZ level. All values are in Å.

structure	R_{F-O}	r_{F-H}	r_1[a]	r_2[b]
eq. $F^-(H_2O)$	2.4496	1.3874	1.0629	0.96
vib. av. $F^-(H_2O)$	2.432	1.33	1.1024	0.9646
vib. av. $F^-(D_2O)$	2.4422	1.3523	1.0904	0.9636

[a]H bonded O−H distance.
[b]Free O−H distance.

drogen or deuterium atoms participating in the hydrogen bond cause an enhanced interaction between the fluoride anion and the water molecule. The physical basis of the enhanced hydrogen bonding interaction resulting from the nuclear quantum effects can be understood by analyzing the vibrationally averaged isotropic nuclear magnetic shielding constants. The nuclear magnetic shielding constants are sensitive to the electronic environments around the nuclei. Moreover, the vibrationally averaged shielding constants provide an indirect means to detect changes in the electronic structure of the $F^-(H_2O)$ system due to the nuclear quantum effects.

Table 5.7. Isotropic nuclear magnetic shielding constants (ppm) for $F^-(H_2O)$ and $F^-(D_2O)$ computed at the B3LYP/aug-cc-pVTZ level.

structure	^{19}F	^{17}O	$^{1}H_1$	$^{1}H_2$
eq.	396.20	307.37	17.15	33.73
vib. av. H_2O	387.43	299.15	16.52	33.71
vib. av. D_2O	389.62	299.38	16.85	33.65

The equilibrium and vibrationally averaged isotropic nuclear magnetic shielding constants for $F^-(H_2O)$ and $F^-(D_2O)$ are presented in Table 5.7. The difference between ^{19}F shielding constants between $F^-(H_2O)$ and $F^-(D_2O)$ is 2.2 ppm. This value differs by less than 1 ppm from the experimental isotope effect on the ^{19}F shielding constant, 3.0 ± 0.1 ppm [105], measured in solution. In order to explore the effect of solvation for the H/D isotope effect on the ^{19}F shielding constant further, we performed a VPT2 analysis on $F^-(H_2O)_2$. Unfortunately, the vibrationally averaged structure for $F^-(H_2O)_2$ contains contracted O−H distances relative to the equilibrium structure as was seen in the hydrogen fluoride clusters. As shown earlier, these contracted distances are un-physical and are due to the truncation of the many-mode expansion. This approximation is not valid for systems such as $F^-(H_2O)_2$ which contain several anharmonic low-frequency vibrational modes. These un-physical structural trends prevent any further analysis of the vibrationally averaged magnetic properties for the $F^-(H_2O)_2$ system.

The H/D isotope effect for the shielding constants of all other nuclei is less than 1 ppm. The fluorine nucleus is more deshielded with H_2O than with D_2O, which is consistent with the frequency and stuctural data presented in Tables 5.5 and 5.6. The ^{19}F shielding constant is decreased with H_2O relative to D_2O because the proton is more delocalized than the deuteron in the hydrogen bond. Therefore, the electron density around the fluoride anion interacts more strongly with H_2O than with D_2O. The same trends apply for comparing the equilibrium and vibrationally averaged ^{19}F shielding constants for $F^-(H_2O)$. The vibrationally averaged ^{19}F shielding constant is $\sim$ 9 ppm lower than the ^{19}F shielding constant evaluated for the equilibrium geometry with no vibrational averaging. Therefore, including nuclear quantum effects results in a stronger hydrogen bonding interaction between

the fluoride anion and the water molecule.

5.4 Conclusions

Two hydrogen bonded systems, $(HF)_{n=2-6}$ and $F^-(H_2O)$ were studied using two different methods for including nuclear quantum effects, PICPMD and VPT2. In PICPMD [41, 69], path integrals are combined with Car-Parrinello [88] molecular dynamics. In the path integral formulation, each quantum nucleus is represented by a ring of p quasi-particles. Each quasi-particle interacts with the two adjacent quasi-particles via a harmonic potential corresponding to the quantized kinetic energy, and each quasi-particle feels only $1/p$ of the actual potential energy. In the VPT2 method [87, 3], the zeroth-order vibrational wave functions are generated from the harmonic approximation, and the second-order perturbation theory corrections are calculated from the cubic and semidiagonal quartic force constants. Our objectives were to gain insights into the impact of nuclear quantum effects on hydrogen bonding and examine the robustness of the VPT2 approach for studying hydrogen bonded systems.

For the HF clusters, the comparison of the PICPMD and CPMD hydrogen bond donor−acceptor distances, ΔR_{FF}, indicated a directional change in the impact of nuclear quantum effects on the hydrogen bonding as the size of the HF clusters increases from $(HF)_4$ to $(HF)_5$. The directional change arises from a competition between zero point energy effects of librational modes and enhanced electrostatics arising from the delocalization of quantum protons. As the size of the HF clusters increases, the hydrogen atoms become more delocalized. This trend, in conjunction with the redistribution of electronic density toward the fluorine atoms, results in the enhanced electrostatics when nuclear quantum effects are included with the PICPMD approach.

The VPT2 method was able to qualitatively reproduce the directional change for the impact of nuclear quantum effects on the donor−acceptor distances in the HF clusters. However, the vibrationally averaged covalent F−H distances were contracted relative to the corresponding equilibrium values. We investigated this further using a variational approach, VSCF, applied to the HF dimer. Our analysis indicates that the cause of this problem is a breakdown in the perturbation series

due to truncating the many-mode expansion potential.

The $F^-(H_2O)$ system is a hydrogen bonded system where the truncation of the many-mode expansion is a valid approximation. We conducted a detailed analysis on the influence of nuclear quantum effects on hydrogen bonding in the $F^-(H_2O)$ and $F^-(D_2O)$ systems by computing anharmonic vibrational effects, vibrationally averaged molecular structures, and vibrationally averaged isotropic nuclear magnetic shielding constants. For the $F^-(H_2O)$ system, inclusion of nuclear quantum effects resulted in enhanced hydrogen bonding. A large anharmonic redshift on the order of 1000 cm^{-1} was calculated for the vibrational stretching frequency corresponding to the shared hydrogen. There are a number of changes for the vibrationally averaged structure in this system as a result of the anharmonicity associated with the shared hydrogen. The decrease in donor−acceptor, F−O, distance and hydrogen bond length as well as the corresponding increase in covalent O−H distance for the shared hydrogen are all indicative of enhanced hydrogen bonding resulting from nuclear quantum effects. The H/D isotope effect for the structural and vibrational properties is consistent with the Ubbelohde [106] effect.

Our analysis of the vibrationally averaged isotropic nuclear magnetic shielding constants showed that the fluorine nucleus becomes more deshielded as a result of the quantum delocalization of the shared hydrogen. The H/D isotope effect on the ^{19}F shielding constant was within 1 ppm of the experimental [105] value measured in solution. The trends for the vibrationally averaged ^{19}F shielding constants show that the enhanced hydrogen bonding is a result of a stronger electrostatic interaction between the fluoride anion and the delocalized quantum proton.

There were two opposite impacts of nuclear quantum effects on the hydrogen bonding in the $(HF)_{n=2-4}$ and $F^-(H_2O)$ systems. The opposite trends in these systems arise because for $(HF)_{n=2-4}$, zero-point energy effects dominate, whereas for $F^-(H_2O)$ electrostatics are impacted more by the nuclear quantum effects. Moreover, the impact of nuclear quantum effects in the $(HF)_{n=5-6}$ and $F^-(H_2O)$ systems are qualitatively similar since the hydrogen-bonded hydrogens in both of these systems interact with negatively charged F atoms.

Our analysis provides insights regarding the influence of nuclear quantum effects on hydrogen bonding. The present findings indicate that the qualitative impact of nuclear quantum effects on hydrogen bonding is related to the underly-

ing electronic structure of the system. For systems with more polarizable hydrogen bond acceptors, such as $F^-(H_2O)$ and $(HF)_{n>5}$, the delocalization of the quantum hydrogens enhances the electrostatics resulting in stronger hydrogen bonds. In systems containing less polarizable hydrogen bond acceptors, such as $(HF)_2$, zero point energy effects dominate, resulting in weaker hydrogen bonds.

In the context of the nuclear-electronic orbital (NEO) framework, the structural impact of nuclear quantum effects in HF clusters provides an important *qualitative* benchmark. In Chapter 4, we showed that when nuclear quantum effects were included at the NEO-MP2 level for the HF dimer, the F−F distance was reduced relative to the conventional electronic structure MP2 equilibrium F−F distance. Several approaches including experiment [78], PICPMD, VPT2, and VSCF indicate that the F−F distance in the HF dimer should increase when nuclear quantum effects are included. The low frequency, large amplitude bending motions in the HF dimer are responsible for the increased F−F distance. The NEO-MP2 approach is not able to capture these highly delocalized bending motions in the ground state nuclear-electronic wavefunction because it does not recover enough dynamical electron-proton correlation. In the next Chapter, we formulate a method for including *explicit* dynamical electron-proton correlation in the NEO framework in order to address the lack of dynamical electron-proton correlation recovered using orbital-based NEO methods.

Chapter 6

Explicit electron-proton correlation in the nuclear-electronic orbital framework

Reproduced in part with permission from:
Swalina, C.; Pak, M. V.; Chakraborty, A.; Hammes-Schiffer, S. *Journal of Physical Chemistry A* **2006**, *110*, 9983-9987.

6.1 Introduction

Nuclear quantum effects such as zero point motion and hydrogen tunneling are often significant for hydrogen bonding interactions and hydrogen transfer reactions. In conventional treatments based on the Born-Oppenheimer approximation, nuclei are represented as classical point charges. In this case, the nuclear quantum effects are typically neglected or are included in the form of harmonic zero point energy corrections and Bell tunneling corrections[6]. Grid-based methods[5] can provide accurate nuclear wavefunctions for the Born-Oppenheimer potential energy surface but are computationally expensive for multidimensional systems.

Recently methods have been developed to include nuclear quantum effects in electronic structure calculations without invoking the Born-Oppenheimer approximation. In the nuclear-electronic orbital (NEO) approach[10, 12, 13, 14, 15, 18],

specified nuclei are treated quantum mechanically on the same level as the electrons by solving a mixed nuclear-electronic Schrödinger equation using molecular orbital techniques. The NEO approach is designed for the quantum mechanical treatment of a relatively small number of nuclei, such as the hydrogen nuclei involved in key hydrogen bonding interactions or hydrogen transfer reactions. This approach has been implemented at the Hartree-Fock (NEO-HF), configuration interaction (NEO-CI), multiconfigurational self-consistent-field (NEO-MCSCF), and second-order perturbation theory (NEO-MP2) levels. Similar techniques have been developed by other groups[35, 33, 29, 26, 34, 28, 32, 27, 36].

These molecular orbital-based methods typically produce nuclear wavefunctions that are too localized, leading to severe overestimations of hydrogen vibrational frequencies. The magnitudes of the errors in the calculated hydrogen vibrational stretch frequencies are often 2000-3000 cm^{-1} (i.e., on the same order as the frequencies themselves)[34, 28, 32, 27, 36, 73, 74, 17]. The bending mode frequencies involving hydrogen are also often qualitatively incorrect. The over-localization of the nuclear wavefunction impacts not only the frequencies, but also the geometries, the isotope effects, and the tunneling splittings. We have demonstrated that the over-localization of the ground state nuclear wavefunction can result in qualitative errors for the geometric isotope effects in hydrogen-bonded systems[17, 16]. For example, grid-based methods and experimental data indicate that deuteration decreases the fluorine-fluorine distance in the hydrogen fluoride dimer, whereas the molecular orbital-based methods predict that deuteration increases this distance[17].

We have shown that dynamical electron-proton correlation strongly influences the delocalization of nuclear wavefunctions[12, 13]. Unfortunately, the recovery of electron-proton correlation using orbital-based treatments suffers from slow convergence reminiscent of that found for precise treatments of electron-electron correlation. The qualitative impact of electron-proton dynamical correlation on the wavefunction is greater than that of electron-electron dynamical correlation because of the attractive electrostatic interaction between the electron and the proton and the difference between the masses. The physical basis for the problems with the molecular orbital-based approaches for treating electron-proton correlation can be understood by comparison to a Born-Oppenheimer grid-based calculation of the nuclear wavefunction. In this treatment, the external potential is computed at

discrete points of a grid representing the nuclear coordinates by calculating a new electronic wavefunction for each set of nuclear coordinates. Thus, the electrons adjust instantaneously to the positions of the nuclei. The conventional molecular orbital-based approaches do not include this type of explicit correlation between the electrons and the quantum nuclei. At the Hartree-Fock level, the quantum nuclei move in an average field of the electrons, and the electrons move in an average field of the quantum nuclei. Corrections at the MP2 level and multiconfigurational methods are unable to fix the severe problems with the Hartree-Fock nuclear-electronic wavefunction.

In this chapter, we present the nuclear-electronic orbital explicitly correlated Hartree-Fock (NEO-XCHF) method, which includes explicit electron-proton correlation directly into the nuclear-electronic orbital self-consistent-field framework. This scheme is formulated using Gaussian basis functions for the electrons and the quantum nuclei in conjunction with Gaussian-type geminal functions that depend on the distance between an electron and a quantum nucleus. Previously explicit electron-electron correlation has been included in MP2 corrections for electronic structure calculations[107, 108] but, to our knowledge, not in the self-consistent-field procedure. Geminals have also been used in other contexts within electronic structure theory[109, 110]. Adamowicz and coworkers have developed a non-Born-Oppenheimer approach in which all electrons and nuclei are treated quantum mechanically with explicit correlation between all particles[39]. This approach is restricted to relatively small systems. In the NEO-XCHF approach, only a small number of nuclei are treated quantum mechanically, and only electron-proton correlation is treated explicitly with Gaussian-type geminals. As a result, the NEO-XCHF approach is applicable to larger systems of chemical and biological interest. We demonstrate that the hydrogen vibrational frequencies calculated at the NEO-HF level are improved significantly with the NEO-XCHF method for a model system. We also present a general form of the NEO-XCHF nuclear-electronic wavefunction that will enable calculations of larger many-electron systems.

6.2 Theory

For a system with one electron, one proton, and N_c classical point charges, the Hamiltonian is

$$\hat{H} = -\frac{1}{2}\nabla_e^2 - \frac{1}{2m_p}\nabla_p^2 - \sum_A^{N_c} \frac{Z_A}{|\mathbf{r}^e - \mathbf{r}_A^c|} + \sum_A^{N_c} \frac{Z_A}{|\mathbf{r}^p - \mathbf{r}_A^c|} - \frac{1}{|\mathbf{r}^e - \mathbf{r}^p|} \tag{6.1}$$

Here $\mathbf{r}^e$ and $\mathbf{r}^p$ denote the spatial coordinates of the electron and proton, respectively, and $\mathbf{r}_A^c$ and Z_A denote the spatial coordinates and the charges of the classical point charges. At the NEO-XCHF level, the total nuclear-electronic wavefunction for a system comprised of one electron and one proton is

$$\Psi_{tot}\left(\mathbf{r}^e, \mathbf{r}^p\right) = \psi^e\left(\mathbf{r}^e\right)\psi^p\left(\mathbf{r}^p\right)\left(1 + \sum_k^{N_{gem}} b_k \exp\left[-\gamma_k\left(\mathbf{r}^e - \mathbf{r}^p\right)^2\right]\right) \tag{6.2}$$

where $\psi^e\left(\mathbf{r}^e\right)$ and $\psi^e\left(\mathbf{r}^e\right)$ are spatial orbitals representing the electron and the proton, respectively. In Eq. 6.2, the summation term is the Gaussian-type geminal (GTG) expansion, which couples the electron and the proton. For notational convenience, we define the GTG factor as

$$G\left(\mathbf{r}^e, \mathbf{r}^p\right) \equiv \left(1 + \sum_k^{N_{gem}} b_k \exp\left[-\gamma_k\left(\mathbf{r}^e - \mathbf{r}^p\right)^2\right]\right) \tag{6.3}$$

We have derived modified Hartree-Fock equations using the standard variation method to minimize the energy $\left\langle \Psi_{tot} \middle| \hat{H} \middle| \Psi_{tot} \right\rangle$ with respect to both the electronic and the nuclear molecular orbitals subject to the normalization constraint $\langle \Psi_{tot} | \Psi_{tot} \rangle = 1$. The resulting Hartree-Fock equations for the electron and the proton are

$$f^e\left(\mathbf{r}^e\right)\psi^e\left(\mathbf{r}^e\right) = \varepsilon^e s^e\left(\mathbf{r}^e\right)\psi^e\left(\mathbf{r}^e\right) \tag{6.4}$$

$$f^p\left(\mathbf{r}^p\right)\psi^p\left(\mathbf{r}^p\right) = \varepsilon^p s^p\left(\mathbf{r}^p\right)\psi^p\left(\mathbf{r}^p\right) \tag{6.5}$$

where the Fock operators are defined as

$$f^e\left(\mathbf{r}^e\right) = \int d\mathbf{r}_p \psi^p\left(\mathbf{r}^p\right) G\left(\mathbf{r}^e, \mathbf{r}^p\right) \hat{H} \psi^p\left(\mathbf{r}^p\right) G\left(\mathbf{r}^e, \mathbf{r}^p\right) \tag{6.6}$$

$$f^p\left(\mathbf{r}^p\right) = \int d\mathbf{r}_e \psi^e\left(\mathbf{r}^e\right) G\left(\mathbf{r}^e, \mathbf{r}^p\right) \hat{H} \psi^e\left(\mathbf{r}^e\right) G\left(\mathbf{r}^e, \mathbf{r}^p\right) \tag{6.7}$$

and the overlap operators $s^e\left(\mathbf{r}^e\right)$ and $s^p\left(\mathbf{r}^p\right)$ are defined analogously without the operator $\hat{H}$.

The spatial orbitals for the electron and the proton are expanded in Gaussian basis sets:

$$\psi_i^e\left(\mathbf{r}^e\right) = \sum_{\mu}^{N_{bf}^e} c_{\mu i}^e \varphi_\mu^e\left(\mathbf{r}^e\right) \tag{6.8}$$

$$\psi_i^p\left(\mathbf{r}^p\right) = \sum_{\mu}^{N_{bf}^p} c_{\mu i}^p \varphi_\mu^p\left(\mathbf{r}^p\right) \tag{6.9}$$

where the unprimed indices refer to electronic basis functions and the primed indices refer to nuclear basis functions. Substitution of these expansions into Eqs. 6.4 and 6.5 leads to the Hartree-Fock-Roothaan equations for the electron and the proton:

$$\sum_{\nu}^{N_{bf}^e} F_{\mu\nu}^e c_{\nu i}^e = \varepsilon_i^e \sum_{\nu}^{N_{bf}^e} S_{\mu\nu}^e c_{\nu i}^e \tag{6.10}$$

$$\sum_{\nu'}^{N_{bf}^p} F_{\mu'\nu'}^p c_{\nu' i'}^p = \varepsilon_{i'}^p \sum_{\nu'}^{N_{bf}^p} S_{\mu'\nu'}^p c_{\nu' i'}^p \tag{6.11}$$

where the Fock matrix elements are defined as

$$F^e_{\mu\nu} = \sum_{\mu'\nu'}^{N^p_{bf}} c^p_{\mu' i'} c^p_{\nu' i'} H_{\mu\mu'\nu\nu'} \tag{6.12}$$

$$F^p_{\mu'\nu'} = \sum_{\mu\nu}^{N^e_{bf}} c^e_{\mu i} c^e_{\nu i} H_{\mu\mu'\nu\nu'} \tag{6.13}$$

$$H_{\mu\mu'\nu\nu'} = \iint d\mathbf{r}^e d\mathbf{r}^p \varphi^e_\mu\left(\mathbf{r}^e\right) \varphi^p_{\mu'}\left(\mathbf{r}^p\right) G\left(\mathbf{r}^e, \mathbf{r}^p\right) \hat{H} \varphi^e_\nu\left(\mathbf{r}^e\right) \varphi^p_{\nu'}\left(\mathbf{r}^p\right) G\left(\mathbf{r}^e, \mathbf{r}^p\right) \tag{6.14}$$

and the overlap matrix elements $S^e_{\mu\nu}$ and $S^p_{\mu'\nu'}$ are defined analogously without the operator $\hat{H}$. Note that these Fock and overlap matrices are different from those used in conventional electronic structure theory. As long as the overlap matrices are invertible, however, Eqs. 6.10 and 6.11 can be solved using standard matrix methods for generalized eigenvalue equations. The integrals over GTGs are evaluated using the McMurchie-Davidson approach by expanding them as linear combinations of Gaussian Hermite integrals[108, 111, 112, 113]. The NEO-XCHF approach has been incorporated into the GAMESS electronic structure code[23].

In addition, we have derived alternative modified Hartree-Fock equations using the variation method to minimize the total energy $\left\langle \Psi_{tot} \middle| \hat{H} \middle| \Psi_{tot} \right\rangle \Big/ \langle \Psi_{tot} | \Psi_{tot} \rangle$ with respect to both the electronic and the nuclear molecular orbitals subject to orthonormalization constraints for the electronic and nuclear molecular orbitals. In this case, the total wavefunction is not normalized. The resulting Hartree-Fock equations for the electron and the proton are

$$\left[\frac{1}{\langle \Psi_{tot} | \Psi_{tot} \rangle} f^e\left(\mathbf{r}^e\right) - \frac{\left\langle \Psi_{tot} | \hat{H} | \Psi_{tot} \right\rangle}{\langle \Psi_{tot} | \Psi_{tot} \rangle^2} \Lambda^e\left(\mathbf{r}^e\right) \right] \psi^e\left(\mathbf{r}^e\right) = \tilde{\varepsilon}^e \psi^e\left(\mathbf{r}^e\right) \tag{6.15}$$

$$\left[\frac{1}{\langle \Psi_{tot} | \Psi_{tot} \rangle} f^p\left(\mathbf{r}^p\right) - \frac{\left\langle \Psi_{tot} | \hat{H} | \Psi_{tot} \right\rangle}{\langle \Psi_{tot} | \Psi_{tot} \rangle^2} \Lambda^p\left(\mathbf{r}^p\right) \right] \psi^p\left(\mathbf{r}^p\right) = \tilde{\varepsilon}^p \psi^p\left(\mathbf{r}^p\right) \tag{6.16}$$

where the operators $\Lambda^e(\mathbf{r}^e)$ and $\Lambda^p(\mathbf{r}^p)$ are defined as

$$\Lambda^e(\mathbf{r}^e) = \int d\mathbf{r}_p \psi^p(\mathbf{r}^p) \left[G^2(\mathbf{r}^e, \mathbf{r}^p) - 1\right] \psi^p(\mathbf{r}^p) \tag{6.17}$$

$$\Lambda^p(\mathbf{r}^p) = \int d\mathbf{r}_e \psi^e(\mathbf{r}^e) \left[G^2(\mathbf{r}^e, \mathbf{r}^p) - 1\right] \psi^e(\mathbf{r}^e) \tag{6.18}$$

Expansion of the molecular orbitals in Gaussian basis sets using Eqs. 6.8 and 6.9 leads to Hartree-Fock-Roothaan equations that are identical to those in NEO-HF except that the Fock operators are modified to be the expressions in square brackets in Eqs. 6.15 and 6.16. As the GTG factor $G(\mathbf{r}^e, \mathbf{r}^p)$ approaches unity, Eqs. 6.15 and 6.16 approach the NEO-HF equations. Note that the molecular orbital energies are different in the two formulations of NEO-XCHF.

We have confirmed that the two formulations of NEO-XCHF give identical ground and excited state energies for the model systems studied in this chapter. We used the first formulation given by Eqs. 6.4 and 6.5 to calculate the vibrational stretching frequencies presented below. The frequencies were calculated as the energy difference between the proton eigenvalues defined in Eq. 6.11 for the excited state corresponding to the hydrogen vibrational stretching mode and the ground state. Similar frequencies were obtained by performing a separate NEO-XCHF calculation for the relevant excited state.

This approach can be extended to systems composed of multiple electrons and multiple quantum nuclei by using the following form of the total nuclear-electronic wavefunction:

$$\Psi_{tot} = \Phi^e(\mathbf{r}^e)\Phi^p(\mathbf{r}^p)\left\{1 + \sum_{i=1}^{N_e}\sum_{j=1}^{N_p}\sum_{k=1}^{N_{gem}} b_k \exp\left[-\gamma_k\left(\mathbf{r}_i^e - \mathbf{r}_j^p\right)^2\right]\right\} \tag{6.19}$$

Here $\Phi^e(\mathbf{r}^e)$ and $\Phi^p(\mathbf{r}^p)$, respectively, are antisymmetrized wavefunctions (i.e., determinants of spin orbitals) representing the electrons and fermionic nuclei such as protons. The total wavefunction is antisymmetric with respect to interchange of any two electrons or any two quantum nuclei because the GTG factor is symmetric with respect to these interchanges. The extension to bosonic nuclei is straightforward[16]. Including the GTGs as a summation of Gaussians multiplied

by the NEO-HF wavefunction is more computationally practical than including them as a product of Gaussians or at the basis function level because this form requires only 4-particle and simpler integrals. Since the geminal expansion parameters, b_k and γ_k, represent fundamental properties of an electron and a proton, these parameters can remain fixed at values predetermined from variational calculations on small systems. We expect that a relatively small number of GTGs (i.e. $N_{gem} \leqslant 4$) will be required to obtain the desired accuracy of the nuclear-electronic wavefunction. For the case of multiple electrons and quantum nuclei, modified Hartree-Fock equations analogous to those in Eqs. 6.15 and 6.16 can be solved iteratively to self-consistency. For large systems, the computational efficiency can be enhanced by avoiding the calculation of many of the demanding 3- and 4-particle integrals with a distance cutoff.

6.3 Application to model system

In order to validate the NEO-XCHF approach, we apply it to a model system containing one electron and one proton. The model system, $X^+[H]$, is depicted in Figure 6.1. This model consists of a hydrogen atom moving in the field of an infinitely massive positive point charge. The electron and the proton of the hydrogen atom are treated quantum mechanically, and the positive point charge X^+ is treated classically. We emphasize that the NEO approach is designed for systems in which at least two nuclei are treated classically, thereby eliminating the difficulties associated with translations and rotations[30]. In this model system, however, only a single nucleus is treated classically, so the ground state should be a rotational state that is spherically symmetric about the classical nucleus. We are able to describe the vibrational states along the X−H axis by placing the basis function centers for the nucleus and the electron at a single point. The same basis function center is used for both the electronic and the nuclear basis functions.

The frequencies corresponding to the stretching motion of hydrogen, deuterium, and tritium in the $X^+[H]$ system were calculated using the NEO-HF and the NEO-XCHF methods. The cc-pVDZ electronic basis set was used for all calculations[52]. For the NEO calculations, the distance between the classical nucleus and the centers of the electronic and nuclear basis functions was chosen to be the equilibrium

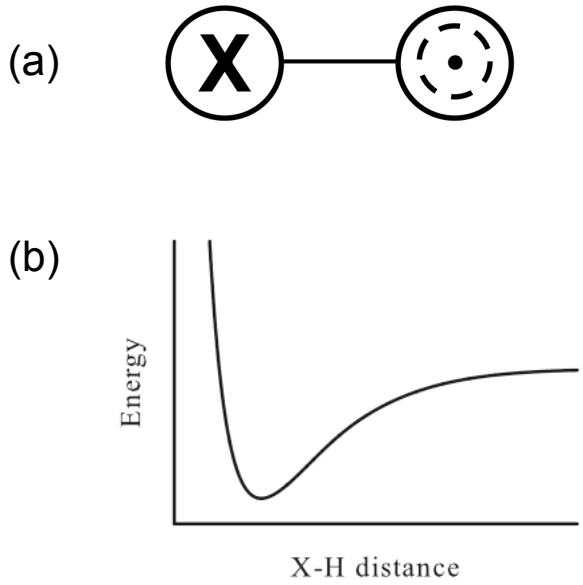

Figure 6.1. (a) Schematic picture of the $X^+[H]$ model system. The solid circles represent the electronic basis functions, and the dashed circle represents the nuclear basis functions. (b) The ROHF potential energy as a function of the X−H distance for the model system.

distance obtained from a conventional ROHF/cc-pVDZ calculation of H_2^+. An even-tempered (ET) nuclear basis set including $5s$, $5p$, and $5d$-type Gaussian basis functions was constructed for hydrogen, deuterium, and tritium using the method of Bardo and Ruedenberg[114]. The exponents for this basis set are given in Table 6.1. To avoid significant contamination of the vibrational states with rotational character, the d basis functions with the two lowest-frequency exponents were excluded for the calculations on hydrogen, and the d basis functions with the lowest-frequency exponent were excluded for the calculations on deuterium and tritium. Four GTGs were included in the NEO-XCHF calculations. The values of b and γ in the geminal expansion were variationally optimized simultaneously with the exponent of the nuclear basis function for NEO-XCHF/1s calculations with only a single 1s Gaussian nuclear basis function. The values of these parameters are presented in Table 6.2. The values of these parameters were fixed for the subsequent NEO-XCHF/ET calculations. The NEO-HF nuclear wavefunctions for the ground state and the excited state corresponding to the hydrogen vibrational

stretching mode are depicted in Figure 6.2.

Table 6.1. Exponents for the ET-5s5p5d nuclear basis set for H, D, and T isotopes.

n	$\nu_n(\mathrm{cm}^{-1})$	$\zeta_n\,(\mathrm{bohr}^{-2})$ H^a	$\zeta_n\,(\mathrm{bohr}^{-2})$ D^a	$\zeta_n\,(\mathrm{bohr}^{-2})$ T^a
1	500	2.091532	4.180988	6.274596
2	866	3.622534	7.241472	10.867601
3	1500	6.274596	12.542965	18.823789
4	2598	10.867601	21.724415	32.602802
5	4500	18.823789	37.628895	56.471366

[a] The exponents in the Table are related to frequencies using the harmonic approximation. The range of frequencies used for determining the exponents was generated using the even-tempered scheme developed by Bardo and Ruedenberg[114]. $\nu_n = \alpha\beta^n$.

The results for the X$^+$[H] model system are presented in Table 6.3. For comparison, we calculated the frequencies at the ROHF level from the Hessian and with the vibrational self-consistent-field (VSCF) method[5, 66] which is a grid-based method that includes anharmonic effects. The VSCF method is expected to be accurate for this model system because the electron is predominantly adiabatic with respect to the proton. The NEO-HF frequencies are greater than the frequencies calculated using the Hessian and VSCF approaches for all three isotopes by approximately a factor of two, corresponding to an error with magnitude of ~ 2000 cm^{-1} for hydrogen. When four GTGs are included in the NEO-XCHF calculation, the frequencies are within 5 cm^{-1} of the VSCF frequencies for H and T and within 100 cm^{-1} of the VSCF frequency for D. Since dynamical electron-proton correlation is responsible for the dramatic improvement in the frequencies, we also computed the frequencies using the NEO-full CI approach. Note that even the NEO-full CI method does not provide frequencies as accurate as the NEO-XCHF approach. In addition, we found that the variationally optimized exponent of the 1s basis function from the NEO-XCHF/1s calculation corresponds to a frequency much lower and closer to the harmonic ROHF frequency than the exponent from an analogous NEO-HF/1s calculation. Thus, the NEO-XCHF method provides a more accurate description of the nuclear wavefunction than the NEO-HF method.

Table 6.2. Values for the geminal expansion parameters determined by non-linear optimization.

Isotope	b_1	γ_1	b_2	γ_2	b_3	γ_3	b_4	γ_4	ζ [a]	E (au)
	–	–	–	–	–	–	–	–	14.29	-0.573863
	0.852	1.962	–	–	–	–	–	–	9.101	-0.582212
H	0.5054	8.97	0.784	1.342	–	–	–	–	8.286	-0.584926
	5.046	0.1928	5.407	1.2366	3.467	8.275	–	–	5.297	-0.592260
	9.1737	0.4496	9.54	2.0777	6.072	0.0917	5.605	13.799	5.264	-0.592833
D	2.399	26.16	4.304	3.869	5.548	0.8769	5.287	0.1601	7.391	-0.595467
T	2.337	26.361	4.199	3.936	5.439	0.8902	5.284	0.1604	9.041	-0.596599

[a]Nuclear Gaussian 1s basis function exponent value.

Table 6.3. Vibrational stretching frequencies calculated from the energy level splittings for the model system.

Isotope	NEO-HF	NEO-XCHF	NEO-full CI	Harmonic ROHF	VSCF ROHF
H	3621	1649	2263	1710	1645
D	2729	1081	1707	1210	1177
T	2302	963	1457	988	966

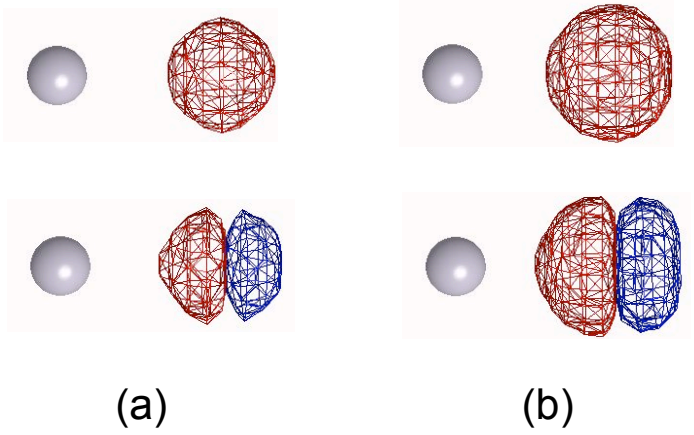

Figure 6.2. Nuclear molecular orbitals for the ground and excited proton vibrational states for the $X^+[H]$ model system computed at the (a) NEO-HF and (b) NEO-XCHF levels. 2 GTGs were used in the NEO-XCHF calculation.

We emphasize that the goal of the NEO-XCHF approach is not to obtain quantitatively accurate frequencies for spectroscopic purposes, but rather to obtain qualitatively reasonable frequencies that enable the calculation of geometries, isotope effects, vibronic couplings, and tunneling splittings for relatively large systems. The improvement observed for this model system suggests that the NEO-XCHF approach will alleviate the qualitative errors observed previously for properties such as the geometric isotope effects[17].

6.4 Conclusions

We presented a method that includes explicit electron-proton correlation directly into the nuclear-electronic orbital self-consistent-field framework. Our application of the NEO-XCHF method to a model system illustrates that the description of the nuclear wavefunction is significantly improved by the inclusion of explicit electron-proton correlation. In particular, the nuclear wavefunction becomes more delocalized, and the hydrogen vibrational frequencies are decreased when explicit electron-proton correlation is included. An accurate description of the nuclear wavefunction is essential for the calculation of geometries, isotope effects, vibronic couplings, and tunneling splittings.

The NEO-XCHF approach is computationally practical for many-electron systems because only a relatively small number of nuclei are treated quantum mechanically and only electron-proton correlation is treated explicitly. Electron-electron dynamical correlation can be included within the framework of this approach using density functional theory or second-order perturbation theory. Non-dynamical correlation can be included with multiconfigurational methods such as MCSCF[12, 13] and non-orthogonal CI[18]. This approach will facilitate computational studies of a wide range of chemically and biologically significant hydrogen transfer and hydrogen bonding systems.

Chapter 7

Conclusions

The nuclear-electronic orbital approach was designed to include nuclear quantum effects directly into electronic structure calculations in a computationally efficient way by calculating mixed nuclear-electronic wavefunctions with molecular orbital methods. Analagous to conventional electronic structure theory where electron-electron correlation is an important effect, in nuclear-electronic structure theory, electron-nuclear correlation is even more important. The focus of this dissertation was on the development of methods for including electron-nuclear correlation in the NEO framework and its impact on nuclear wavefunctions. In addition, the impact of nuclear quantum effects on hydrogen bonding was studied using NEO and other state-of-the-art approaches including vibrational self-consistent field (VSCF), vibrational perturbation theory (VPT), and path integral Car-Parrinello molecular dynamics (PICPMD).

In order to include dynamical electron-proton correlation in the NEO framework, we implemented the NEO second-order perturbation theory (NEO-MP2) approach in Chapter 2. The NEO-MP2 approach contains individual perturbation corrections for electron-electron and electron-proton correlation. We have shown that for systems containing only a single quantum nucleus, there are two distinct formulations of NEO-MP2 theory, depending on whether or not the nuclear Coulomb exchange operator was included in the reference Hamiltonian. We proved analytically that the removal of the proton-proton Coulomb-exchange operator from the reference Hamiltonian leads to a lower NEO-MP2 energy for a system composed of one electron and one proton represented by two electronic

and two nuclear basis functions. We also demonstrated empirically that this trend holds by calculating second order electron-proton corrections for three different chemical systems.

In Chapter 3, a number of key issues related to the application of the NEO approach to hydrogen transfer reactions were addressed. We discussed the representation of each hydrogen with multiple basis function centers and the variational optimization of the positions of the basis function centers. Our analysis demonstrated that two nuclear basis function centers can adequately describe both single and double well proton potential energy surfaces. Since hydrogen transfer reactions often sample both single and double well proton potential energy surfaces, this type of flexibility in the nuclear basis set is important. We performed a comparative study of the NEO-HF, NEO-MP2, and NEO-full CI methods for a symmetric proton transfer system containing a double well proton potential energy surface. The results demonstrated that electron-proton correlation is critical for the variational optimization of the nuclear basis function centers and the delocalization of the nuclear wavefunctions for these types of systems. The NEO approach was compared to grid-based methods for the calculation of vibronic splittings. It was shown that the splittings calculated with the NEO method converge toward the grid-based splittings as the quality of the nuclear basis set is improved.

We have shown that nuclear quantum effects of the hydrogen atom motions significantly impact the structures and other properties of hydrogen bonded systems. In Chapters 4 and 5, we studied the impact of nuclear quantum effects on the structures of several hydrogen bonded systems using the NEO approach, multi-dimensional grid-based methods, VSCF, VPT2, and PICPMD.

The structural impact of nuclear quantum effects for a set of bihalides, $[XHX]^-$ with X = F, Cl, and Br, and the hydrogen fluoride (HF) dimer were investigated in Chapter 4. For the bihalides, inclusion of the nuclear quantum effects of the hydrogen significantly increased the X−X distances. The X−X distances calculated with the NEO-MP2(ee)/1D grid method were in excellent agreement with the distances calculated with the Born-Oppenheimer two-dimensional method. The NEO-MP2(ee+ep) and VSCF methods lead to smaller X−X distances that are in better agreement with the experimental R_0 values available for X = F and Cl. This improvement is due to a more accurate description of the bending modes, which

are neglected in the two-dimensional grid method. The better agreement between the experimental and NEO-MP2(ee+ep) X−X distances shows that including dynamical electron-proton correlation leads to a better description of the hydrogen bending motions in these systems.

Since the HF dimer contains bending motions which are an order of magnitude lower in frequency than the F−H stretching motions, it is a more challenging hydrogen bonded system to study with these methods. Experimental data for the F−F distance is available for both a model which removes the large amplitude bending motions and another model which includes them. Inclusion of the hydrogen quantum effects using the NEO-MP2 approach decreases the F−F distance in the HF dimer and agrees well with the F−F distance obtained experimentally for the model that removes large amplitude bending motions. Inclusion of nuclear quantum effects with the VSCF, VPT2, and path integral methods increases the F−F distance. The VPT2 F−F distance is in close agreement with the experimental F−F distance for the model which includes the bending motions.

In Chapter 5, we studied the structural impact of nuclear quantum effects for a series of hydrogen fluoride clusters using PICPMD and VPT2. We found that for the $(HF)_{2-4}$ clusters, inclusion of nuclear quantum effects lead to increased F−F distances and for $(HF)_{5-8}$ clusters, inclusion of nuclear quantum effects produces shorter F−F distances. Thus, as the HF clusters evolve toward the condensed phase, a directional change in the impact of nuclear quantum effects on the hydrogen bonding occurs. The directional change for the $(HF)_{2-6}$ clusters does not appear for the F−F distances calculated at the NEO-MP2(ee+ep) level. Instead, the F−F distances calculated with NEO are always shorter than the F−F distances calculated at the MP2 level. This difference arises because the NEO-MP2(ee+ep) approach does not treat the bending/librational motions in the HF clusters correctly.

The reason that the NEO method was not able to treat the lower frequency bending modes properly is a lack of dynamical electron-proton correlation. As demonstrated earlier in Chapter 3, dynamical electron-proton correlation impacts the delocalization of nuclear wavefunctions. The fact that orbital-based methods with CI and MP2 do not recover enough dynamical electron-proton correlation is due to the attractive nature between the electron and proton and also because of

the larger mass of the proton. Because of the attractive nature of the electron-proton interaction, the overall nuclear-electronic wavefunction must be capable of describing the system when the electrons and protons are very close, i.e. the electron-proton cusp must be described accurately.

In order to include explicit dynamical electron-proton correlation into the nuclear-electronic orbital framework, we implemented the NEO explicitly correlated Hartree-Fock (NEO-XCHF) approach. In the NEO-XCHF approach the electrons and quantum protons are expanded using Gaussian basis sets in conjunction with Gaussian-type geminal functions, which depend on the distance between an electron and a quantum nucleus. We have applied the NEO-XCHF approach to a model system comprised of one electron, one quantum proton, and one infinitely massive positive point charge. The description of the nuclear wavefunction was significantly improved by the inclusion of explicit electron-proton correlation. In particular, the nuclear wavefunction became more delocalized, and the hydrogen vibrational frequencies were decreased when explicit electron-proton corelation was included. The NEO-XCHF approach is currently being extended to treat systems containing multiple electrons and protons.

Overall, we have used two different approaches to include dynamical electron-proton correlation in the NEO framework. The NEO-MP2 method is an orbital-based approach for including electron-proton correlation as a second-order perturbation correction. The NEO-XCHF method includes local corrections for dynamical electron-proton correlation *during* the variational calculation of mixed nuclear-electronic wavefunctions using Gaussian basis sets in conjunction with Gaussian-type geminals. Our results indicate that dynamical electron-proton correlation significantly impacts the *qualitative* characteristics of nuclear wavefunctions. Moreover, dynamical electron-proton correlation is essential for treating systems containing low frequency, large amplitude atomic motions such as hydrogen bonded clusters. Methods based on orbital expansions for recovering dynamical electron-proton correlation suffer from slow convergence reminiscent of that found for precise treatments of electron-electron correlation. Therefore, in order to include nuclear quantum effects even qualitatively, a many-particle formulation of the NEO-XCHF method is needed.

Considering the increased complexity of the integrals required in the NEO-

XCHF method, it is unlikely that this approach will be useful for treating systems requiring a large number of quantum nuclei. Rather, the NEO-XCHF method will be more useful in studying hydrogen transfer systems in which only a small number of nuclei require quantum mechanical treatment. For these systems, the efficiency can be significantly increased by screening out small integrals involving geminal functions.

In the future, dynamical electron-electron correlation must be incorporated into the NEO-XCHF framework. This can be done using density functional theory or second-order perturbation corrections. Another interesting direction will be to remove the adiabatic separation between the light and heavy nuclei in the NEO framework.

Bibliography

[1] Astrand, P. O.; Ruud, K.; Taylor, P. R. *Journal of Chemical Physics* **2000**, *112*, 2655–2667.

[2] Barone, V. *Journal of Chemical Physics* **2004**, *120*, 3059–3065.

[3] Barone, V. J. *Journal of Chemical Physics* **2005**, *122*, 014108.

[4] Bowman, J. M. *Journal of Chemical Physics* **1978**, *68*, 608–610.

[5] Bowman, J. M. *Accounts of Chemical Research* **1986**, *19*, 202–208.

[6] Bell, R. P. *The Tunnel Effect in Chemistry;* Chapman and Hall: London, 1980.

[7] Liu, Y.; Lu, D. H.; Gonzalez-Lafont, A.; Truhlar, D. G.; Garrett, B. C. *Journal of the American Chemical Society* **1993**, *115*, 7806–7817.

[8] Webb, S. P.; Hammes-Schiffer, S. *Journal of Chemical Physics* **2000**, *113*, 5214–5227.

[9] Webb, S. P.; Agarwal, P. K.; Hammes-Schiffer, S. *Journal of Physical Chemistry B* **2000**, *104*, 8884–8894.

[10] Webb, S. P.; Iordanov, T.; Hammes-Schiffer, S. *Journal of Chemical Physics* **2002**, *117*, 4106–4118.

[11] Iordanov, T.; Hammes-Schiffer, S. *Journal of Chemical Physics* **2003**, *118*, 9489–9496.

[12] Pak, M. V.; Hammes-Schiffer, S. *Physical Review Letters* **2004**, *92*, Art.No. 103002.

[13] Pak, M. V.; Swalina, C.; Hammes-Schiffer, S. *Chemical Physics* **2004**, *304*, 227–236.

[14] Swalina, C.; Pak, M. V.; Hammes-Schiffer, S. *Chemical Physics Letters* **2005**, *404*, 394–399.

[15] Swalina, C.; Pak, M. V.; Hammes-Schiffer, S. *Journal of Chemical Physics* **2005**, *123*, 014303.

[16] Reyes, A.; Pak, M. V.; Hammes-Schiffer, S. *Journal of Chemical Physics* **2005**, *123*, 064104.

[17] Swalina, C.; Hammes-Schiffer, S. *Journal of Physical Chemistry A* **2005**, *109*, 10410–10417.

[18] Skone, J. H.; Pak, M. V.; Hammes-Schiffer, S. *Journal of Chemical Physics* **2005**, *123*, 134108.

[19] Swalina, C.; Pak, M. V.; Chakraborty, A.; Hammes-Schiffer, S. *Journal of Physical Chemistry A* **2006**, *110*, 9983–9987.

[20] Handy, N. C.; Yamaguchi, Y.; Schaefer, H. F., I. *Journal of Chemical Physics* **1986**, *84*, 4481–4484.

[21] Kutzelnigg, W. *Molecular Physics* **1997**, *90*, 909.

[22] Csaszar, A. G.; Allen, W. D.; Schaefer, H. F., I. *Journal of Chemical Physics* **1998**, *108*, 9751–9764.

[23] Schmidt, M. W.; Baldridge, K. K.; Boatz, J. A.; Elbert, S. T.; Gordon, M. S.; Jensen, J. H.; Koseki, S.; Matsunaga, N.; Nguyen, K. A.; Su, S.; Windus, T. L.; Dupuis, M.; Montgomery, J. A. *Journal of Computational Chemistry* **1993**, *14*, 1347–1363.

[24] Thomas, I. L. *Physical Review* **1969**, *185*, 90–94.

[25] Thomas, I. L.; Joy, H. W. *Physical Review A* **1970**, *2*, 1200–1208.

[26] Tachikawa, M.; Mori, K.; Nakai, H.; Iguchi, K. *Chemical Physics Letters* **1998**, *290*, 437–442.

[27] Nakai, H. *International Journal of Quantum Chemistry* **2002**, *86*, 511–517.

[28] Nakai, H.; Sodeyama, K.; Hoshino, M. *Chemical Physics Letters* **2001**, *118-124*, 345.

[29] Nakai, H.; Sodeyama, K. *Journal of Chemical Physics* **2003**, *118*, 1119–1127.

[30] Nakai, H.; Hoshino, M.; Miyamoto, K.; Hyodo, S. *Journal of Chemical Physics* **2005**, *122*, 164101.

[31] Hoshino, M.; Nakai, H. *Journal of Chemical Physics* **2006**, *124*, 194110.

[32] Kreibich, T.; Gross, E. K. U. *Physical Review Letters* **2001**, *86*, 2984–2987.

[33] Shigeta, Y.; Nagao, H.; Nishikawa, K.; Yamaguchi, K. *Journal of Chemical Physics* **1999**, *111*, 6171–6179.

[34] Shigeta, Y.; Ozaki, Y.; Kodama, K.; Nagao, H.; Kawabe, H.; Nishikawa, K. *International Journal of Quantum Chemistry* **1998**, *69*, 629–637.

[35] Shigeta, Y.; Takahashi, S.; Yamanaka, S.; Mitani, M.; Nagao, H.; Yamaguchi, K. *International Journal of Quantum Chemistry* **1998**, *70*, 659–669.

[36] Bochevarov, A. D.; Valeev, E. F.; Sherrill, C. D. *Molecular Physics* **2004**, *102*, 111–123.

[37] Kozlowski, P. M.; Adamowicz, L. *Chemical Reviews* **1993**, *93*, 2007–2022.

[38] Kinghorn, D. B.; Adamowicz, L. *Physical Review Letters* **1999**, *83*, 2541–2543.

[39] Cafiero, M.; Bubin, S.; Adamowicz, L. *Physical Chemistry Chemical Physics* **2003**, *5*, 1491–1501.

[40] Roos, B. O., Ed. *Lecture Notes in Quantum Chemistry;* Springer-Verlag, Berlin, 1992.

[41] Marx, D.; Tuckerman, M. E.; Marthyna, G. J. *Computer Physics Communications* **1999**, *118*, 166–184.

[42] Benkovic, S. J.; Hammes-Schiffer, S. *Science* **2003**, *301*, 1196–1202.

[43] Borgis, D.; Hynes, J. T. *Chemical Physics* **1993**, *170*, 315–346.

[44] Deumens, E.; Ohrn, Y. *Journal of Physical Chemistry A* **2001**, *105*, 2660–2667.

[45] Bartlett, R. J. *Annual Review of Physical Chemistry* **1981**, *32*, 359–401.

[46] Raghavachari, K. *Annual Review of Physical Chemistry* **1991**, *42*, 615–642.

[47] Huzinaga, S.; Arnau, C. *Journal of Chemical Physics* **1971**, *54*, 1948.

[48] Potts, D. M.; Taylor, C. M.; Chaudhuri, R. K.; Freed, K. F. *Journal of Chemical Physics* **2001**, *114*, 2592.

[49] Szabo, A.; Ostlund, N. S. *Modern Quantum Chemistry;* McGraw-Hill, Inc., New York, 1989.

[50] Moller, C.; Plesset, M. S. *Physical Review* **1934**, *46*, 618.

[51] Surjan, P. R.; Szabados, A. *Journal of Chemical Physics* **2000**, *112*, 4438–4446.

[52] Dunning Jr., T. H. *Journal of Chemical Physics* **1989**, *90*, 1007–1023.

[53] Woon, D. E.; Dunning Jr., T. H. *Journal of Chemical Physics* **1993**, *98*, 1358–1371.

[54] Woon, D. E.; Dunning Jr., T. H. *Journal of Chemical Physics* **1994**, *100*, 2975–2988.

[55] Light, J. C.; Hamilton, I. P.; Lill, J. V. *Journal of Chemical Physics* **1985**, *82*, 1400–1409.

[56] Marston, C. C.; Balint-Kurti, G. G. *Journal of Chemical Physics* **1989**, *91*, 3571–3576.

[57] Hehre, W. J.; Ditchfield, R.; Pople, J. A. *Journal of Chemical Physics* **1972**, *56*, 2257–2261.

[58] Jensen, F. *Chemical Physics Letters* **1996**, *261*, 633–636.

[59] Brooks, C. L., I.; Karplus, M.; Pettitt, B. M. *Advances in Chemical Physics* **1988**, *71*, 1.

[60] Moriuchi, T.; Tamura, T.; Hirao, T. *Journal of the American Chemical Society* **2002**, *124*, 9356–9357.

[61] Finney, J. L. *Faraday Discussions* **1996**, *103*, 1–18.

[62] Headrick, J. M.; Bopp, J. C.; Johnson, M. A. *Journal of Chemical Physics* **2005**, *121*, 11523–11526.

[63] Hammer, N. I.; Diken, E. G.; Roscioli, J. R.; Johnson, M. A.; Myshakin, E.; Jordan, K. D.; McCoy, A. B.; Huang, X.; Bowman, J. M.; Carter, S. *Journal of Chemical Physics* **2005**, *122*, 244301.

[64] Gregory, J. K.; Clary, D. C. *Journal of Physical Chemistry* **1996**, *100*, 18014–18022.

[65] Clary, D. C.; Benoit, D. M.; van Mourik, T. *Accounts of Chemical Research* **2000**, *33*, 441–447.

[66] Chaban, G. M.; Jung, J. O.; Gerber, R. B. *Journal of Chemical Physics* **1999**, *111*, 1823–1829.

[67] Carter, S.; Bowman, J. M.; Handy, N. C. *Theoretical Chemistry Accounts* **1998**, *100*, 191–198.

[68] Diri, K.; Myshakin, E.; Jordan, K. D. *Journal of Physical Chemistry A* **2005**, *109*, 4005–4009.

[69] Tuckerman, M. E.; Marx, D.; Klein, M. L.; Parrinello, M. J. *Journal of Chemical Physics* **1996**, *104*, 5579–5588.

[70] Raugei, S.; Klein, M. L. *Journal of the American Chemical Society* **2003**, *125*, 8992–8993.

[71] Chen, B.; Ivanov, I.; Klein, M. L.; Parrinello, M. J. *Physical Review Letters* **2003**, *91*, 215503.

[72] Tachikawa, M.; Mori, K.; Osamura, Y. *Molecular Physics* **1999**, *96*, 1207–1215.

[73] Tachikawa, M. *Molecular Physics* **2002**, *100*, 881–901.

[74] Udagawa, T.; Ishimoto, T.; Tokiwa, H.; Tachikawa, M.; Nagashima, U. *Chemical Physics Letters* **2004**, *389*, 236–240.

[75] Shibl, M. F.; Tachikawa, M.; Kuhn, O. *Physical Chemistry Chemical Physics* **2005**, *7*(Shibl, M. F.; Tachikawa, M.; Kuhn, O. Phys. Chem. Chem. Phys), 1368–.

[76] Del Bene, J.; Jordan, M. *Spectrochimica Acta Part A: Molecular and Biomolecular Spectroscopy* **1999**, *55*, 719–729.

[77] Dyke, T. R.; Howard, B. J.; Klemperer, W. J. *Journal of Chemical Physics* **1972**, *56*, 2442–2454.

[78] Howard, B. J.; Dyke, T. R.; Klemperer, W. J. *Journal of Chemical Physics* **1984**, *81*, 5417–5425.

[79] Simon, S.; Duran, M.; Dannenberg, J. J. *Journal of Chemical Physics* **1996**, *105*, 11024–11031.

[80] Boys, S. F.; Bernardi, F. *Molecular Physics* **1970**, *19*, 553–566.

[81] Frisch, M. J.; Trucks, G. W.; Schlegel, H. B.; Scuseria, G. E.; Robb, M. A.; Cheeseman, J. R.; Montgomery, J. A., J.; Vreven, T.; Kudin, K. N.; Burant, J. C.; Millam, J. M.; Iyengar, S. S.; Tomasi, J.; Barone, V.; Mennucci, B.; Cossi, M.; Scalmani, G.; Rega, N.; Petersson, G. A.; Nakatsuji, H.; Hada, M.; Ehara, M.; Toyota, K.; Fukuda, R.; Hasegawa, J.; Ishida, M.; Nakajima, T.; Honda, Y.; Kitao, O.; Nakai, H.; Klene, M.; Li, X.; Knox, J. E.; Hratchian,

H. P.; Cross, J. B.; Adamo, C.; Jaramillo, J.; Gomperts, R.; Stratmann, R. E.; Yazyev, O.; Austin, A. J.; Cammi, R.; Pomelli, C.; Ochterski, J. W.; Ayala, P. Y.; Morokuma, K.; Voth, G. A.; Salvador, P.; Dannenberg, J. J.; Zakrzewski, V. G.; Dapprich, S.; Daniels, A. D.; Strain, M. C.; Farkas, O.; Malick, D. K.; Rabuck, A. D.; Raghavachari, K.; Foresman, J. B.; Ortiz, J. V.; Cui, Q.; Baboul, A. G.; Clifford, S.; Cioslowski, J.; Stefanov, B. B.; Liu, G.; Liashenko, A.; Piskorz, P.; Komaromi, I.; Martin, R. L.; Fox, D. J.; Keith, T.; Al-Laham, M. A.; Peng, C. Y.; Nanayakkara, A.; Challacombe, M.; Gill, P. M. W.; Johnson, B.; Chen, W.; Wong, M. W.; Gonzalez, C.; Pople, J. A. **2003**.

[82] Kawaguchi, K.; Hirota, E. *Journal of Chemical Physics* **1987**, *87*, 6838–6841.

[83] Kawaguchi, K. *Journal of Chemical Physics* **1988**, *88*, 4186–4189.

[84] Rasanen, M.; Seetula, J.; Kunttu, H. *Journal of Chemical Physics* **1993**, *98*, 3914–3918.

[85] Collins, C. L.; Morihashi, K.; Yamaguchi, Y.; Schaefer, H. F., I. *Journal of Chemical Physics* **1995**, *103*, 6051–6056.

[86] Peterson, K. A.; Dunning, T. H., J. *Journal of Chemical Physics* **1995**, *102*, 2032–2041.

[87] Astrand, P. O.; Karlstrom, G.; Engdahl, A.; Nelander, B. *Journal of Chemical Physics* **1995**, *102*, 3534–3554.

[88] Car, R.; Parrinello, M. J. *Physical Review Letters* **1985**, *55*, 2471–2474.

[89] Janzen, J.; Bartell, L. S. *Journal of Chemical Physics* **1969**, *50*, 3611–3618.

[90] Kreitmeir, M.; Heusel, G.; Bertagnolli, H.; Todheide, K.; Mundy, C. J.; Cuello, G. J. *Journal of Chemical Physics* **2005**, *122*, 154511.

[91] Rincon, L.; Almeida, R.; Garcia-Aldea, D.; Diez y Riega, H. *Journal of Chemical Physics* **2001**, *114*, 5552–5561.

[92] Guedes, R. C.; do Couto, P. C.; Costa Cobral, B. J. *Journal of Chemical Physics* **2003**, *118*, 1272–1281.

[93] Weis, P.; Kemper, P. R.; Bowers, M. T.; Xantheas, S. S. *Journal of the American Chemical Society* **1999**, *121*, 3531–3532.

[94] The piny md simulation package. Marthyna, G. J.; Tuckerman, M. E.

[95] Becke, A. D. *Physical Review A* **1988**, *38*, 3098–3100.

[96] Lee, C.; Yang, W.; Parr, R. G. *Physical Review B* **1988**, *37*, 785–789.

[97] Becke, A. D. *Journal of Chemical Physics* **1993**, *98*, 5648–5652.

[98] Stephens, P. J.; Devlin, F. J.; Chablowski, C. F.; Frisch, M. J. *Journal of Physical Chemistry* **1994**, *98*, 11623–11627.

[99] Ruud, K.; Astrand, P. O.; Taylor, P. R. *Journal of Chemical Physics* **2000**, *112*, 2668–2683.

[100] Ruud, K.; Astrand, P. O.; Taylor, P. R. *Journal of the American Chemical Society* **2001**, *123*, 4826.

[101] Dalton, a molecular electronic structure program. Helgaker, T.; Jensen, H. J. A.; Jorgensen, P.; et. al.. **2005**.

[102] Chaban, G. M.; Gerber, R. B. *Spectrochimica Acta Part A: Molecular and Biomolecular Spectroscopy* **2002**, *58*, 887–898.

[103] Yagi, K.; Taketsugu, T.; Hirao, T.; Gordon, M. S. *Journal of Chemical Physics* **2000**, *113*, 1005–1017.

[104] Roscioli, J. R.; Diken, E. G.; Johnson, M. A.; Horvath, S.; McCoy, A. B. *Journal of Physical Chemistry A* **2006**, *110*, 4943–4952.

[105] Loewenstein, A.; Shporer, M.; Lauterbur, P. C.; Ramirez, J. E. *Chemical Communications* **1968**, pages 214–215.

[106] Robertson, J. M.; Ubbelohde, A. R. *Proceedngs of the Royal Society of London Series A* **1939**, *170*, 222.

[107] Kutzelnigg, W.; Klopper, W. *Journal of Chemical Physics* **1991**, *94*, 1985–2001.

[108] Persson, B. J.; Taylor, P. R. *Journal of Chemical Physics* **1996**, *105*(5915-5926).

[109] Silver, D. M.; Mehler, E. L.; Ruedenberg, K. *Journal of Chemical Physics* **1970**, *52*, 1174–1180.

[110] Valeev, E. F.; Schaefer, H. F., I. *Journal of Chemical Physics* **2000**, *113*, 3990–3995.

[111] McMurchie, L. E.; Davidson, E. R. *Journal of Computational Physics* **1978**, *26*, 218–231.

[112] Persson, B. J.; Taylor, P. R. *Theoretical Chemistry Accounts* **1997**, *97*, 240–250.

[113] Boys, S. F. *Proceedngs of the Royal Society of London Series A* **1960**, *258*, 402–411.

[114] Bardo, R. D.; Ruedenberg, K. *Journal of Chemical Physics* **1974**, *60*, 918–931.

Vita

Chet Swalina

Education

- B.S. Chemistry, University of the Sciences in Philadelphia, 2001
  magna cum laude, Highest Honors in Chemistry
- Ph.D. Chemistry, The Pennsylvania State University
  Thesis Advisor: Prof. Sharon Hammes-Schiffer

Publications

1. C. W. Swalina, R. J. Zauhar, M. DeGrazia, and G. Moyna "Derivation of ^{13}C chemical shift surfaces for the anomeric carbons of oligosaccharides and glycopeptides using ab-initio methodology," *J. Biomol. NMR* **21**, 49-61 (2001).
2. C. W. Swalina, E. P. Obrien, and G. Moyna "Study of the temperature-dependent conformational averaging of ^{1}H NMR resonances in vinylcyclopropane using ab-initio methodology and Boltzmann statistics," *Magn. Reson. Chem.* **40**, 195-201 (2002).
3. M. Pak, C. Swalina, S. P. Webb, and S. Hammes-Schiffer "Application of the nuclear-electronic orbital method to hydrogen transfer systems: Multiple centers and multiconfigurational wavefunctions," *Chem. Phys.* **304**, 227-236 (2004).
4. C. Swalina, M. Pak, and S. Hammes-Schiffer "Alternative formulation of many-body perturbation theory for electron-proton correlation," *Chem. Phys. Lett.* **404**, 394-399 (2005).
5. C. Swalina, M. Pak, and S. Hammes-Schiffer "Analysis of the nuclear-electronic orbital method for model hydrogen transfer systems," *J. Chem. Phys.* **123**, Art No. 014303 (2005).
6. C. Swalina and S. Hammes-Schiffer "Impact of nuclear quantum effects on the molecular structure of bihalides and the hydrogen fluoride dimer," *J. Phys. Chem. A* **109**, 10410-10417 (2005).
7. C. Swalina, M. Pak, A. Chakraborty, and S. Hammes-Schiffer "Explicit electron-proton correlation in the nuclear-electronic orbital framework," *J. Phys. Chem. A* **110**, 9983-9987 (2006).